

**Modulation of the tumor microenvironment by the CXCR4 antagonist
AMD3100 in pancreatic and colorectal adenocarcinoma**

This dissertation is submitted for the degree of Doctor of Philosophy

**Martin Smoragiewicz
King's College**

Professor Duncan Jodrell Group

Submitted February 2019



Modulation of the tumor microenvironment by the CXCR4 antagonist AMD3100 in pancreatic and colorectal adenocarcinoma

Martin Smoragiewicz

Immunotherapy with checkpoint inhibitors has not been effective thus far in patients with micro-satellite stable pancreatic ductal adenocarcinoma (PDAC), which suggests an immunosuppressive mechanism operates within the tumour microenvironment (TME) of PDAC. In the *KRasG12D; p53R172H; Pdx1-Cre* (KPC) genetically engineered mouse model of PDAC, T cells are excluded from tumour nests and this effect is related to the chemokine CXCL12 produced by FAP+ stromal cells. Targeting the CXCL12/CXCR4 pathway with AMD3100, a CXCR4 antagonist, resulted T cell infiltration and tumor regression with anti-PD-L1 therapy in the KPC model. The CAMPLEX clinical trial was initiated to assess the safety of a 7-day AMD3100 infusion and provide proof-of-concept that AMD3100 reverses CXCL12 mediated immune-suppression in the TME.

The safety and pharmacokinetic results from the CAMPLEX dose escalation phase are presented. A dose-rate of AMD3100 80ug/kg/hr was safe, reasonably well tolerated, and achieved relevant plasma concentrations at steady state. However, pharmacodynamic markers of CXCR4 inhibition, including peripheral white blood cell and CD34+ cell mobilization, were maximal at the lowest dose-rate of 20ug/kg/hr, with little drug-related adverse events. An increase in T cell infiltration was observed in paired pre/post infusion tumour biopsies in a subset of patients, consistent with the pre-clinical KPC data. To further characterize the pharmacodynamic effects of AMD3100 on the TME, additional pre-clinical experiments in the KPC model were performed. Increased CXCR4 protein expression within the TME is a robust effect of AMD3100, which was also observed in the CAMPLEX biopsies. Furthermore, there was a large increase in the infiltration of F4/80+ macrophages at 6 days in KPC mice receiving a high dose of AMD3100. Further studies are warranted to determine their source, polarization, and whether they are related to the anti-tumour effects of AMD3100.

1. PREFACE.....	7
2. ABSTRACT.....	8
3. INTRODUCTION	9
4. MATERIALS AND METHODS	21
4.1. CAMPLEX patient eligibility.....	21
4.2. CAMPLEX study design.....	21
4.3. CAMPLEX safety evaluations	22
4.4. CAMPLEX response evaluation	23
4.5. CAMPLEX pharmacokinetic methods	23
4.6. CAMPLEX pharmacokinetic analysis	24
4.7. CAMPLEX pharmacodynamic correlates in the peripheral circulation	25
4.8. Mice	25
4.9. Histologic analysis.....	28
4.9.1. Immunohistochemistry	29
4.9.2. IHC image analysis	31
4.9.3. Immunofluorescence	34
4.9.4. Immunofluorescence image analysis	36
4.10. CAMPLEX TCRseq	39
4.10.1. DNA extraction.....	39
4.10.2. TCRseq.....	40
4.11. Statistical testing.....	42
4.12. Summary of work done by myself and others.....	42
5. PHARMACODYNAMICS OF CXCR4 INHIBITION IN MICE.....	44
5.1. High dose AMD3100 modestly decreases tumour growth and may improve survival in KPC mice	44

5.2. Pharmacodynamic effects of AMD3100 on tumour and normal tissue.....	46
5.2.1. Increased CXCR4 expression in tumour and normal tissue is a pharmacodynamic effect of AMD3100.....	46
5.2.2. High dose AMD3100 increases tumour infiltration of F4/80+ cells ..	49
5.3. Tumour cell proliferation, death and necrosis with AMD3100 treatment ...	51
5.4. Pharmacodynamic effects of AMD3100 in peripheral blood.....	52
5.5. Discussion.....	56
6. COMPLEX CLINICAL TRIAL: AMD3100 IS SAFE AND WELL TOLERATED AT TARGET 2µG/ML PLASMA CONCENTRATION	63
6.1. Patient population	63
6.1.1. Patient demographics.....	63
6.1.2. Impact of eligibility criteria on patient recruitment - an audit of patients referred to the Addenbrooke's Early Phase Clinical Trial Clinic	64
6.2. Safety data – AMD3100 is safe and well tolerated up to 80ug/kg/hr	65
6.2.1. Adverse events	65
6.2.2. Dose limiting toxicities	68
6.3. Pharmacokinetics.....	69
6.3.1. Target plasma AMD3100 concentrations achieved at 80 µg/kg/hr ..	69
6.3.2. AMD3100 terminal T _{1/2} may be longer than previously identified	70
6.3.3. AMD3100 clearance correlates with renal function, but not with measures of body composition	72
6.4. AMD3100 mobilizes white blood cell subsets into the peripheral circulation	74
6.5. Discussion.....	78
7. COMPLEX CLINICAL TRIAL: AMD3100 MAY INCREASE T CELL INFILTRATION AND TURNOVER IN A SUBSET OF PATIENTS	88

7.1. Clinical outcome endpoints (secondary and exploratory) following a 7 day AMD3100 continuous intravenous infusion	88
7.2. Paired biopsies for pharmacodynamic analysis from CAMPLEX dose escalation phase	91
7.3. CXCR4 expression in tumour is a pharmacodynamic effect of AMD3100	92
7.4. AMD3100 increased TILs in a subset of patients and a change in T cell repertoire	96
7.4.1. Image analysis algorithm validation and immunofluorescence variability	96
7.4.2. AMD3100 increased TILs in a subset of patients	97
7.4.3. AMD3100 may induce significant T cell turnover in the tumour.....	100
7.5. CXCL12 expression is variable between patients and does not correlate with the number of TILs	104
7.6. Changes in cancer and immune cell PD-L1 expression following AMD3100 infusion	106
7.7. Discussion	107
8. CONCLUSION	117
9. ACKNOWLEDGMENTS	119
10. ABBREVIATIONS	120
11. REFERENCES	121

1. PREFACE

- This dissertation is the result of my own work and includes nothing which is the outcome of work done in collaboration except as declared in the Preface and specified in the text.
- It is not substantially the same as any that I have submitted, or, is being concurrently submitted for a degree or diploma or other qualification at the University of Cambridge or any other University or similar institution except as declared in the Preface and specified in the text. I further state that no substantial part of my dissertation has already been submitted, or, is being concurrently submitted for any such degree, diploma or other qualification at the University of Cambridge or any other University or similar institution except as declared in the Preface and specified in the text
- It does not exceed the prescribed word limit for the relevant Degree Committee.

2. ABSTRACT

Immunotherapy with checkpoint inhibitors has not been effective thus far in patients with micro-satellite stable pancreatic ductal adenocarcinoma (PDAC), which suggests an immunosuppressive mechanism operates within the tumour microenvironment (TME) of PDAC. In the *KRasG12D; p53R172H; Pdx1-Cre* (KPC) genetically engineered mouse model of PDAC, T cells are excluded from tumour nests and this effect is related to the chemokine CXCL12 produced by FAP+ stromal cells. Targeting the CXCL12/CXCR4 pathway with AMD3100, a CXCR4 antagonist, resulted T cell infiltration and tumor regression with anti-PD-L1 therapy in the KPC model. The CAMPLEX clinical trial was initiated to assess the safety of a 7-day AMD3100 infusion and provide proof-of-concept that AMD3100 reverses CXCL12 mediated immune-suppression in the TME.

The safety and pharmacokinetic results from the CAMPLEX dose escalation phase are presented. A dose-rate of AMD3100 80ug/kg/hr was safe, reasonably well tolerated, and achieved relevant plasma concentrations at steady state. However, pharmacodynamic markers of CXCR4 inhibition, including peripheral white blood cell and CD34+ cell mobilization, were maximal at the lowest dose-rate of 20ug/kg/hr, with little drug-related adverse events. An increase in T cell infiltration was observed in paired pre/post infusion tumour biopsies in a subset of patients, consistent with the pre-clinical KPC data.

To further characterize the pharmacodynamic effects of AMD3100 on the TME, additional pre-clinical experiments in the KPC model were performed. Increased CXCR4 protein expression within the TME is a robust effect of AMD3100, which was also observed in the CAMPLEX biopsies. Furthermore, there was a large increase in the infiltration of F4/80+ macrophages at 6 days in KPC mice receiving a high dose of AMD3100. Further studies are warranted to determine their source, polarization, and whether they are related to the anti-tumour effects of AMD3100.

3. INTRODUCTION

Immunotherapy for pancreatic and colorectal adenocarcinoma

The incidence and mortality of pancreatic ductal adenocarcinoma (PDAC) has been steadily increasing in Europe[1] and the United States[2]. Only 15 to 20% of patients are potentially resectable on presentation, though most relapse despite adjuvant chemotherapy [3–5]. Recent advances chemotherapy have improved the prognosis for patients with advanced disease, but median survival remains under 1 year[6, 7]. There is therefore an unmet need for this increasing patient population.

Colorectal adenocarcinoma (CRC) is the second leading cause of cancer death in Europe[1]. Over the last 15 years, there has been significant improvement in the overall survival of patients with advanced colorectal cancer, with median survival approximately 30 months[8]. The improvement in survival is due to the development of new treatments, including cytotoxic chemotherapeutic agents (5-FU, irinotecan, oxaliplatin, TAS-102), agents targeting the Vascular Endothelial Growth Factor pathway (bevacizumab, aflibercept, ramucirumab, and regorafenib) and agents targeting the Epidermal Growth Factor Receptor pathway (cetuximab and panitumumab). However, the majority of patients with advanced CRC will die from their disease, with 5-year survival of approximately 5%[1]. Once they progress on standard therapies, the median overall survival for patients with advanced CRC is 5 to 6 months with best supportive care[9]. Therefore, there is an unmet need for patients with advanced CRC who have progressive disease on standard therapies.

Interest in cancer immunotherapy has been reborn over the last decade due to impressive results from a new class of agents, the checkpoint inhibitors. Blocking monoclonal antibodies to the T-cell immunologic checkpoint proteins

cytotoxic T-lymphocyte antigen 4 (CTLA-4), programmed cell death protein 1 (PD-1) and programmed death-ligand 1 (PD-L1) have shown activity across multiple tumours, including including melanoma, lung, renal, bladder, Hodgkin's lymphoma, head and neck cancers [10–16].

Immunotherapy for biomarker unselected patients with PDAC and CRC has thus far been disappointing. Unselected patients with PDAC did not show responses to treatment with anti-PD-L1[17] or anti-CTLA-4[18] antibodies. Similarly, unselected patients with CRC had response rates of <5% to treatment with anti-PD-(L)1[17, 19] and CTLA-4[20] antibodies. However, a landmark study in patients with CRC with mismatch repair deficient (dMMR) or microsatellite instability-high (MSI-H) solid tumours showed an impressive 40% objective response rate and durable responses with anti-PD-1 antibody pembrolizumab, while those with microsatellite stable (MSS) had no responses [16] The addition of anti-CTLA-4 to anti-PD-1 antibodies may further increase the response rate to 55% in MSI-H CRC [21]. The leading hypothesis to explain the differential response to checkpoint inhibitors is that MSI-H tumours have a high tumour mutational burden, and consequently more neoantigens, relative to MSS tumours[16]. However, these exciting results are likely of limited therapeutic value since the prevalence of MSI-H is only about 15% in CRC[22], and 5% in advanced CRC[23]. The prevalence of MSI-H in PDAC is even lower, less than 1%[24], but responses to anti-PD-1 therapy have been reported[25].

Therefore, there is an urgent need to understand whether additional and more fundamental immune suppression mechanisms operate within the tumour microenvironment of PDAC and CRC to explain the lack of responses to anti-CTLA-4 and anti-PD-(L)1 antibodies in this population with high unmet need.

CXCR4/CXCL12 mediated T cell exclusion from the tumour microenvironment

A variety of cells within the tumour microenvironment are being targeted to improve responses to checkpoint inhibition in pre-clinical models of PDAC, and

many are targeting myeloid cells such as tumour-associated macrophages (TAMs). CSF1/CSF1R blockade reprograms TAM to enhance antigen-presentation, reduce immunosuppression activity, increase anti-tumour T cell activity, and results in PDAC regression with PD-1/CTLA-4 checkpoint blockade[26]. CXCR2 blockade limits the accumulation of myeloid-derived suppressor cells (MDSCs) within the tumour microenvironment, and enables tumour regression with anti-PD-1 treatment[27]. Other promising approaches targeting myeloid cells include agents against CD40[28], Bruton tyrosine kinase (BTK)/ PI3K γ [29], and CCL2/CCR2[30]. Targeting tumour cells by Focal adhesion kinase (FAK) inhibition overcomes the fibrotic and inflammatory microenvironment, which potentiated the efficacy of anti-PD-1 and anti-CTLA-4 antibodies[31].

A collaboration between the Jodrell, Tuveson, and Fearon laboratories demonstrated that exclusion of tumour infiltrating lymphocytes (TILs) from the tumour microenvironment prevents responses to PD-L1 checkpoint inhibition in the autochthonous LSL- KrasG12D/+;LSL-Trp53R172H/+;Pdx-1-Cre (KPC) model of PDAC, despite the presence of a spontaneous adaptive immune response. The FAP+ stromal cells mediate this immunosuppressive mechanism, potentially by the production of the chemokine ligand 12 (CXCL12), which coats cancer cells. By administering AMD3100, an antagonist of the CXCL12 receptor CXCR4, TILs accumulate within the tumour microenvironment and KPC mice exhibit immune mediated control of tumour growth. AMD3100 synergized with anti-PD-L1 therapy, causing tumour regression and elimination of p53+ cancer cells in an immune dependent mechanism[32]. These observations suggest the hypothesis that AMD3100 enables T cells to come into contact with their tumour target, allowing anti-PD-L1 to exert its effect.

The exact mechanism by which CXCL12 excludes TILs from the microenvironment remains unknown. One possible mechanism may be due to T cell induced apoptosis[33]. The investigation of the high turnover rate of CD8 T

cells in HIV infection led to the discovery that the HIV envelop glycoprotein gp120 of strain X4 induced CD8 T cell apoptosis in a dose-dependent manner. Gp120 binds to the CXCR4 on CD8 T cells and macrophages, and upregulates the expression of tumour necrosis factor receptor II (TNFRII) on CD8 T cells and TNF α bound to the membrane of macrophages (mbTNF). The interaction of mbTNF and TNFRII induces CD8 T cell apoptosis. CXCL12 also induces a similar CD8 T cell apoptosis in a dose-dependent manner.

Alternatively, CXCL12 may have a concentration-dependent bi-functional effect on T-cell migration, where T-cells migrate towards a low concentration (chemotaxis), but away from high concentrations (terms chemofugetaxis) [34]. CXCL12 levels have not been directly measured in the tumour microenvironment and compared to other tissues. However, the chemofugetaxis properties of CXCL12 are being investigated to prevent islet cell transplantation for the treatment of type 1 diabetes. Islets coated with CXCL12 or encapsulated with alginate incorporating CXCL12 display long term survival and function in pre-clinical models, and suggests that CXCL12 may have similar effects in the tumor microenvironment[35].

To explain the paradox that CXCL12 is produced by FAP+ stromal cells yet localizes to the cancer cells, our group has previously hypothesized that CXCL12 is captured by high mobility group box 1 (HMGB1), which is overexpressed by metabolically stressed cancer cells[36], and forms a heterocomplex[37]. However, it is also unknown whether the free or membrane bound CXCL12 contribute to the exclusion of T cells from cancer nests, or both.

Regardless of the exact mechanism, clinical correlative studies support the notion that CXCL12 is relevant. Indeed, high expression of CXCL12 assessed by immunohistochemistry in primary tumours confers a worse prognosis in PDAC and CRC [38, 39], though correlations between CXCL12 expression and TIL infiltrates were not assessed.

CXCL12 and CXCR4 in health and disease

There are over 50 different chemokines and over 20 different chemokine receptors have been identified, which implies substantial redundancy in chemokine receptor binding[40]. CXCR4 is unique in that CXCL12 is the only known endogenous ligand for CXCR4[41]. CXCL12 also binds to the chemokine receptor CXCR7 (CXCR7), whose function is to control CXCL12 gradients by high affinity binding and degradation of CXCL12[42]. CXCL12 binding to CXCR4 initiates signaling through a variety of pathways. CXCR4 is a seven transmembrane G-protein-coupled receptor. G protein mediated signaling activates downstream phosphoinositide-3 kinase (PI3K), phospholipase C- β (PLC- β), and mitogen-activated protein kinase (MAPK). G protein independent signaling has also been reported to activate the JAK/STAT pathway[43]. The various signaling pathways activated by CXCL12/CXCR4 result in a plethora of responses including gene transcription, chemotaxis, cell survival, and proliferation.

CXCR4 is expressed in a variety of non-hematopoietic tissues (heart, brain, lung, kidney, and liver) in addition to a variety of hematopoietic cells (T and B cells, monocytes, macrophages, neutrophils, dendritic cells, and hematopoietic stem cells) [44–47]. The amino acid sequence of CXCL12 and CXCR4 are highly conserved in mammals. Underscoring the importance of CXCL12/CXCR4 signalling, CXCL12 is the only chemokine that is required for survival. Ablation of either CXCL12 or CXCR4 gene is embryonically lethal in mice, with very similar characteristics consisting of defects in B-cell lymphopoiesis, myelopoiesis, and cerebellar and heart development[48, 49]. Therapeutically, the CXCR4/CXCL12 role in the maintenance of hematopoietic stem cell pool in the bone marrow has been successfully targeted, as discussed below[45].

Few CXCR4 mutations have been reported but are responsible for a rare genetic syndrome with manifestations of warts, hypogammaglobulinemia,

infections and myelokathexis (WHIM syndrome)[50]. Normally, the CXCR4 receptor undergoes slow constitutive internalization (1%/min), and CXCL12 rapidly induces CXCR4 receptor endocytosis (50%/5min) and degradation in lysosomes [51–53]. In WHIM syndrome, mutations in the C-terminal of CXCR4 prevent receptor internalization, and results in persistent CXCR4 activation. Consequently, mature neutrophils do not leave the bone marrow, causing neutropenia and subsequent recurrent infections. There is also an increased susceptibility to human papilloma virus, suggesting a defect in cell mediated immunity.

The CXCR4 antagonist AMD3100

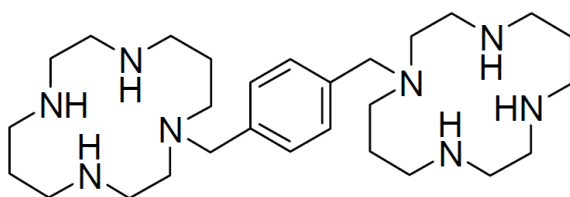


Figure 1 Molecular structure of AMD3100

AMD3100 is a molecule with 2 cyclam rings connected by an aromatic bridge and a molecular mass of 502.79 g/mol (anhydrous) (Figure 1). It is a strong base due to the basic nitrogens of each bicyclam ring, which enable electrostatic interaction with the acid carboxylates of aspartic acid residues at positions 171 and 262 of the CXCR4 receptor. Mutation of these 2 residues abrogates AMD3100 antagonism and impairs the function of CXCR4 as a co-receptor for HIV[54]. In a human T cell lymphoblast-like cell line (CCRF-CEM) expressing endogenous CXCR4, AMD3100 was shown to inhibit CXCL12 binding to CXCR4, CXCL12 mediated calcium flux, G-protein activation, and chemotaxis with half maximal inhibitory concentration (IC₅₀) values of 651±37, 572±190, 15.4±4, and 51±17 nM, respectively. AMD3100 also demonstrated lack

of inhibition of ligand-induced calcium flux and/or ligand binding for a series of chemokine and 7-transmembrane receptors including CXCR1-3, CXCR7, CCR1-9, and BLTR, demonstrating that AMD3100 is a potent, selective antagonist of CXCR4[55, 56].

AMD3100 was initially developed for the treatment of HIV[57], but this clinical program was discontinued due to poor antiviral activity [58] and oral bioavailability [59]. However, the observed mobilization of white blood cells (WBC) into the peripheral circulation in early trials was further investigated and found to also mobilize CD34+ cell counts [60]. CD34+ cells are collected by apheresis for autologous stem cell transplantation protocols. Single agent AMD3100 yielded modest CD34+ mobilization in a small study with patients with multiple myeloma [61]. However, the combination of granulocyte colony stimulating factor (G-CSF) and AMD3100 (240µg/kg subcutaneous [S/C] daily, starting on day 4) compared to G-CSF alone increased the proportion of patients with multiple myeloma or non-Hodgkin's lymphoma achieving the optimal CD34+ cell count target for transplantation in fewer apheresis days [62–64]. This is currently the only approved indication for AMD3100.

The current highest approved dose of AMD3100 (240 µg/kg) achieves a maximum plasma concentration (C_{max}) of ~1 µg/ml with a terminal half-life of 3.6-5hr [59, 65]. Given the short half-life and C_{max} below the biologically active dose in the pre-clinical studies discussed above (2 µg/ml, unpublished data), daily S/C dosing would not be adequate and multiple S/C dosing, not feasible. AMD3100 has previously been administered as a 10-day continuous IV infusion to HIV patients, safely achieving mean plasma concentrations of 3.28 µg/ml in the highest dose cohort (160 µg/kg/hr)[58]. The COMPLEX clinical trial (NCT02179970) was initiated to assess the safety of administering continuous infusion of AMD3100 and achieving an AMD3100 concentration at steady state \geq 2 µg/ml in patients with CRC, PDAC and high grade serous ovarian adenocarcinomas (HGSO). Patients HGSO were also included as they do not

show responses to anti-PD-(L)1 therapy[17, 19], high expression of CXCL12 is associated with worse prognosis [39, 66], and T cells are excluded from tumour nests[67, 68]. The CAMPLEX safety and pharmacokinetic data are the basis of Chapter 6.

Quantification of tumour infiltrating lymphocytes

Exploratory objectives of the CAMPLEX trial include an assessment of the modulation of tumour microenvironment from paired biopsies of metastases pre and post AMD3100 infusion. The exploratory objectives are an important addition to the trial as, although the KPC mouse model is currently the best experimental system for assessment of therapy for PDAC, previous studies demonstrating efficacy in this model have not translated into successful human therapies[69–71]. This is the first opportunity to assess whether AMD3100 can reverse CXCL12 mediated TIL exclusion from the tumour microenvironment in humans. This thesis has a special emphasis on histologic TIL quantification methodology.

A review of the literature suggests a variety of histologic TIL quantification methodologies, reflecting both available quantification tools and tumour immunology understanding. Central to these methods is the hypothesis that specific immune cell densities within different tumour compartments can be meaningfully correlated with clinical outcomes.

TIL density has prognostic value across multiple tumours and treatment modalities. Increasing TIL density has been linked to less advanced pathologic stage and improved survival in PDAC[72, 73] and CRC[74]. TIL density has been found to have equivalent [67] or even a superior and independent prognostic value to the Union for International Cancer Control TNM clinical staging in CRC[75, 76]. High TIL density at the invasive margin of incompletely resected metastatic liver disease prognosticated for response to palliative chemotherapy[77]. In breast cancer, estimates of lymphocyte densities within

both stroma and tumour nests have been linked to higher rates of pathologic complete response (pCR) to neo-adjuvant chemotherapy, a favorable prognostic factor[78]. In a series of melanoma patients treated with the PD-1 checkpoint inhibitor pembrolizumab, CD8 density at the invasive margin and centre of the tumour associated with clinical response[79].

However, there is no agreement on the definition of tumour compartments, or how to measure and compare them. TILs have been quantified within cancer cell nests compared to the surrounding stroma[67, 73, 78, 80], at the invasive margin[77, 81], in the center of a tumour compared to the invasive margin irrespective of their distribution within cancer cell nests or stroma[75, 79, 81], and other permutations of these compartments[67, 72]. Many have defined stroma as all the tissue between tumour nests, while others have subdivided it into distant and proximal stroma to account for TILs within the proximal stroma contacting tumour nests[80]. Others have included the proximal stromal TILs within the tumour nest counts[73, 78]. The invasive margin has been suggested to have more prognostic significance than the center of the tumour[75, 79], though a more detailed compartment analysis suggested TILs within tumour nests may be more prognostic than at the invasive margin[67].

The tools employed to quantify TIL densities within tumour compartments vary from semi-quantitative methods to software-based image analysis. Most semi-quantitative methods rely on trained pathologist to assess variables such as the percentage of stroma or tumour nests infiltrated by TILs[67, 78]. Though the inter-observer correlation within a study may be high[78], it is not clear how generalizable the method is and, therefore, whether values between studies can be compared. Another common method involves the subjective identification of one or several high-powered microscopy fields with the highest TIL infiltrate[67, 81], followed by a manual count of TILs. Beyond being labor-intensive and subject to inter-observer variability, it is not clear that the regions of highest subjective infiltrate are in fact the best, or only, regions to compare between

samples. Increasingly, image analysis software is being used for TIL quantification, offering the prospect of high throughput analyses that could be compared between studies[73, 75, 77, 79].

There is lack of agreement of which TIL subsets to measure. A recent review, summarizing over 120 different papers across various cancers, showed a very consistent association between increasing densities of CD8+, CD45RO+ and Th1+ cells with better prognosis. On the other hand, Th2+, Th17+, and T_{reg} cells have been inconsistently associated with improved, worse or not correlated with prognosis. This may reflect their plasticity within different tumour microenvironments across different tumours[82].

Currently, the Immunoscore™ is the most advanced scoring system that incorporates the above concepts of TIL location, density, and subtype with software image analysis. Immunoscore™ was developed in early stage CRC and may soon be changing clinical practice[74, 75]. Large H&E slides of primary tumours are first examined by a pathologist to determine the areas of highest TIL density within the center of the tumour and at the invasive margin. Subsequently, these regions are stained for CD8+ and CD45RO+ resident memory T cells. A subgroup of patients with low densities in both compartments have a particularly poor prognosis among a patient population with a generally good prognosis[76, 81]. A large consortium has been initiated to validate the Immunoscore™ in clinical practice for early stage CRC, and may identify patients that could benefit from adjuvant chemotherapy[83].

However, Immunoscore™ is unlikely to be an appropriate end-point for the CAMPLEX trial. Firstly, Immunoscore™ does not assess TIL densities between tumour nests and stroma, and may therefore miss any relative changes in TIL density in these compartments with AMD3100 treatment. Secondly, Immunoscore™ is not feasible due to a lack of an invasive margin on many biopsy specimens. Correlative studies from an anti-PD-1 trial with

Pembrolizumab in melanoma patients suggested that assessment of the invasive margin is feasible on biopsy specimens[79]. Melanoma patients may have easier to access metastases for larger biopsies, which would enable a clear definition of an invasive margin.

The literature suggests that TIL density and location matters. Given the proposed mechanism of AMD3100, we hypothesize that an increase in TIL density in tumour nests will be a pharmacodynamic read-out of the CAMPLEX clinical trial. Thus, a key objective was to develop a TIL quantification method for use with the CAMPLEX trial biopsies and a major section of Chapter 7.

The recently developed technique of sequencing the T-cell receptor beta (TCRb) third complementarity-determining region 3 (CDR3) may complement and add to the histologic pharmacodynamic readouts of the CAMPLEX trial (ImmunoSeq, Adaptive Biotechnologies). The TCRb CDR3 region directly contacts antigens on MHC molecules, and is unique to a T cell clone. Correlative studies from a clinical trial with an anti-PD-1 agent in melanoma patients demonstrated ten-fold more expanding clones in responding patients relative to non-responders[79]. We hypothesize that AMD3100 will result in a more clonal T cell population tumour biopsies. Additionally, this technology permits quantification of T cells by estimating TCR gene rearrangements per diploid genomes. This would complement the histologic TIL quantification, though the spatial distribution of TILs between stroma and tumour nests is lost.

If the CAMPLEX trial demonstrates AMD3100 reverses TIL exclusion in some patients, the question of predictive biomarkers will arise. The pre-clinical KPC experiments show that AMD3100 controlled tumour growth, but responses occurred in combination with anti-PD-L1[32]. It is reasonable to anticipate a similar situation in human PDAC, and therefore the next trial should combine AMD3100 with either anti-PD-1 or anti-PD-L1 checkpoint blockade. Enriching for patients most likely to respond would be valuable for this proof of concept trial.

The paired pre and post treatment biopsies on the CAMPLEX clinical trial will be an excellent opportunity to explore potential predictive biomarkers, such as CXCL12 expression.

Interpreting pharmacodynamic readouts on biopsies can be challenging for several reasons, including limited sample, and variability due to intra-patient TIL density heterogeneity. It is also unclear how the trauma of a biopsy may alter the immune infiltrate on a repeat biopsy. The Feig et al.[32] paper showed a large infiltration of CD3+ cells within p53+ cancer cell regions, although the effect was not quantified. Therefore, the intratumoural pharmacodynamic readouts of AMD3100 need to be better characterized to help interpret the biopsies from the CAMPLEX trial. Additionally, it would be important to understand if AMD3100 mediated CD3+ infiltration occurs at the invasive margin, in the centre of the tumour or both. These questions will be explored in KPC mice administered AMD3100 alone in Chapter 5.

4. MATERIALS AND METHODS

4.1. CAMPLEX patient eligibility

Patients with advanced or metastatic PDAC, HGSO or CRC, refractory to or declining conventional chemotherapy were eligible for the dose escalation phase. A 10 patient expansion cohort has been initiated in patients with PDAC using the recommended phase 2 dose (RP2D) of 80 µg/kg/hr. Other eligibility criteria included mandatory biopsy of the same metastasis at baseline and within +/- 4 hr of infusion end, an Eastern Cooperative Oncology Group (ECOG) performance status of 0 or 1, and life expectancy of at least 12 weeks. Patients were excluded if they met any of the following criteria: 1) inadequate hematologic function (including a lymphocyte count below the lower limit of normal), 2) inadequate renal function (creatinine clearance <50ml/min), 3) inadequate hepatic function, 4) treatment with chemotherapy, corticosteroids or other immunosuppressive agents within 28 days, 5) cardiac co-morbidity, including any history of significant arrhythmias or myocardial infarction < 6 months, 6) active infection, 7) pregnant, or 8) known hepatitis B, hepatitis C, or HIV infection. Patients were accrued at Addenbrooke's Hospital, Cambridge, UK in the dose escalation phase, and a second centre at Weill Cornell Medical College, NY, USA accrued additional patients to the dose expansion cohort.

4.2. CAMPLEX study design

This phase 1, multicentre, open-label, non-randomized study followed a 3+3 dose escalation design. The primary endpoint was to determine the safety of administering AMD3100 to achieve a plasma AMD3100 concentration at steady state ≥ 2 µg/ml in $\geq 80\%$ of patients at the RP2D. Based on a previous study of continuous IV infusion of AMD3100 in patients with HIV that achieved plasma AMD3100 concentrations at steady state of 1.8 and 3.2 µg/ml at doses of 80 and

160 µg/kg/hr [58], respectively, we anticipated a dose of 120µg/kg/hr to achieve the primary endpoint. AMD3100 was administered as a 7 day continuous infusion in planned dose cohorts of 20, 40, 80 and 120µg/kg/hr, and patients had the option of a second 7 day infusion in the event of a confirmed partial or complete response. Intra-patient dose escalation was not permitted. Safety was evaluated using the Common Terminology Criteria for Adverse Events (CTCAE) 4.03. A dose-limiting toxicity (DLT) was defined as any grade 3 or greater adverse event (AE) occurring within 21 days of completion when considered certainly, probably or possibly drug related. The RP2D will be confirmed in a 10 patient dose expansion cohort. Secondary endpoints included the determination of overall objective response rate, and metabolic changes in tumour using ¹⁸FDG-PET. Exploratory objectives included immune changes in tumour biopsies.

All patients provided written informed consent under a Research Ethics Committee-approved protocol, and in compliance with Good Clinical Practice (GCP), local regulatory requirements and legal requirements. A Clinical Trial Authorisation (CTA) was obtained from the Medicine and healthcare regulatory authority (MHRA). This study is sponsored by Cambridge University Hospitals NHS Foundation Trust and the University of Cambridge. Sanofi-Aventis Groupe provided study drug free of charge. The clinical trial was funded by Stand Up 2 Cancer and the Lustgarten Foundation.

4.3. CAMPLEX safety evaluations

Clinical review was performed at baseline, daily during the infusion, and weekly until day 21 after infusion discontinuation. Complete blood counts, biochemistry and C-reactive protein levels were obtained with a similar schedule, except only on days 2/4/8 during the infusion. Due to potential concerns of cardiac arrhythmias, patients were monitored by cardiac telemetry for the initial 48hr of the infusion (later amended to 72hr), and subsequently transitioned to a Holter monitor for the remaining part of the infusion. Patients were admitted to

the Clinical Research Facility at Addenbrooke's Hospital for cardiac telemetry, with the option to receive the remaining infusion in the outpatient setting.

4.4. CAMPLEX response evaluation

Overall response rate was determined according to the Response Evaluation Criteria in Solid Tumours (RECIST) 1.1 criteria[84]. Baseline CT scans were performed within 14 days before the start of the infusion, and at 14 (+/-2) days after the infusion. Patients with a partial or complete response were required to undergo a confirmatory CT scan at Day 56 prior to being eligible for a second infusion. ¹⁸FDG-PET/CT scans were performed within 14 days before the start of the infusion, and within 1 day of infusion completion. Analysis was performed in collaboration with radiology registrar Eva Serrao and supervised by consultant Ferdia Gallagher. ¹⁸FDG-PET/CT responses were determined according to PET Response Criteria in Solid Tumours (PERCIST) 1.0[85]. The standardized uptake value lean (SUL) peak was determined from a 1mm³ – volume spheric region of interest (ROI) centred on the hottest point in a tumour foci. The biopsied lesion was excluded from the PERCIST 1.0 analysis due to the uncertain effect of a biopsy on the metabolic uptake. Exploratory analyses were also performed on the biopsied metastasis, or sum of up to 5 target lesion SUL_{peak}.

4.5. CAMPLEX pharmacokinetic methods

Samples for plasma AMD3100 concentration analysis were taken at the following nominal time points: predose, 24, 72 and 168 hrs of the infusion. A time point at day 7(+/-2) after infusion discontinuation was added from patient 1017 onwards.

Plasma concentration of AMD3100 in CAMPLEX trial samples was measured by liquid chromatography-tandem mass spectrometry (LC-MS/MS)

using an assay developed by the PK/Bioanalytics Core Facility at CRUK-CI. AMD3100 calibration standards were prepared in the range of 40-4,000 ng/mL using blank control human plasma obtained from the NHS blood transfusion service (lower limit of quantification (LLOQ) 40 ng/mL). After the addition of the internal standard (AMD3100-D4) and EDTA (10mM), plasma samples, quality control (QC) and calibration standards were extracted using 1% formic acid in methanol to precipitate the plasma protein. Following vortex mixing and centrifuging, a portion of the supernatant was removed and the solvent evaporated. The residue was reconstituted in 1% formic acid in water prior to analysis on the LC-MS/MS. High-performance liquid chromatography was performed with the Thermo Scientific Accela Pump and Phenomenex Kinetex column (2.6 μ m, 100 x 2.1mm) using mobile phases A and B containing 0.1% formic acid in water or methanol, respectively. MS/MS detection was carried out using the Thermo Scientific TSQ Vantage with an electrospray source heated to 350°C. QC samples (40, 120, 400 and 3000 ng/mL) were used to determine the precision (coefficient of variation [%CV]) and accuracy (relative error [%RE]). Acceptability of bioanalytical batches was determined by the following criteria: at least 75% of calibration standards with $\pm 15\%$ RE (within $\pm 20\%$ RE at the LLOQ of their target concentrations; at least four of the six QC samples within $\pm 15\%$ RE of their respective target values. Two of the six QC samples may be outside the $\pm 15\%$ limit but not at the same concentration. During assay validation, QC intra-day %CV ranged between 1.3 to 5.7%, and %RE ranged between -0.3 to 9.2%. All instrument control, data collection, peak area integration, regression and quantification was performed using Thermo Scientific LCQuan. A weighted ($1/x^2$) least square linear regression was used to construct the calibration line.

4.6. CAMPLEX pharmacokinetic analysis

Non-compartmental pharmacokinetic analyses were performed using Graphpad Prism software (version 7). Pharmacokinetic parameters were calculated and summarized by dose cohorts for proportionality estimates

(Pearson correlation coefficient). Concentration at steady state (C_{ss}) was determined at 168hr of the infusion, or at 72hr or later if the infusion was discontinued early and renal function was at baseline. The area under the concentration-time curve AUC_{0-168} was calculated using the linear trapezoidal rule. Clearance (CL) was determined using the following equation[86]:

$$C_{ss} = \frac{K_0}{CL}$$

where K_0 is the infusion rate (mg/hr).

4.7. CAMPLEX pharmacodynamic correlates in the peripheral circulation

At baseline, 24/72/168hr of the infusion, and 21(+/-2) days after infusion, blood was collected into Sarstedt EDTA blood tubes and CD34+ cells quantified by flow cytometry at the Haemato-Oncology Diagnostic Service at Addenbrooke's Hospital. The CD34+ absolute count was derived from a bead based assay using BD Bioscience Trucount tubes and an ISHAGE gating strategy. CD34+ cell counts, and other WBC subsets obtained by standard clinical full blood counts for safety evaluations, were summarized using descriptive statistics for each dose cohort. On treatment means or day 28 counts and baseline counts were compared using two-way ANOVA with Dunnett's multiple comparison test. Pharmacodynamic modelling was performed using Graphpad Prism software (version 7) to estimate the half-maximal effect (EC_{50}) and maximum effect (EC_{max}).

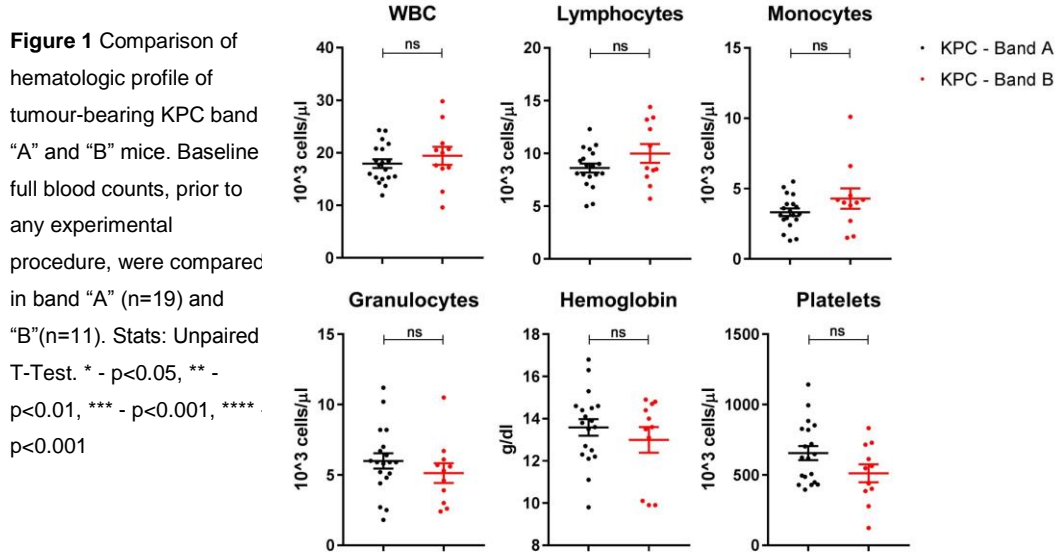
4.8. Mice

Experiments were carried out within the CRUK-CI Biological Resources Unit (BRU), in accordance with the Animals (Scientific Procedures) Act 1986, and with the approval of the Institute Animal Welfare and Ethical Review Body. The generation of *LSL-Kras^{G12D/+};LSL-Trp53^{R172H/+};Pdx1-Cre (KPC)* mice has previously been described [32, 87]. Mice received ad libitum diet and were

housed at a 12-hour light/ 12-hour dark cycle. Tumour-bearing were identified by palpation and tumour sizes were verified by high-resolution abdominal ultrasonography (Vevo2100, VisualSonics), by the CRUK-CI Preclinical Genome Editing Core's Tumour Models Team. The BRU classifies mice into bands "A" and "B", where the former are optimal for intervention studies assessing tumour volume changes. Mice can be classified as band "B" for different reasons, including poor health, but mainly when the tumour measurements are difficult to accurately assess by ultrasound (e.g. cystic, multi-lobed tumours). There is an approximate 5 fold difference in cost between band "A" and "B" mice.

Band "A" mice with 5-8mm tumours were enrolled for the 144hr experiment to investigate the effect of AMD3100 on tumour growth. Tumour volumes were determined 2 days before enrolment and on day 6 by ultrasound, and measurements in the same field of view were compared. Healthy band "B" mice were enrolled for shorter experiments (24hr and 48hr) to characterize the intra-tumoural pharmacodynamic effects of AMD3100. There was no difference in the hematologic profile of enrolled band "A" and "B" KPC mice (Figure 1) or in their age (mean 164 vs 194 days, $p=0.26$). AMD3100 (SigmaAldrich, A5602) or PBS was administered by osmotic pumps (Alzet, Charles River) implanted on Day 0. In the 144hr experiment, osmotic pumps (model 1007D) were loaded with a 400mg/ml solution of AMD3100 and released the solution at 0.5 $\mu\text{l/hr}$ (or 200 $\mu\text{g/hr}$). Mice weighed between 22.7-35.3g (mean 29.9g) at baseline, and therefore weight-based dosing ranged between 5.6-8.8mg/kg/hr (mean 6.7mg/kg/hr). In the 24hr and 48hr experiment, osmotic pumps (model 1003D) were loaded with a 45mg/ml solution of AMD3100 and released the solution at 1.0 $\mu\text{l/hr}$ (or 45 $\mu\text{g/hr}$). Mice weighed between 27.7-33.4g (mean 30.0g) at baseline, and therefore weight-based dosing ranged between 1.3-1.6mg/kg/hr (mean 1.5mg/kg/hr) At the end-point, tumours were en bloc dissected with normal surrounding tissue to adequately capture the invasive margin. Tumours were cut into 3 equal parts: one part was embedded in OCT and snap frozen; a second part was fixed in neutral buffered 10% formaldehyde for 24hr and

paraffin-embedded; the last part was trimmed of adjacent normal tissue and snap frozen.



8 to 10 week old non-tumour prone littermates of KPC mice with genotype LSL-Trp53^{R172H/+};Pdx1-Cre (PC) mice were enrolled for experiments investigating the mobilization of WBC subsets in the peripheral circulation. AMD3100 was administered either by osmotic pumps or S/C injection at different doses.

Complete blood cell (CBC) counts, including 3-part WBC count differential, were determined by a haematology bench-top analyser (Mythic 18, Woodley Equipment Company Ltd). The benchtop analyzer provides precise measurements of all counts (Figure 2). 10 μ l of blood were collected in EDTA-coated capillaries from tail bleeds and analyzed within 1 hour of collection.

	WBC	Lymphocytes	Monocytes	Granulocytes	Hemoglobin	Hematocrit	Platelets
Pooled CV %	5.4	5.7	10.4	11.0	3.4	3.9	6.3

$$\text{pooled CV} = \sqrt{\frac{\sum_{k=1}^K (n_k - 1) (CV_k)^2}{\sum_{k=1}^K n_k}}$$

Figure 2 Precision of the Mythic 18 blood cell analyser. Blood from cardiac bleeds were collected in EDTA anticoagulant from 6 PC mice, and three 10µl aliquots were analysed. Coefficient of variation (CV) for each triplicate was pooled using the maximum likelihood estimate formula.

4.9. Histologic analysis

All immunohistochemistry (IHC) and immunofluorescence (IF) staining and scanning was performed by the CRUK-CI Histopathology Core. 3 µm formalin-fixed, paraffin-embedded (FFPE) tissue sections were deparaffinised in xylene and rehydrated in an ethanol series, before staining as described below. H&E and IHC slides were imaged by Aperio AT2 scanner, and IF slides on the Axio Scan.Z1 (Zeiss). All images were imported into Halo software (v2.1, Indica labs) for image analysis. H&E and IHC or IF images were co-registered for simultaneous annotation of images for areas of necrosis, normal tissue, and the invasive margin. The invasive margin was defined as the border between cancer cells at the leading edge of the tumour and surrounding tissue. For the CAMPLEX samples, H&E slides were also reviewed with a Consultant Histopathologist Rebecca Brais (RB) (Cambridge University Hospitals NHS Foundation Trust) to verify the diagnosis and clarify any issues with slide annotation. For mouse experiments, all annotations were verified by Dr Aarthi Gopinathan, an experienced member of the lab in histologic analysis, who was also blind to treatment groups. Archival control paraffin sections of a primary PDAC and normal lymph node were obtained from Addenbrooke's Hospital

tissue bank in accordance with institutional and national policies (LREC 08/H0306/32).

4.9.1. Immunohistochemistry

IHC was performed for CD3, CD4, CD20, FOXP3, F4/80, CXCR4, PD-L1, Ki-67, and Cleaved-Caspase-3 proteins on human and mouse tissue as indicated. Staining conditions had previously been optimized by the CRUK-CI Histopathology Core for all antibodies. Staining was performed on a Leica Bond automated platform and the Leica Polymer Refine Detection System (Vision Biosystems). Specific conditions for antigen retrieval, primary antibody concentration and incubation time are outlined in Table 1.

Table 1 Primary antibodies used for IHC of mouse and CAMPLEX trial tumour tissue

Antigen	Clone	Catalogue	Company	Host	Isotype	Stock concentration	dilution	Incubation time	Antigen retrieval
CXCR4	UMB2	ab124824	Abcam	Rabbit	Mab IgG	2.24mg/mL	1 in 500 (Sanger diluent for human only)	60 min	EDTA , 30min
Cleaved Caspase-3	5A1E	9664	CST	Rabbit	Mab IgG	unknown	1 in 200	15 mins	Tris EDTA , 20min
CD3	Polyclonal	A0452	Dako	Rabbit	Polyclonal	0.60 g/L	1 in 1000	15 mins	Tris EDTA , 20min
CD4	EPR19514	ab183685	Abcam	Rabbit	Mab IgG	unknown	1 in 2000	15 mins	Tris EDTA , 20min
CD20	L26	NCL-L-CD20-L26	Novocastra	Mouse	mab IgG2a	unknown	0.95 ug/ml	15 mins	Tris EDTA , 20min
F4/80	Ci:A3-1	MCA497	Serotec	Rat	mab IgG2b	1mg/ml	1 in 200	15 mins	Sodium Citrate, 20min
FOXP3	FJK-16s	14-5773	eBioscience	Rat	mab IgG2a	0.5mg/mL	5 ug/ml	15 mins	Tris EDTA , 20min
Ki-67	Polyclonal	IHC-00375	Bethyl Laboratories	Rabbit	Polyclonal	unknown	1 in 1000	15 mins	Sodium Citrate, 20min
PD-L1	E1L3N	13684	CST	Rabbit	Mab IgG	Unknown	1 in 100	15 mins	Tris EDTA , 20min

Table 2 Antibodies used for Immunofluorescence staining of CAMPLEX trial tumour tissue

Antigen	Clone	Catalogue	Company	Host	Isotype	Stock concentration	dilution	Incubation time	Antigen retrieval	Directly conjugated
panCK	AE1/AE3	53-9003	eBioscience	Mouse	Mab IgG1	0.5mg/mL	1 in 200	30 mins	Tris EDTA , 20min	AiX488
CD3	Polyclonal	A 0452	Dako	Rabbit	Polyclonal	0.60 g/L	1 in 50	30 mins	Tris EDTA , 20min	no
CXCL12	79018	IC350A	R&D	Mouse	Mab IgG1	Unknown	1 in 5	60 mins	Tris EDTA , 20min	APC
CD8	Sp16	RM-9116-S0	ThermoFisher	Rabbit	Mab IgG	Unknown	1 in 25	30 mins	Tris EDTA , 20min	no
CD11b	M1/70.15	MCA74A647T	BioRad	Rat	IgG2b	0.05mg/mL	1 in 25	30 mins	Tris EDTA , 20min	AiX 647
Isotype control		53-4714-80	ThermoFisher	Mouse	Mab IgG1 k	0.5mg/mL	1 in 200	30 mins	Tris EDTA , 20min	AiX 488
Isotype control		IC002A	R&D	Mouse	Mab IgG1	unknown	1 in 5	60 mins	Tris EDTA , 20min	APC
Isotype control		MCA6006A647	BioRad	Rat	IgG2b	0.05mg/mL	1 in 25	30 mins	Tris EDTA , 20min	AiX 647
Isotype control		31235	Invitrogen	Rabbit	IgG	11.2 mg/mL	1 in 933.3 recurring	30 mins	Tris EDTA , 20min	no
Secondary ab to rabbit	Polyclonal	A11010	Invitrogen	Goat	IgG	2 mg/mL	1 in 250	30 mins	N/A	AiX546

For mouse tissue, adjacent normal tissue served as internal positive controls: lymphoid tissue for CD3, CD4, FOXP3, F4/80 and CXCR4; proliferating cells in crypts of bowel tissue for Ki-67. For human tissue, additional control tissues were included with every staining batch: normal human lymph node for CD20; FFPE cell pellets positive (HDLM-2) and negative (PC-3) for PD-L1 (Cell Signalling Technology, SignalSlide 13747). The PC-3 cell line appeared to stain weakly for PD-L1 (Figure 3A), which was confirmed by customer support at Cell Signalling Technology. HDLM-2 were strongly positive for PD-L1 as expected (Figure 3B). An FFPE cell pellet of the AsPC-1 cell line, known to be negative for CXCR4 expression by RNAseq (unpublished data provided by Fran Richards, Jodrell Group), was included for both mouse and human tissue staining. See chapters 5 and 7 for detailed validation of the CXCR4 antibody on mouse and human tissue, respectively.

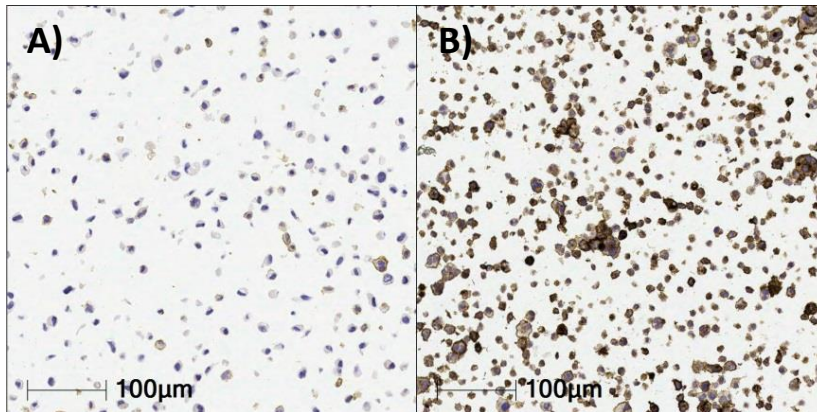


Figure 3 PD-L1 IHC controls. A) PD-L1 IHC of paraffin-embedded cell pellets negative (PC-3) and B) positive for PD-L1 (HDLM-2), respectively.

4.9.2. IHC image analysis

4.9.2.1. COMPLEX tissues

PD-L1 expression was quantified in two different ways by a histopathologist (RB) based on established methodology from companion diagnostic tests in clinical use [88, 89]: the percentage of PD-L1+ tumour cells, and the percentage of tumour area containing PD-L1+ immune cells. The PD-L1

stained slides were quantified in a random order and blinded. Only membranous PD-L1 staining was considered positive.

CXCR4 + cells were quantified across whole tumour sections using the Immune Cell Algorithm v1.2 in Halo software (v2.1, Indica labs), which was calibrated using stained control lymph node tissue. Only membranous CXCR4 staining defined a CXCR4+ cell. Areas of necrosis were excluded from analysis.

4.9.2.2. Mouse tissues

Image analysis algorithms in Halo software (v2.1, Indica labs) were calibrated using internal positive control tissue: proliferating Ki-67⁺ cells in crypts of bowel tissue; CC3⁺ tumour cells; CD3⁺, CD4⁺, FOXP3⁺, F4/80⁺ and CXCR4⁺ cells in lymphoid tissue such as Peyer's patches, tertiary lymphoid organs or spleen (Figure 4). CC3⁺ and Ki-67⁺ cells were quantified using the CytoNuclear v1.4 algorithm within the tumour, defined by the invasive margin but excluding areas of necrosis, and reported as the percentage of all nuclei. % Tumour necrosis was calculated by dividing the area of necrosis by the area of the tumour, defined by the invasive margin. Immune cell subsets were first quantified on whole tumour sections using the Immune Cell Algorithm v1.2. Subsequently, using the Infiltration Algorithm, the spatial distribution of the identified immune cells was analyzed by quantifying their density in 100µm isometric rings from 500 µm outside the invasive margin to the center of the tumour. Adjacent lymphoid tissue and bowel, and necrotic regions were excluded from this analysis.

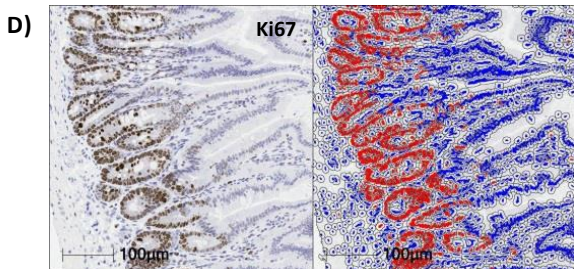
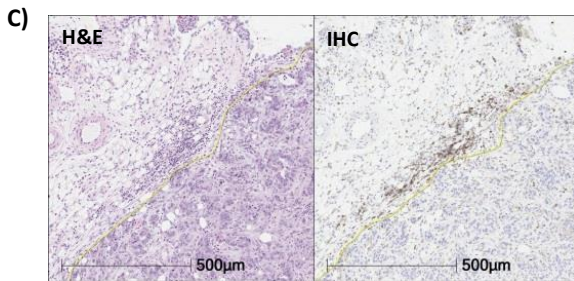
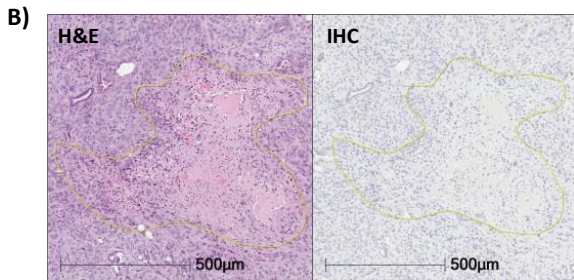
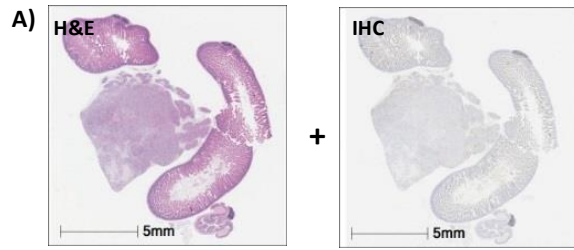
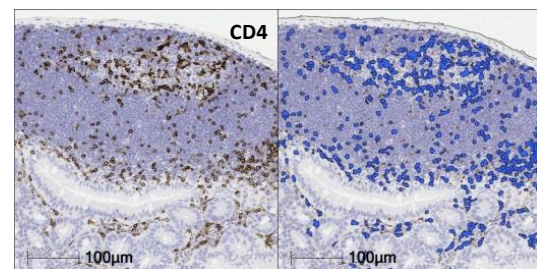
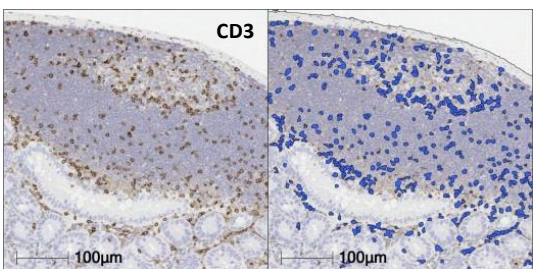
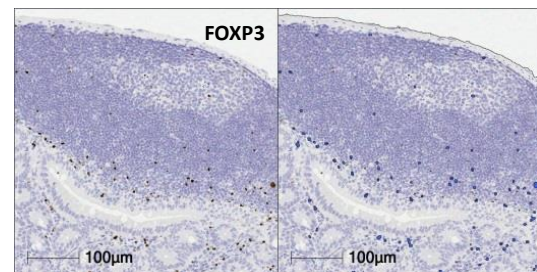
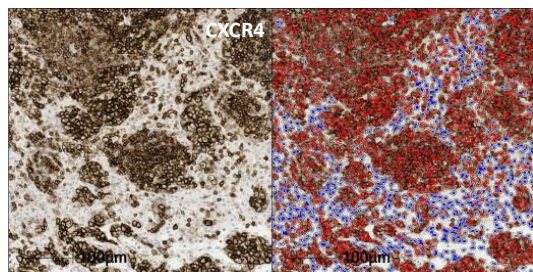
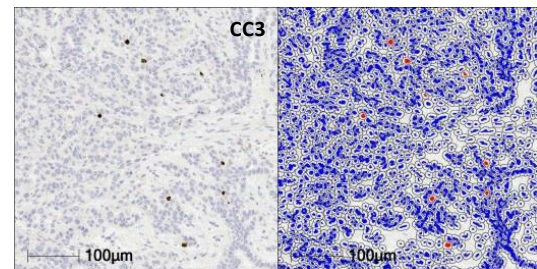
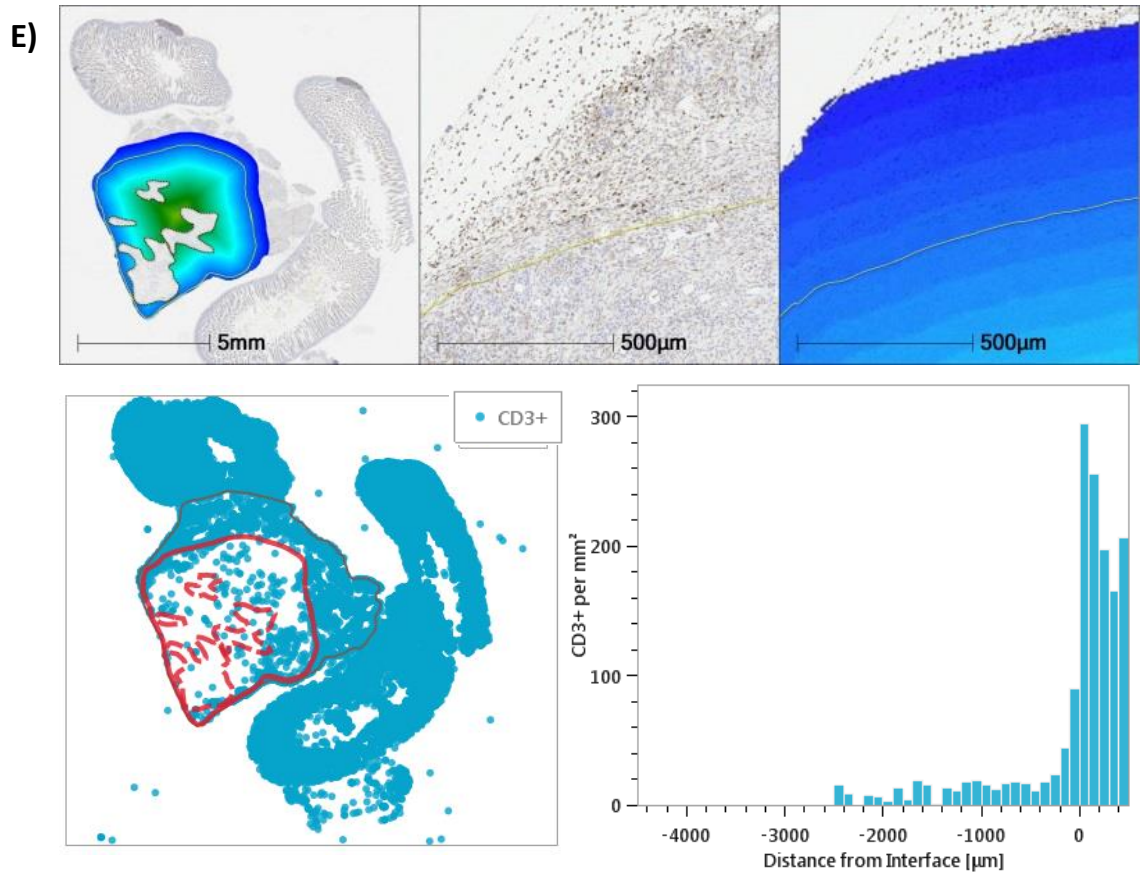


Figure 4 Image analysis of IHC markers. **A)** H&E and IHC images from en-bloc dissections of KPC PDAC tumours are co-registered for annotation. Using the H&E slide, **B)** areas of necrosis are excluded and **C)** the invasive margin identified (yellow lines). **D)** IHC and pseudo colour (left and right images, respectively) from image analysis. Image analysis algorithms are calibrated using internal positive control tissue: proliferating Ki67⁺ cells in crypts of bowel tissue; CC3⁺ tumour cells; CD3⁺, CD4⁺, FOXP3⁺, and CXCR4⁺ cell in lymphoid tissue such as Peyer's patches and tertiary lymphoid organs. (Ki67⁺, CC3⁺, and CXCR4⁺ in red, negative cells in blue; CD3⁺, CD4⁺ and FOXP3⁺ in blue). **E)** The distribution of immune cells is quantified by infiltration analysis in 100µm isometric rings, from 500 µm outside the invasive margin to the centre of the tumour. Image analysis was performed in Halo Software





4.9.3. Immunofluorescence

Staining was performed on the Bond Rx automated platform using the Research Detection Kit (Vision Biosystems). Specific conditions for antigen retrieval, primary antibody concentration and incubation time are outlined in Table 3. Human primary PDAC and lymph node control tissue was included with every run on the autostainer.

Two triple-IF panels (with antibodies against pan-cytokeratin, CXCL12 and either CD3 or CD8) were developed with the CRUK-CI Histopathology Core to stain CAMPLEX tumour biopsies (Figure 5). A pan-cytokeratin (panCK) antibody was used to identify cancer cells in both panels, and PDAC and lymph node served as positive and negative controls, respectively. Lymph node served as a positive control for CD3 and CD8 stains. CXCL12 was previously shown to “coat”

PDAC cancer cells [32].

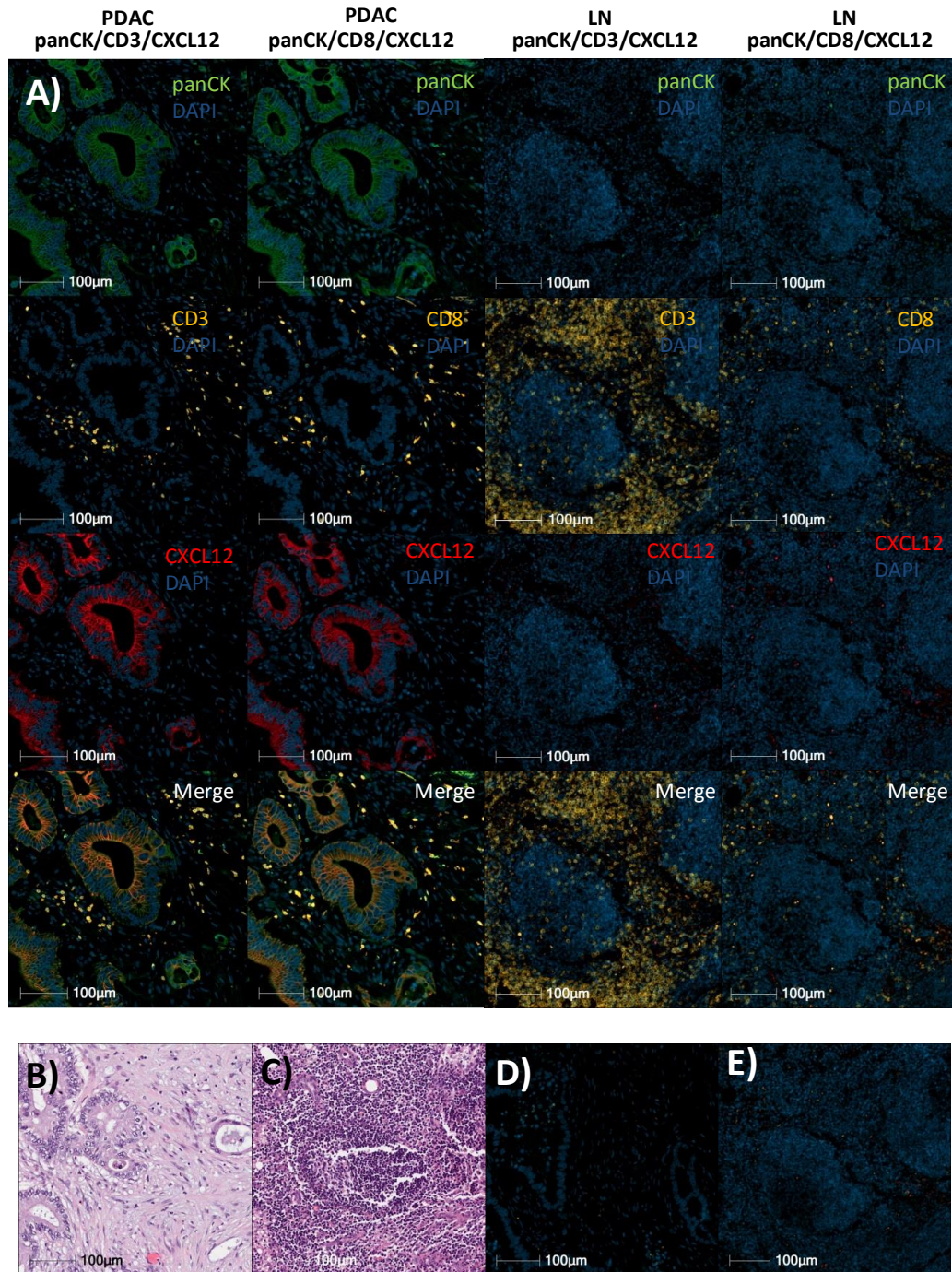


Figure 5 Immunofluorescence panels for CAMPLEX samples A) Two immunofluorescent panels for pan-cytokeratin (panCK, clone AE1/AE3, primary conjugated to Alx488), CXCL12 (primary conjugated to APC) and CD3 or CD8 (secondary antibody in Alx 546) staining of serial sections of human primary pancreatic cancer (PDAC) and lymph node (LN) control tissues. H&E of PDAC (B) and LN (C). Isotype controls for panCK and CXCL12, and secondary only Alx546 on PDAC (D) and LN (E).

4.9.4. Immunofluorescence image analysis

Biopsies of metastases were obtained in the CAMPLEX trial, and the invasive margin is often not identified in biopsy specimens. A previous publication had suggested a significant amount of variability in the densities of TILs at the invasive margin of CRC liver metastases, while being fairly homogenous in the tumour centre [77]. In that study, the invasive margin was defined as a *region* of 500µm width on each side of the border between cancer cells and liver tissue. The objective of the IF analysis was to quantify any changes to TIL densities. In an attempt to remove a potential source of variability, tumour tissue within 500µm of the invasive margin (defined in the current study as the border between cancer cells at the leading edge of the tumour and surrounding tissue), when present, was excluded from image analysis (Figure 6C).

Two approaches were used to quantify TILs using the High-Plex FL2.0 algorithm in Halo software (v2.1, Indica labs) (Figure 6). In the “distance method”, nuclei were first identified by DAPI positivity, and subsequently classified as either tumour or immune cells based on pan-CK and CD3/CD8 staining, respectively. Subsequently, the distance of every cancer cell to the nearest T cell was determined, or vice versa. In the “compartmental density” method, a machine learning algorithm (random forest) was trained to identify cancer cell nests or stroma, and subsequently T cells quantified within the stromal or tumour nest compartments. A T cell was deemed to be within a tumour nest if at least touching a tumour nest.

The calibration of algorithms to detect cancer cells (based on positive staining with panCK) and CD3 or CD8 cells proved challenging due to significant variation in immunofluorescence signal intensity between slides from different biopsies, and one algorithm could not be designed to analyse all samples. A solution was to validate the algorithm on each slide analysed. On each slide, the following objects manually counted in a small area (containing 50 to 100 objects

of interest): nuclei, cancer cells, immune cells, immune cells in stroma, and immune cells touching or within a tumour nest. The algorithms were adjusted until the difference with manual counts was less than 10%. The parameters changed between algorithms were the intensity of fluorescence signal for DAPI and panCK used to identify nuclei and cancer cells, respectively. As additional validation, nuclei were counted in the same area by a second user (Cara Brodie, CRUK-CI Histopathology Core scientist). On the other hand, the algorithm to identify CXCL12+ cells was adjusted to detect as many CXCL12 “coated” cancer cells in the positive control primary PDAC, but no cells in a primary PDAC slide stained with isotype control antibody-fluorophore conjugate.

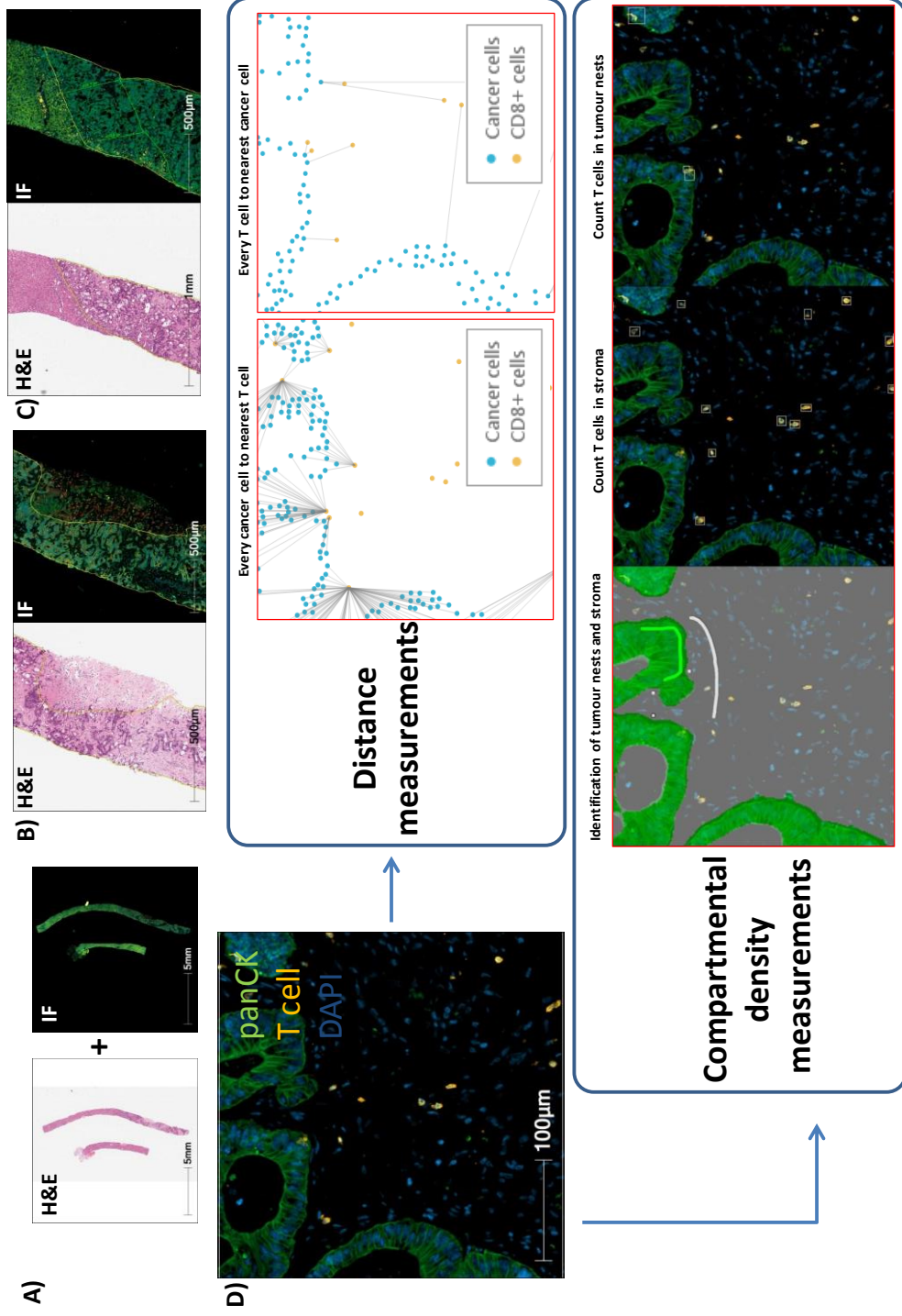


Figure 6 CAMPLEX T cell infiltration analysis. A) H&E and IF images of whole biopsies are co-registered for annotation. Using the H&E slide, the area for analysis (yellow line) is identified by B) excluding areas of necrosis and C) any area within 500 μm from the invasive margin, when present. D) Whole biopsies are then analysed for T cell infiltration using either distance measurements or a compartmental density analysis. In the former, the distance of every cancer cell to the nearest T cell is determined, or vice versa. In the latter, a machine learning algorithm is trained to identify cancer cell nests (green line) or stroma (white line), and subsequently T cells quantified within the stromal or tumour nest compartments.

4.10. CAMPLEX TCRseq

4.10.1. DNA extraction

The snap frozen biopsies from CAMPLEX were processed to extract DNA and RNA. Due to a misunderstanding regarding the processing of biopsies, the biopsy specimens were divided into 4 equal parts prior to snap freezing. This turned out to be a potential advantage as the fragments could be processed individually and only those containing adequate material sent for sequencing. The Caldas lab had previously developed a method to obtain tissue sections for histologic analysis as well as RNA and DNA from the same frozen biopsy. We adapted the protocol to our purposes, mainly incorporating chilled OCT to prevent any biopsy thawing and thus potential RNA degradation. The protocol is illustrated in Figure 7. The H&E was reviewed by a Consultant Histopathologist (RB) to determine cellular content, and additional fragments processed if found to have less than 40% cancer cell content. Patient 1008 had a mucinous adenocarcinoma with predominantly mucin, and a cancer cell content of 5-10%. Lukasz Magiera (LM) performed DNA extraction using the AllPrep DNA/RNA/miRNA Universal Kit (Qiagen, 80224) according to manufacturer instructions from tissues, and DNA quantification by fluorometer according to manufacturer instructions (Qubit 3.0, Life technologies). DNA yield from each biopsy fragment ranged between 0.45µg and 39.6µg (mean 10.4µg).

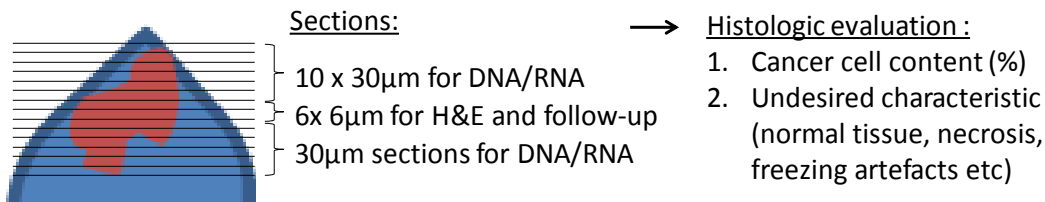
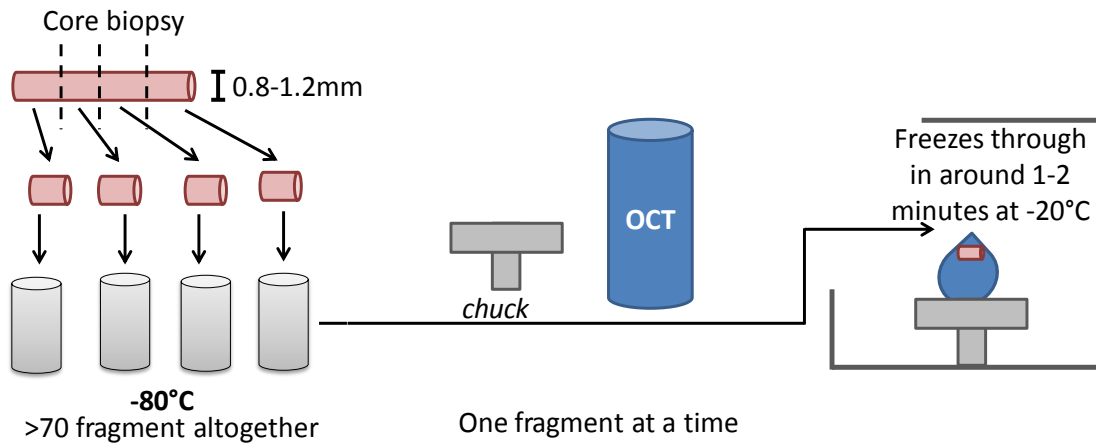


Figure 7 Processing protocol for CAMPLEX frozen biopsies. At collection, the core biopsy was divided into equal smaller fragments, typically four depending on the size of the original biopsy, and snap frozen. For processing, the fragments were embedded in chilled OCT (-4c) and allowed to solidify in the cryotome at -20c. Subsequently, ten 30µm sections were cut and collected in RLT buffer for DNA/RNA extraction, followed by six 6µm sections for histologic analysis. The remaining tissue was cut in 30µm sections until exhausted. All 30µm sections were extracted for DNA/RNA.

4.10.2. TCRseq

Extracted DNA samples were submitted to Adaptive Biotechnology for next generation sequencing of the T-cell receptor β -chain complementarity determining regions (CDR3s) (TCRseq)[90] and computational analysis. Samples were run on the hsTCRB-FFPE assay at survey resolution.

The T cell fraction was determined by dividing the number of productive templates by nucleated cells (a measure based on the amplification of reference gene primers rather than DNA absorbance). Productive rearrangements can produce a functional protein receptor (in-frame and do not contain a stop codon).

TCR clonality (0 to 1) is a measure of population skewing, where high clonality indicates biased expansion of individual T cell clones and implies the presence of a specific immune response to tumour antigens[91]. TCR clonality was calculated as follows:

$$Entropy = H = - \sum_{i=1}^N p_i \log_2(p_i)$$

$$Clonality = 1 - \frac{H}{\log_2(N)}$$

where H is the Shannon entropy, p_i is the proportional abundance of clone i, and N is the total number of unique TCR gene rearrangements.

The number of expanded and contracted T cell clones between baseline and day 8 biopsies was determined using nucleotide sequences of productive rearrangements, with a minimum of 5 clones, and a binomial test for p-value with Benjamini-Hochberg correction (alpha 0.001).

The Morisita Index (MI) compares TCR rearrangement and template counts between 2 samples, where a value of 1 indicates that the same T cell clones are present at the same proportions in the 2 samples [91]. The MI was calculated as follows:

$$MI = \frac{2 \sum_i^s a_i b_i}{\left(\frac{\sum_i^s a_i^2}{A^2} + \frac{\sum_i^s b_i^2}{B^2} \right) AB}$$

where a_i and b_i are the number of templates of clone i in samples A and B, respectively, and A and B are the total number of templates in samples A and B, respectively.

4.11. Statistical testing

Statistical testing was performed GraphPad Prism 6 Software, including paired and unpaired T-Tests, Pearson’s correlation coefficient as indicated in the text and figures.

4.12. Summary of work done by myself and others

CAM-PLEX clinical trial	
Study design	The initial protocol was complete prior to starting my PhD. However, I was involved in several amendments including the addition of saliva cortisol sample collection (not discussed in the thesis).
Patient recruitment and management	I recruited, consented, and managed the overwhelming majority of patients on the dose escalation phase. Important support provided by the nursing staff in the Early Phase Clinical Trial Unit.
Data management	I answered the overwhelming majority of data queries from the monitor related to the data collected.
Safety data	I analyzed the safety data.
Imaging (RECIST 1.1 and PERCIST)	RECIST 1.1 measurements performed by radiologists. Eva Serrao did the actual PERCIST measurements. I was actively involved in the decision to use PERCIST, related exploratory analysis of the PET-CT data, and analysis of the data.
Pharmacokinetics	The measurement of plasma AMD3100 concentrations was done by the PK/Bioanalytics Core Facility at CRUK-CI. I analyzed the data.
Histology and image analysis	I was actively involved in the selection of relevant antibodies (CXCR4, PD-L1, and immunofluorescence), initial antibody work-up, and optimization. Final staining on trial samples performed by CRUK-CI Histopathology Core. I performed all image analyses.
DNA extraction	I was actively involved in optimizing the DNA extraction procedure with the help of Lukasz Magiera
TCRseq	Sequencing and computational analysis performed by Adaptive Biotechnology. I interpreted the data
Mouse experiments	
Study design	I designed the mouse experiments, with input from various lab members

Experimental work	Osmotic pump implantation and ultrasound imaging performed by the CRUK-CI Biological Resources Unit. I performed the collection and processing of most biologic samples.
Ultrasound image analysis	I performed the image analysis
Histology and image analysis	IHC performed by CRUK-CI Histopathology Core. I performed all image analyses.

5. PHARMACODYNAMICS OF CXCR4 INHIBITION IN MICE

5.1. High dose AMD3100 modestly decreases tumour growth and may improve survival in KPC mice

In previous experiments with KPC mice, a dose response in anti-tumour activity of single agent AMD3100 was identified between 15-45 $\mu\text{g/hr}$ [32]. A dose of 45 $\mu\text{g/hr}$ almost completely arrested tumour growth after 6 days with a mean plasma concentration of 2 $\mu\text{g/ml}$. These data were the basis for the target AMD3100 steady state concentration in the CAMPLEX clinical trial. At the time of this experiment, a mean plasma steady state concentration of 738 ng/ml (range 707-770ng/ml) had been reported in the first cohort of patients in the CAMPLEX trial at a dose of 20 $\mu\text{g/kg/hr}$. This is nearly double that which was achieved in a previous study by Hendrix et al.[58] in patients with HIV. This raised the possibility that CAMPLEX would achieve higher steady state concentrations than expected in subsequent dose cohorts. Given the maximal anti-tumour effect of single agent AMD3100 was not previously identified, we hypothesized that administering AMD3100 at 200 $\mu\text{g/hr}$ would have additional anti-tumour activity in KPC mice.

We enrolled and randomized 16 band “A” (see Chapter 4 for definition of mice bands) KPC mice to subcutaneous implantation of osmotic pumps delivering either PBS or AMD3100 at 200 $\mu\text{g/hr}$ for 6 days. Groups were well balanced in terms of baseline characteristics (Figure 1A). 3 mice in the PBS group deteriorated clinically on-study and required early culling without ultrasound tumour measurement, but none in the AMD3100 group (Hazard ratio=0.13, $p=0.08$) (Figure 1B). One mouse in the AMD3100 cohort was excluded from all further analysis due to the unusual histology of acinar carcinoma. There appeared to be a non-significant reduction in mean tumour growth from 117% ($n=5$) to 79% ($n=7$) ($p=0.18$) in PBS vs AMD3100 treated KPC

mice, respectively (Figure 1C). However, the comparison is based on a small sample size. AMD3100 was successfully delivered to all treated mice with a mean plasma concentration of 7.5 µg/ml at the endpoint at 6 days (range 5.8-9.5 µg/ml).

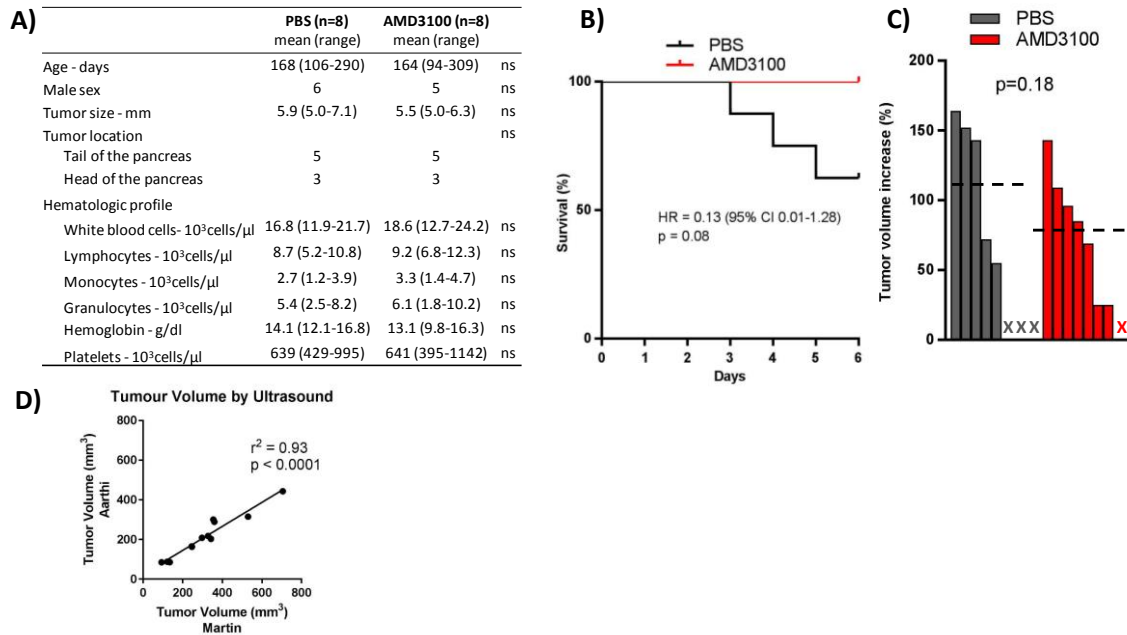


Figure 1 High dose AMD3100 modestly decreases tumour growth and may improve survival in KPC mice **A)** Baseline characteristics of band “A” KPC mice treated with either PBS or AMD3100 at 200µg/hr by osmotic pump for 6 days. A tail bleed was taken before treatment for a full blood count. **B)** Kaplan Meier survival curves. One mouse in the AMD3100 group was excluded from analysis due to unusual acinar carcinoma histology. **C)** Tumour volume changes measured by ultrasound at 6 days of treatment relative to Day -1. Ultrasound measurement was not possible in three PBS treated mice due to clinical deterioration on study (grey X). One mouse in the AMD3100 cohort was excluded from any analysis due to the unusual histology of acinar carcinoma (red X). Dotted line represents the mean volume change in each group. **D)** 12 tumour ultrasounds were quantified by a second operator (Dr Aarthi Gopinathan) to partially validate the ultrasound measurements. Stats: unpaired t-test for baseline characteristics and tumour volume measurements. Mantel-Haenszel hazard ratio (HR) and log-rank test. Pearson correlation coefficient (r).

Ultrasound measurement of tumour volume is challenging and time-consuming. To help partially validate the results from this experiment, Dr Aarthi Gopinathan, who has extensive experience with ultrasound measurements, kindly quantified 12 tumour ultrasounds. There was a strong correlation between the independent tumour volume measurements ($r^2=0.93$) (Figure 1D).

5.2. Pharmacodynamic effects of AMD3100 on tumour and normal tissue

To characterize the pharmacodynamic effects of CXCR4 inhibition on tumour and normal tissue, additional KPC mice were administered PBS or AMD3100 for 24hr and 48hr. Since the characterization of intra-tumoural PD effects was the primary objective of this experiment, healthy band “B” KPC mice were enrolled. Ultrasound measurements of tumour volume were not performed since these mice were classified as band “B” because of difficulties in accurately assessing tumour volume by ultrasound (e.g. cystic, multi-lobed tumours). Tumours were *en bloc* dissected with normal surrounding tissue to adequately capture the invasive margin, which also prevented comparison of tumours by weight or caliper measurements.

For these experiments, the dose rate of AMD3100 was lowered to 45µg/hr for two reasons. Firstly, mean AMD3100 plasma concentrations from emerging data on later CAMPLEX cohorts were closer to previous estimates (see Chapter 6). Secondly, high-dose AMD3100 (200µg/hr) had apparently failed to show dramatic anti-tumour activity as measured by tumour volumes (see above), and the 45µg/hr dose rate is consistent with previous experiments in KPC mice [32].

5.2.1. Increased CXCR4 expression in tumour and normal tissue is a pharmacodynamic effect of AMD3100

CXCR4 is expressed in all cells of the myeloid and lymphoid lineage [92], and treatment with AMD3100 increases surface expression of CXCR4 of cells in the peripheral circulation [93] and *in vitro* [51–53]. To determine whether CXCR4 expression also increases on cells within tumour and normal tissue with AMD3100 treatment, an anti-CXCR4 antibody (UMB2 clone) was first validated in collaboration with the Histology Core at CRUK-CI. Strong and weak membranous staining pattern was observed in a proportion of larger activated germinal centre cells of lymph nodes, probably representing centroblasts and centrocytes within the dark zone (DZ) and light zone (LZ), respectively (Figure 2). Many smaller

lymphoid cells within germinal centres, the mantle zone and T-cell zone displayed perinuclear-dot staining (possibly the Golgi apparatus) without associated membranous staining. These cells would be expected to have membrane CXCR4 expression, but this may be below the detection threshold of CXCR4 IHC. The staining pattern in germinal centres is consistent with data showing that germinal centre B cells upregulate CXCR4 expression and centroblasts in particular have high CXCR4 expression [94]. Centroblasts undergo CXCR4 dependent chemotaxis to the dark zone in response to CXCL12 producing reticular cells in the DZ[95]. Therefore, these results validate the anti-CXCR4 antibody (UMB2) for IHC use on mouse tissue. For the purpose of image analysis, only membranous CXCR4 staining defined a CXCR4+ cell.

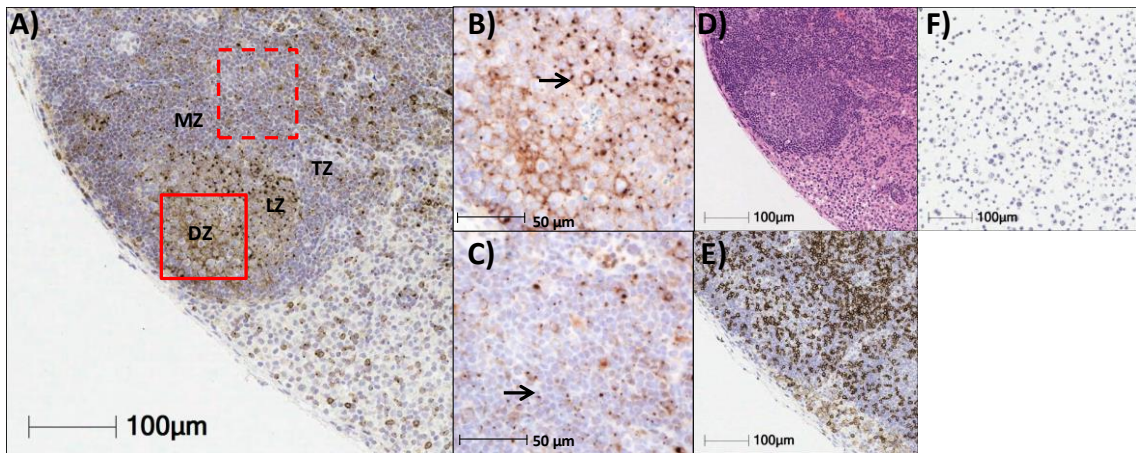


Figure 2 CXCR4 expression in a mouse lymph node. **A)** A proportion of larger activated germinal centre cells display strong and weak CXCR4 membranous staining probably representing centroblasts and centrocytes within the dark zone (DZ) and light zone (LZ), respectively. **B)** Higher magnification of the solid red box in A) also demonstrates the presence of a perinuclear dot-like CXCR4 staining (arrow), possibly the Golgi apparatus, in the smaller lymphoid cells. **C)** Higher magnification of the dotted red box overlapping the mantle zone (MZ) and T-cell zone (TZ) in A) shows predominantly perinuclear-dot CXCR4 staining (arrow). **D)**, and **E)** are H&E and CD4 IHC on serial sections of the lymphoid follicle in A). **F)** CXCR4 IHC on a FFPE cell block of the AsPC-1 cell line known to be CXCR4 negative by RNAseq.

CXCR4 protein expression was examined by IHC in tumour, and adjacent lymphoid and normal tissue. Adjacent lymphoid tissue was most often tertiary lymphoid organs, which can be differentiated from lymph nodes by the lack of encapsulation and afferent lymphatics [96]. In the AMD3100 treated mice, the percentage of CXCR4+ (%CXCR4+) cells increased in lymphoid tissue as early

as 24hr (Figure 3). Nearly all cells displayed membranous staining in lymphoid tissue, but staining intensity was highest in germinal centers. In bowel tissue, the %CXCR4+ cells also increased by 24hr, mainly confined to the lamina propria. In tumour, %CXCR4+ cells increased by a mean 1.9 fold ($p=0.03$) by 48hr, and a mean 3.5 fold ($p<0.001$) by 144hr. Review with pathologist Rebecca Brais suggested that, in PBS treated mice, most of the CXCR4+ cells in the tumour are endothelial cells. In AMD3100 treated mice, CXCR4+ cells are a variety of immune cells and endothelial cells, but cancer cells and bowel epithelial cells remained CXCR4 negative.

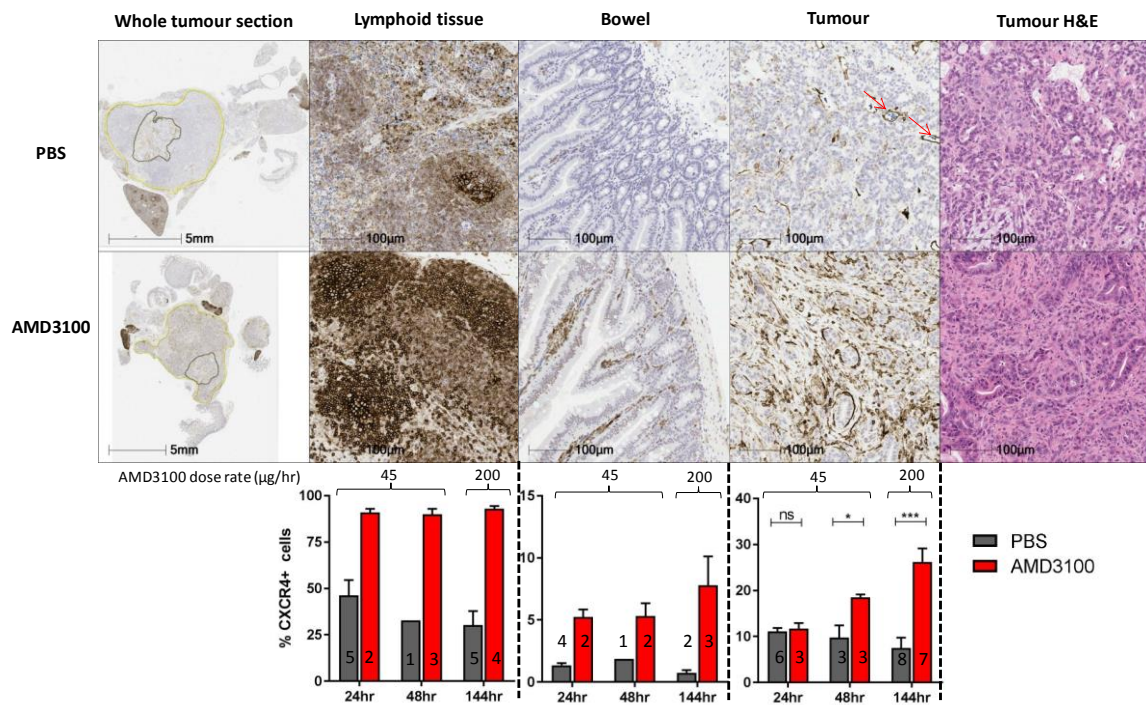


Figure 3 AMD3100 increases CXCR4 expression in lymphoid tissue, bowel, and tumour. KPC mice were treated with either PBS or AMD3100 delivered by osmotic pump for 24hr, 48hr (AMD3100 45 µg/hr) or 144hr (AMD3100 200 µg/hr). Primary pancreatic tumours were *en bloc* dissected to capture adjacent lymphoid tissue (tertiary lymphoid organs, possible lymph nodes, and occasionally an invaded spleen), and occasionally invaded bowel. CXCR4 expression was detected by IHC, and representative images are shown from whole tumour sections (yellow line outlines the tumour), lymphoid tissue and bowel from PBS and AMD3100 treated for 144hr. %CXCR4+ cells were quantified across whole tumours, and lymphoid tissue and bowel when present in the specimen. Review by a pathologist suggested the CXCR4+ cells in AMD3100 treated mice were mixture of immune cells, but cancer or epithelial cells are CXCR4 negative. In PBS treated mice, most of the CXCR4+ cells are endothelial cells (red arrows). Statistical comparison was only performed on tumour tissue %CXCR4+. Numbers of mice available for tissue analysis indicated at the bottom of bars. Stats: unpaired t-test. Mean +/- SEM.

5.2.2. High dose AMD3100 increases tumour infiltration of F4/80+ cells

To investigate whether the increase in intra-tumoural %CXCR4+ cells is at least partially due to an influx of immune cells, immune cell subsets were quantified by software image analysis on whole tumour sections. The invasive margin was manually annotated on H&E sections and co-registered serial sections stained by IHC for individual markers. Immune cell densities were quantified in isometric 100um rings around the invasive margin. The invasive margin was defined as the border between cancer cells at the leading edge of the tumour and surrounding tissue.

There was a marked common pattern of asymmetry in the distribution of CD3+, CD4+, FOXP3+, and F4/80+ immune cells irrespective of treatment (Figure 4A). The density of all immune cells was highest outside the invasive margin (0 to +500 μm), rapidly decreased near the invasive margin, and was relatively low in the tumour center (-500 to -2500um). There was no apparent difference in the pattern of CD3+, CD4+, and FOXP3+ distribution with AMD3100 treatment compared with PBS at any time point. In contrast, the density of F4/80+ cells appeared to increase substantially at the invasive margin, but also intra-tumourally, but only at the 144hr day time point in animals treated at the higher dose rate (200 ug/hr). The asymmetric pattern of F4/80+ cells distribution was maintained in these sections.

To statistically compare the infiltration patterns, whole tumour sections were divided into compartments defined by the distance from the invasive margin (Figure 4B). There were no significant differences between AMD3100 and PBS groups for CD3+, CD4+ or FOXP3+ cells at any timepoint. In contrast, all tumours had higher F4/80+ cell densities in every compartment in the AMD3100 group compared to PBS at 144hr, suggesting a robust pharmacodynamic effect of AMD3100. Representative images of F4/80+ infiltration at 144hr are shown in Figure 4C.

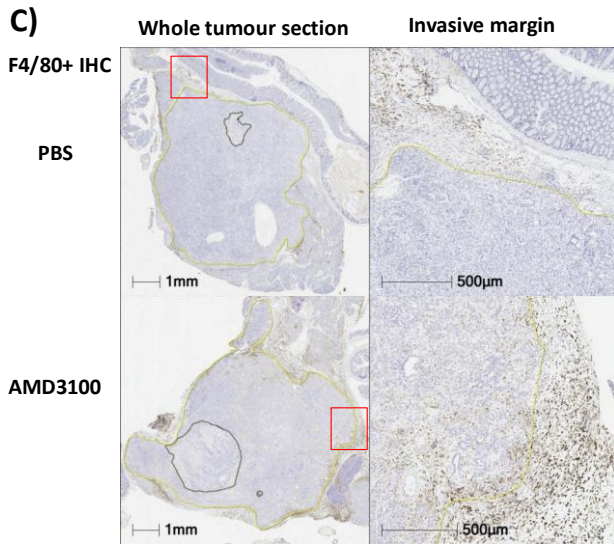


Figure 4 AMD3100 increases tumour infiltration of

F4/80+ cells. **A)** CD3+, CD4+, FOXP3+, and F4/80+ cell

infiltration analysis of KPC mice treated with either PBS or AMD3100 delivered by osmotic pump for 24hr, 48hr (AMD3100 45 µg/hr) or 144hr (AMD3100 200 µg/hr).

Immune cells were identified by IHC and densities were quantified in isometric 100µm rings around the invasive margin by Halo software image analysis (0 to -2500µm is intra-tumor). Number of mice in each group indicated at the top of the figure. **B)** Quantification of different tumour compartments from A), as defined by distance relative to the

invasive margin (green color identifies the compartment analyzed in column). **C)** Images of whole tumors and subjectively highest infiltration at the invasive margin of F4/80+ cells in mice treated for 144hr with either PBS or AMD3100. The invasive margin and necrotic regions are identified by the yellow and black dotted lines, respectively. The red boxes are the areas of subjective highest infiltration.

Stats: unpaired t-test. Mean +/- SEM.

5.3. Tumour cell proliferation, death and necrosis with AMD3100 treatment

To investigate whether the increase in F4/80+ cells is associated with changes in cancer cell proliferation or death, %Ki-67+ cells, %Cleaved Caspase-3+ (CC3+) cells, and %tumour necrosis were quantified in whole tumour sections. There were no significant differences in %CC3+ cells between AMD3100 and PBS treatment groups. Curiously, %Ki-67+ cells were significantly lower at 24hr in the AMD3100 group, but not at 48hr or 144hr. A similar observation was made for % tumour necrosis, although of borderline significance at 24hr ($p=0.05$). On closer inspection, the mean %tumour necrosis of the 24hr AMD3100 group is lower than any other group at any time-point. Tumour necrosis would not be expected to resolve or improve with AMD3100 over 24hr. Furthermore, all 3 variables are significantly correlated: %Ki-67+ cells with %tumour necrosis ($r^2=0.21$, $p=0.03$) or %CC3+ cells ($r^2=0.42$, $p=0.002$), and %CC3+ cells with %tumour necrosis ($r^2=0.49$, $p=0.002$). Given the positive correlation between %Ki-67 and tumour necrosis, the significant difference in %Ki-67+ cells between AMD3100 and PBS groups at 24hr is more likely due to baseline differences in tumours rather than an AMD3100 effect.

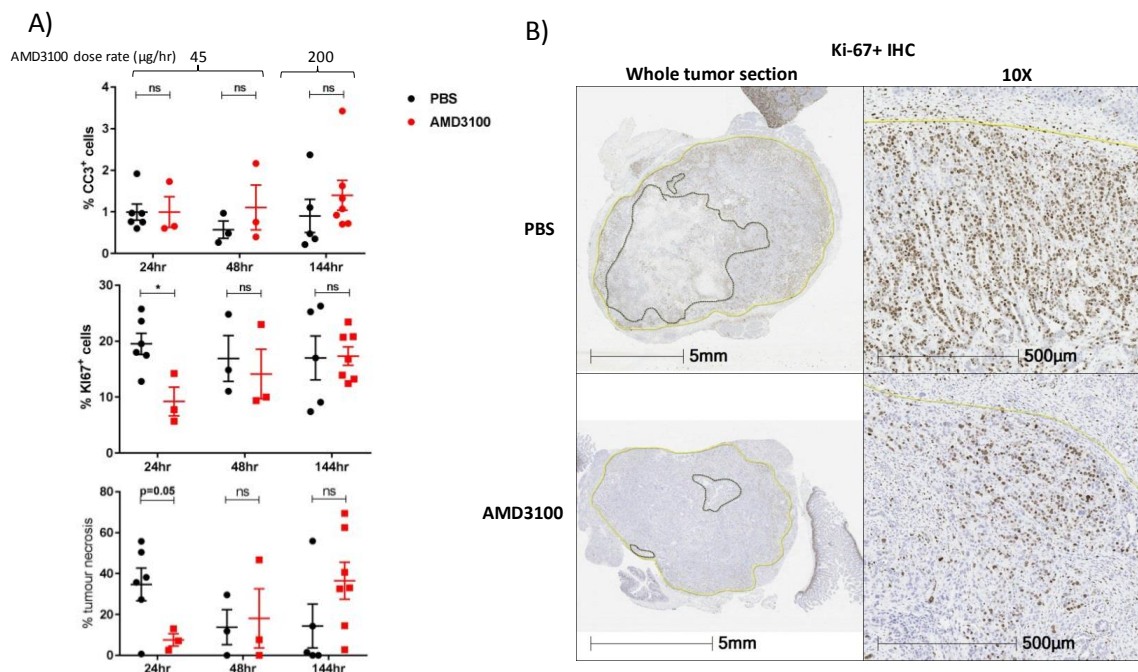


Figure 5 Tumor cell proliferation, death and necrosis with AMD3100 treatment. **A)** %Ki-67+ cells, %CC3+ cells and %tumour necrosis were quantified on whole tumour sections using Halo image analysis software. KPC mice treated with either PBS or AMD3100 delivered by osmotic pump for 24hr, 48hr (AMD3100 45 µg/hr) or 144hr (AMD3100 200 µg/hr). **B)** Representative images of whole tumour sections and 10X view from areas with subjectively highest %Ki-67+ in KPC treated with either PBS or AMD3100 for 24hr. The invasive margin and necrotic regions are identified by the yellow and black dotted lines, respectively. Stats: unpaired t-test. Mean +/- SEM.

5.4. Pharmacodynamic effects of AMD3100 in peripheral blood

The CXCR4 antagonist AMD3100 has previously been shown to robustly mobilize most WBC subsets into the blood rapidly after S/C injection using flow cytometry in mice[97]. A CBC count, including 3-part WBC count differential, can be easily and rapidly obtained from small amounts of blood (10µl) using the Mythic 18 haematology bench-top analyser. Indeed, S/C injection of 5mg/kg AMD3100 to non-tumour bearing PC mice increased lymphocyte and monocyte counts in the peripheral circulation 1hr after injection compared to control PBS (Figure 6A). The PBS control group had significant decreases and increases in lymphocyte and granulocyte counts, respectively, compared to baseline, whereas monocytes were unchanged. Additional PC mice were treated with single doses of AMD3100 S/C of 1.25, 2.5 and 5 mg/kg, and plasma drug concentrations were

measured after 1 hour, together with CBC. AMD3100 plasma concentrations increased linearly with dose ($r^2=0.84$, $p<0.001$) (Figure 6B). Pharmacodynamic modelling demonstrated maximal mobilization by 5mg/ kg S/C (Figure 6C).

Continuous delivery of AMD3100 at 200 μ g/hr by osmotic pump for 72hr to non-tumour bearing PC mice mobilized monocytes and granulocytes by 1hr, and largely maintained throughout (Figure 6D). The dynamics of lymphocyte mobilization are slightly more complex. The difference observed at 1hr and 4hr is attributable to both an increase in lymphocytes in the AMD3100 group, as well as a decrease in the PBS group, similar to that observed with S/C administration. However, lymphocytes returned to baseline within 24hr in the group administered AMD3100 at 200 μ g/hr by osmotic pump and were no longer significantly increased compared to PBS. The plasma concentrations of AMD3100 appear to peak at 1hr post osmotic pump implantation and remain relatively constant after 4hr. The most likely explanation for the peak is that a small amount of AMD3100 is coated on the osmotic pumps during pump preparation and priming.

On the other hand, continuous delivery of AMD3100 at 45 μ g/hr by osmotic pump to KPC mice induced less robust WBC subset mobilization. Similar to non-tumour bearing mice, lymphocyte counts were increased early after pump implantation (2.5hr) in the AMD3100 group vs PBS, but no difference could be detected at subsequent time-points (Figure 6E). Monocytes only modestly mobilized at 2.5 and 24hr, while there were no statistically significant differences in granulocyte mobilization.

Continuous delivery of AMD3100 at 200 μ g/hr by osmotic pump to KPC mice showed only a non-significant trends in WBC subset mobilization at 144hr in cardiac bleeds (Figure 6F), despite mean plasma AMD3100 concentration of 7.5 μ g/ml (range 5.8-9.5 μ g/ml). No interim tail bleeds were performed at the 200 μ g/hr dose.

To investigate possible reasons for the modest WBC subset mobilization to AMD3100 in KPC compared to non-tumour PC bearing mice, the baseline hematologic profile of these mice was compared. Compared to PC mice, KPC mice had strikingly higher monocyte, granulocyte and platelet counts, but not lymphocytes at baseline (Figure 6G).

To investigate whether high WBC counts in the KPC model are representative of human PDAC, baseline CBCs counts were retrieved from the SIEGE clinical trial (unpublished internal data, NCT03529175). Siege enrolled 147 patients with newly diagnosed metastatic PDAC, and excluded patients who completed adjuvant chemotherapy within 6 months. 27% and 18% patients had neutrophil and platelets counts above the upper limit of normal, respectively. Monocytes and lymphocytes were not recorded in the SIEGE database. Therefore, the KPC mice enrolled in this study may only be representative of a sub-group of patients with PDAC when considering the hematologic profile.

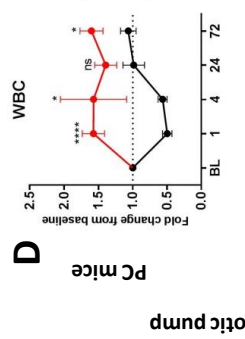
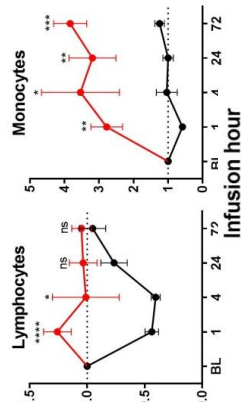
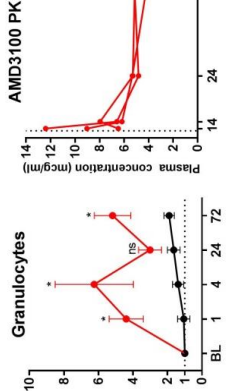
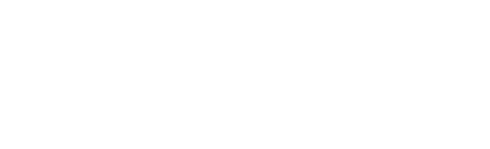
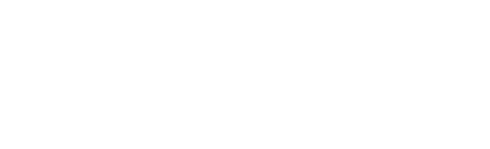
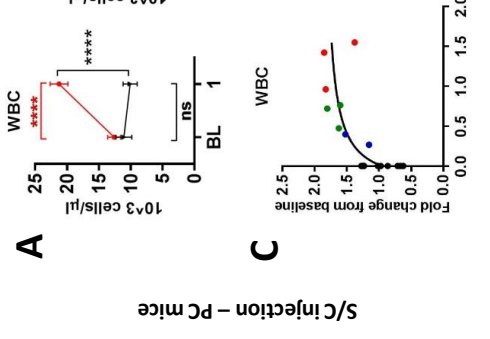
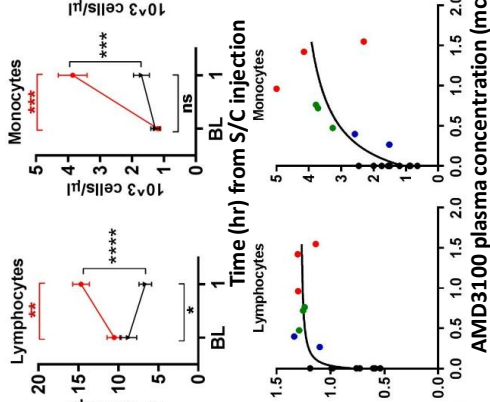
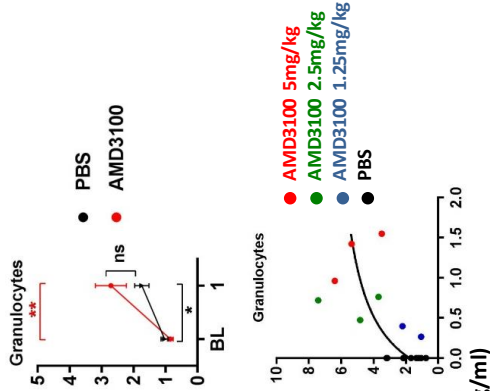
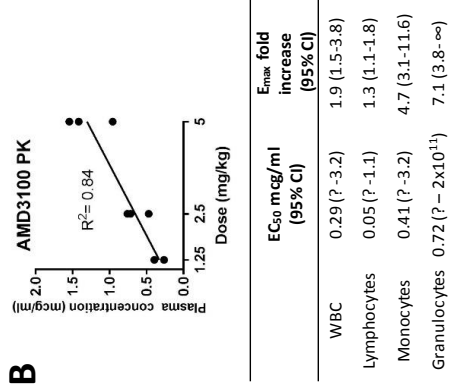


Figure 6 AMD3100 mobilization of WBC subsets in non-tumour bearing PC mice and KPC mice. A) WBC subsets at 1hr post injection of AMD3100 5mg/kg or PBS S/C in non-tumour bearing PC mice, tail bleed (n=9 per group). **B)** Plasma AMD3100 concentration at 1hr post injection of AMD3100 at different doses in non-tumour bearing PC mice, tail bleed (N=3 1.25mg/kg and 5mg/kg, N=2 2.5mg/kg). **C)** Pharmacodynamic modelling of WBC subset mobilization according to AMD3100 plasma concentration at 1hr following S/C injection of PBS (N=9) or AMD3100 (N=3 1.25mg/kg and 5mg/kg, N=2 2.5mg/kg) in non-tumour bearing PC mice, tail bleed. **D)** WBC subsets at indicated time-points following implantation of osmotic pump releasing AMD3100 200mcg/hr (N=3) or PBS (N=3) in non-tumour bearing PC mice, tail bleed. Plasma AMD3100 concentration at the indicated time-points are displayed in the far-right panel . **E)** WBC subsets at indicated time-points following implantation of osmotic pump releasing AMD3100 45mcg/hr or PBS in KPC mice, tail bleed (2.5hr, N=6 AMD3100, N=9 PBS; 24hr, N=3 AMD3100, N=6 PBS; 48hr, N=3 AMD3100, N=3 PBS). **F)** WBC subset at 144hr after implantation of osmotic pump releasing AMD3100 200mcg/hr (N=8) or PBS (N=6) in KPC mice, cardiac bleeds. **G)** Comparison of baseline WBC subsets in non-tumour bearing PC mice (N=59) and KPC mice (N=30), tail bleeds. Mean +/- SEM. Stats: Paired T-Test for comparison BI vs 1hr in A), all others unpaired T-Test. * - $p < 0.05$, ** - $p < 0.01$, *** - $p < 0.001$, **** - $p < 0.001$

5.5. Discussion

The objective of the experiments was to investigate the pharmacodynamic effects of AMD3100 in the KPC model, at a higher dose rate. AMD3100 had been shown previously to have striking anti-tumour activity in this model, and which was the basis of the CAMPLEX clinical trial [32]. The results support the notion that AMD3100 has anti-tumour activity, and identify pharmacodynamic effects for further study to better understand the anti-tumour mechanism of action of AMD3100.

Given the dose response in anti-tumour activity of single agent AMD3100 that had been identified between 15-45 μ g/hr [32], we hypothesized that administering AMD3100 at 200 μ g/hr would have additional anti-tumour activity in KPC mice. In these experiments, there was a non-significant trend towards tumour growth reduction and increasing survival in KPC mice treated with AMD3100. These results are consistent with previously published results by Feig et al.[32], but inconclusive as whether the 200 μ g/hr dose is more or less active than lower doses. There was a trend towards improved survival at 200 μ g/hr, which was not specifically commented on by Feig et al [32]. However, in contrast, the mean tumour volume increased by 79% with AMD3100 200 μ g/hr, compared to approximately 5-10% with 45 μ g/hr in Feig et al. The experiments are

comparable in most other ways: KPC mice enrolled with similar tumour sizes (5-8mm), treated with either PBS or AMD3100 for 6 days, and ultrasound tumour measurements at the same timepoints. A review of the ultrasounds from both experiments by the same experienced operator may help address if technical reasons exist to explain the apparent difference in anti-tumour activity. The mean tumour volume increased in the PBS control groups similarly (approximately 110% vs 117% in this study), but there may be AMD3100 specific ultrasound characteristics that make tumour measurements more challenging. In particular, given the large increase in F4/80+ cells at the invasive margin in AMD3100 treated mice, it is possible that the 200µg/hr dose increases the phenomenon of pseudoprogression [98, 99] relative to the lower 45µg/hr dose. The ultrasound characteristics of pseudoprogression remain undefined.

The difference in tumour growth inhibition could be considered to be due to partial agonist activity of AMD3100 [100] reducing the anti-tumour activity at the 200µg/hr dose. However, the CXCR4 expression in normal and tumour tissue in this experiment does not support this. The CXCR4 receptor undergoes slow constitutive internalization (1%/min), and CXCL12 rapidly induces CXCR4 receptor endocytosis (50%/5min) and degradation in lysosomes [51–53]. AMD3100 inhibits CXCL12 mediated CXCR4 internalization and degradation [55]. Normal lymphocytes and CD34+ cells incubated with CXCL12 producing stromal cells show decreased CXCR4 surface expression, which is reversed by AMD3100. In patients with acute myeloid leukemia (AML), a single S/C dose of AMD3100 induced an increase in CXCR4 surface expression by 6hr on AML blasts and was maintained for 24hr [93]. Taken together, the literature suggests that CXCR4 expressing cells exposed to CXCL12 would be expected to increase surface CXCR4 expression on treatment with AMD3100. We observed a marked increase in CXCR4+ cells across all tissues examined in mice treated with AMD3100 at 200µg/hr. Compared to KPC mice treated with 45µg/hr in this experiment, 200µg/hr treated mice had similar %CXCR4+ cells in all tissues

(Figure 3). However, direct comparisons are limited due to different time points of mice treated at 45µg/hr and 200µg/hr.

CXCR4 protein expression is a pharmacodynamic readout of AMD3100 target engagement. As discussed, the increase in %CXCR4+ cells within normal tissue, lymphoid tissue and tumour likely mostly reflects changes in surface expression of CXCR4 receptor. For example, except for stromal cells, all cells within lymphoid tissue would be expected to express some surface CXCR4 [92], as indeed was the case in KPC mice treated with AMD3100. In PBS treated KPC mice, surface CXCR4 expression was limited to centroblasts and centrocytes within germinal centers as shown by others [94, 95]. However, many smaller lymphoid cells within germinal centers, the mantle zone and T-cell zone displayed perinuclear-dot staining (possibly the Golgi apparatus or an internal storage of CXCR4 protein) without associated membranous staining. These cells would be expected to have membrane CXCR4 expression [92], but this may be below the detection threshold of CXCR4 IHC.

However, it remains possible that the increase in %CXCR4+ cells in all tissues reflects infiltration of a different immune cell population expressing high surface CXCR4 protein. Indeed, the field of HIV focused on CXCR4 given the receptor can be used by the HIV to enter T cells. The literature suggests higher surface expression on naïve or central memory T cells, but lower on memory effector and effector subsets [46, 101, 102]. Flow cytometry experiments would help define whether AMD3100 changes the phenotype of immune cells within lymphoid tissue and tumour, beyond CXCR4 surface expression.

Interestingly, the increase in %CXCR4 cells was evident by 24hr of AMD3100 treatment in lymphoid and normal tissue, but only at 48hr in tumour. This may be due to delayed tissue distribution of AMD3100 due to poor tumour vascularization [70], Alternatively, it may be due to delayed infiltration of a CXCR4+ high expressing immune cell population, both supporting the hypothesis

that continuous, longer term exposure is required, as evaluated in the COMPLEX trial.

The use of software image analysis on whole sections from en-bloc dissected tumours allowed the quantification and characterization of immune cell subsets distribution at the invasive margin and tumour center. There was a marked asymmetry in the distribution of CD3+, CD4+, FOXP3+, and F4/80+ immune cells. Indeed, the density of all immune cells was highest outside the invasive margin, rapidly decreased near the invasive margin, and was relatively low in the tumour center. This pattern has previously been referred to as an excluded infiltrate [103]. With AMD3100 treatment, the density of F4/80+ cells increased substantially at the invasive margin and intra-tumourally at the 144hr day time point, but the exclusion pattern was maintained. Curiously, we did not observe an increase in CD3+ T cell infiltration at any timepoint, which is seemingly discrepant with the previous study by Feig et al.[32].

Feig et al.[32] reported an accumulation of CD3+ T cells within cancer-cell containing regions at 24hr, as defined by p53 staining, but only reported an increased CD45+ inflammatory infiltrate in AMD3100 + aPD-L1 treated mice at 6 days relative to PBS. The CD45+ or CD3+ infiltrate with AMD3100 alone for 6 days was not reported. Nonetheless, as CD45+ is a pan-leukocyte marker, this is potentially consistent with the current finding of increased F4/80+ macrophages at 6 days. The discrepancy in CD3+ infiltration may have several explanations. In Feig et al. [32], cancer cells were defined by p53 IHC staining, which is intensely expressed only in invasive cancers. PanIN lesions may sparsely show moderate levels of detectable p53 [87], and thus p53 is an imperfect cancer cell marker. However, misidentifying PanIN as cancer cells would seem an unlikely explanation for the discrepancy. In this study, however, CD3+ infiltration was evaluated along the tumour invasive margin, which was identified by H&E and is the gold standard for identifying cancer. The markings were confirmed by another experienced lab member, and reviewed by a pathologist. It is possible that

AMD3100 induces a subtle shift in CD3+ localization from intratumoural stroma into tumour cell nests without necessarily an increase in CD3+ cell numbers- therefore, there may be no change in the distribution curve in Figure 4. A similar CD3+ infiltration may also occur from the peritumoural stroma into tumour nests at the invasive margin. In this case, one might expect slight shift to the right of the CD3+ distribution curve in Figure 4. In either case, quantifying such a phenomenon would require a very precise identification of individual cancer cells to examine the spatial distribution of CD3+ cells. The identification of the invasive margin in the current study may be too imprecise to detect such a subtle effect.

On the other hand, there was a striking accumulation of F4/80+ cells with AMD3100 (200 ug/hr) administration at 6 days. F4/80 is a pan-macrophage marker [104, 105], which is weakly expressed on monocytes and increases with maturation of monocytes into macrophages over 6 days [106]. These data are therefore consistent with an AMD3100 mediated recruitment of monocytes into the TME and subsequent maturation into TAMs. The maturation process would also potentially explain why an increase of F4/80+ cells was not observed at 24 and 48hr in this experiment. It should be noted, again, that the dose of AMD3100 was lower (45 ug/hr) at these time-points and, therefore, a dose effect cannot be ruled out. AMD3100 is known to mobilize most mature leukocyte subsets from the bone marrow into the peripheral circulation in non-tumour bearing mice [97] and humans [107], including the inflammatory monocytes (Ly6C+/CCR2+ in mice, CD14+CCR2+ in humans) believed to be the primary source of TAMs [108]. While the mobilization of monocytes in non-tumour bearing mice was marked, it was relatively muted in KPC mice. This is likely because KPC already have substantially mobilized monocytes due to CCL2 expression in the tumour (and chemokine for CCR2), as has previously been shown in an orthotopic model of PDAC[30]. Additional flow-cytometric analysis of PBS and AMD3100 treated KPC mice could help define the changes in leukocytes in the peripheral blood.

Although a striking pharmacodynamic effect, it is unclear whether the increase in F4/80+ cells is responsible for the anti-tumour activity of AMD3100, an adaptive resistance mechanism, or simply an AMD3100 epiphenomenon unrelated to either anti-tumour activity or resistance. Indeed, monocytes are recruited to the tumour microenvironment by a variety of chemokines (CCL2, CCL5) and cytokines (CSF-1, VEGF)[108]. Local factors skew the differentiation of monocytes towards either M1-like macrophages with anti-tumour activity and dendritic cells (IFN- γ , GM-CSF, LPS), or M2-like macrophages (IL-4, IL-13, CSF-1, TGF- β) with tumour promoting and immunosuppressive activity[108]. CXCL12 may have a role in monocyte differentiation, but is incompletely understood. Incubating human peripheral blood monocytes with CXCL12 skews macrophage differentiation towards an M2-like phenotype [109, 110]. Monocytes differentiated into dendritic cells in the presence of CXCL12 had decreased ability to stimulate antigen-specific T cell proliferation [110]. Furthermore, a certain proportion of TAMs may in fact originate from tissue-resident macrophages, which were seeded in tissue during embryonic development [111]. It is unknown how CXCL12 might be involved in the differentiation of this sub-population of TAMs. Phenotyping of the TAMs by flow cytometry or RNAseq expression would help identify the polarization of the new TAMs in AMD3100 treated KPC mice.

There is a growing literature relating to targeting TAMs in PDAC with agents directed against the CSF1/CSFR1[26], CD40[28], Bruton tyrosine kinase (BTK)/ PI3K γ [29], and CCL2/CCR2[30] pathways. It is unclear if the anti-tumour effects are due to depletion of M2-like macrophage, or reprogramming to M1-like phenotype. In the KPC model, agonistic anti-CD40 antibody had anti-tumour activity, and was related to F4/80+ TAM reprogramming from an M2-like phenotype without depleting the overall number of TAMs[28]. Anti-tumour activity was not mediated by CD4+ or CD8+ cells. A clinical trial with anti-CD40 combined with gemcitabine in 1st line metastatic PDAC showed encouraging clinical activity with a response rate of 19% and a progression free survival of 5.6 months, whereas historical single agent gemcitabine is 5.4% and 2.3 months,

respectively [112]. Interestingly, biopsies from 2 patients with responding lesions showed a heavy infiltrate of macrophages but devoid of lymphocytes. Although the infiltration of F4/80+ cells by AMD3100 may not be directly related to single agent AMD3100 anti-tumour activity, there is a rationale to combine AMD3100 with an anti-CD40 agent in the KPC model.

AMD3100 has also been shown to mobilize the non-classical or patrolling monocytes in humans (CD16+/CCR2-/CX3CR1+)[107] and mice (Ly6C-/CCR2-/CX3CR1)[97]. These monocytes have been shown to have anti-tumour activity through scavenging tumour debris and NK cell recruitment and activation. However, they are believed to primarily reside in the vasculature and rarely enter tissue to differentiate into TAMs [113]. Therefore, while a possible mechanism of AMD3100 anti-tumour activity, these cells may not have contributed to the observed increase in F4/80+ cells in the tumour.

In conclusion, the results support the notion that AMD3100 leads to an anti-tumour effect, but further study is required to determine the mechanism of action. While increased CD3+ cell infiltration has previously been proposed [32], the quantification methodology used in the current study may have been insensitive to detect this effect. However, we identified a large increase in the infiltration of F4/80+ macrophages at 6 days in animals receiving AMD3100 200ug/hr. In particular, it would be important to repeat the *in vivo* experiments at the 6 day time point using the original dose of AMD3100 in the Feig et al. paper to rule out a dose effect as a reason for the infiltration of F4/80+ macrophages [32]. Further studies are warranted to determine their source, polarization, and whether they are related to the anti-tumour effects of AMD3100. Combination studies with AMD3100 and other TAM directed agents, particularly agonistic CD40, could prove synergistic in the KPC model. Lastly, CXCR4 protein expression is a robust pharmacodynamic effect of tissue target engagement by AMD3100, and is being explored in the CAMPLEX clinical trial.

6. COMPLEX CLINICAL TRIAL: AMD3100 IS SAFE AND WELL TOLERATED AT TARGET 2µG/ML PLASMA CONCENTRATION

6.1. Patient population

6.1.1. Patient demographics

Table 1 Patient Characteristics in the dose escalation phase

Characteristic	N=17
Age - yr	
Mean	66
Range	51-75
Female sex – no (%)	4 (24)
Histology - no. (%)	
Pancreatic adenocarcinoma	2 (12)
Colorectal adenocarcinoma	15 (88)
KRAS wild-type	5 (33)
ECOG - no. (%)	
0	7 (41)
1	10 (59)
Lymphocyte count (10 ⁹ /L)	
Median	1.24
Range*	0.83-2.01
Albumin < 35 g/L - no. (%)	11 (65)
Sites of metastasis >2 - no. (%)	10 (59)
Prior lines of chemotherapy- no. (%)	
2	12 (70)
3	3 (18)
4	2 (12)

*1 patient had a normal count at enrolment that decreased to 0.83 on day 1 of the infusion with no identifiable cause

18 patients were enrolled and 17 received at least part of a 7-day AMD3100 infusion in the dose escalation phase. 1 patient was withdrawn prior to receiving drug due to a new biliary obstruction. 15 patients with CRC and 3 patients with PDAC were enrolled. The population was typical for an early phase clinical trial, with good performance status and extensive prior systemic therapy (Table 1). Importantly, the baseline lymphocyte count was above the lower limit of normal (1.0, later raised to 1.1 by the hematology lab) in all patients, suggesting adequate immune status and resolution of immunosuppression from previous chemotherapy. 1 patient had a normal count at enrolment that decreased to 0.83 on day 1 of the infusion with no identifiable cause, highlighting the variability in clinical testing of lymphocyte counts.

6.1.2. Impact of eligibility criteria on patient recruitment - an audit of patients referred to the Addenbrooke's Early Phase Clinical Trial Clinic

The dose escalation phase took 23 months to complete. To understand barriers to patient recruitment, an audit was conducted after 14 months, on all patients referred to the Addenbrooke's Hospital Early Phase Clinical Trial Clinic with a diagnosis of either CRC or PDAC. Only 12% and 18% of referred patients with PDAC or CRC, respectively, were consented to begin screening, despite the trial being prioritized for patient recruitment and, for the most part, there being no competing trials (Figure 1). The most common reason was a combination of medical factors, often a borderline or poor performance status. Several patients with PDAC deteriorated clinically while waiting for a trial slot. This delay was often related to the 2-week observation period in between patients in the dose escalation phase, a testimony to the aggressive biology of PDAC. PDAC referrals were subsequently triaged more promptly for appointments.

A lymphocyte count below the lower limit of normal (LLN) was the only ineligibility criterion in a significant proportion of patients, 12% and 9% of patients with PDAC and CRC, respectively. Furthermore, the hospital laboratory raised the LLN from 1.0 to 1.1×10^6 cells/L in the middle of the study. This raised questions about the predictive value of baseline lymphocyte counts for response to a potential immunotherapeutic agent. Due to the relative absence of evidence, reviewed in the discussion, and concerns for potential false negative results on translational studies, the criterion was maintained at 1.0×10^6 cells/L.

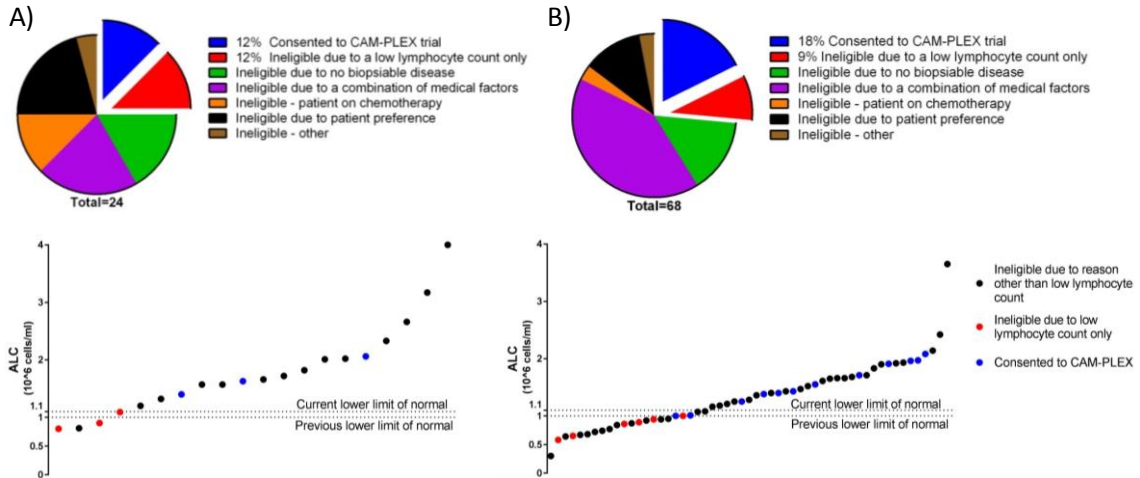


Figure 1 Audit of patient referrals to the Addenbrooke's Hospital Early Phase Clinical Trial Clinic. The clinical charts of all patients referred over a 14 month period with a diagnosis of PDAC (A) or CRC (B) were reviewed for reasons of ineligibility for the CAMPLEX trial. Absolute lymphocyte count (ALC).

6.2. Safety data – AMD3100 is safe and well tolerated up to 80ug/kg/hr

6.2.1. Adverse events

Table 2 AMD3100-related adverse events

CTCAE v 4.03		Adverse event grade																
		20 mcg/kg/hr			40 mcg/kg/hr				80 mcg/kg/hr			120 mcg/kg/hr						
Category	Term	1001	1002	1003	1004	1005	1007	1008	1009	1010	1011	1012	1013	1014	1015	1016	1017	1018
Cardiac	Supraventricular ectopic beats																	
	Supraventricular tachycardia																	
	Ventricular arrhythmia																	
Eye	Watering eyes																	
Gastrointestinal	Abdominal pain																	
	Abdominal distention																	
	Diarrhea																	
	Nausea																	
General	Vomiting																	
	Chills																	
	Fatigue																	
Hematologic	Fever																	
	Anemia																	
Investigations	Platelet count decreased																	
	ALT increased																	
	ALK Phosphatase increased																	
Metabolism and nutrition	Creatinine increased																	
	Anorexia																	
Nervous system	Hypoalbuminemia																	
	Dysgeusia																	
	Headache																	
	Abnormal dreams																	
Psychiatric	Paresthesia																	
	Vasovagal reaction																	
	Anxiety																	
Vascular	Insomnia																	
	Claustrophobia																	
	Hypotension																	
	Hot flashes																	

In the dose escalation phase, the most common subjective AEs, regardless of causality to AMD3100, included insomnia (82%), paresthesia

(59%), diarrhea (53%), abdominal pain (47%), nausea (41%), vomiting (41%), and hot flashes (35%). There were no respiratory AEs. AMD3100 was overall well tolerated, with only grade 1-2 AMD3100 related AEs at the 20/40/80µgkg/hr dose levels (Table 2).

Paresthesia was dose-related (0/3, 1/4, 3/3, and 6/7 patients by dose cohort) and mostly grade 1. Onset was usually within 24-48hr of the start of infusion, but resolved within a few days (median 6 days) after discontinuing AMD3100 (Figure 2A). A previous dose escalation trial of continuous IV infusion of AMD3100 in patients with HIV by Hendrix et al.[58] also found a high frequency of paresthesia at higher doses (Figure 2B). Although direct comparison is difficult with the small numbers of patients, patients on the CAMPLEX trial may have a higher frequency of paresthesia. Many patients had a baseline peripheral sensory neuropathy related to previous oxaliplatin exposure, and this may increase the risk of paresthesia. Several patients reported worsening of paresthesia with cold water, a commonly described symptom in oxaliplatin related peripheral neuropathy. Oxaliplatin acute neurotoxicity is thought to be related to chelation of intracellular calcium and alteration of voltage-gated sodium channels [114]. Plasma calcium concentration did decrease in all cohorts but there was no correlation with dose ($r^2=0.09$, $p=0.11$) (Figure 2C).

Insomnia was dose-related (0/3, 3/4, 3/3, and 7/7 of patients by dose cohort). Onset was relatively rapid on infusion (Figure 2D), and pharmacologic sleeping aids were only marginally effective in improving sleep. However, insomnia often did not resolve by the last follow-up, which was 21 days after drug discontinuation. A number of patients experienced other neuro-psychiatric AEs, such as anxiety, claustrophobia, and abnormal dreams (Table 2). Lastly, gastrointestinal AEs were also dose-related (0/3, 2/4, 3/3, and 7/7 of patients by dose cohort). Diarrhea onset was usually within 24hr of the start of infusion and resolved within a few days with as needed anti-motility medication (Figure 2E).

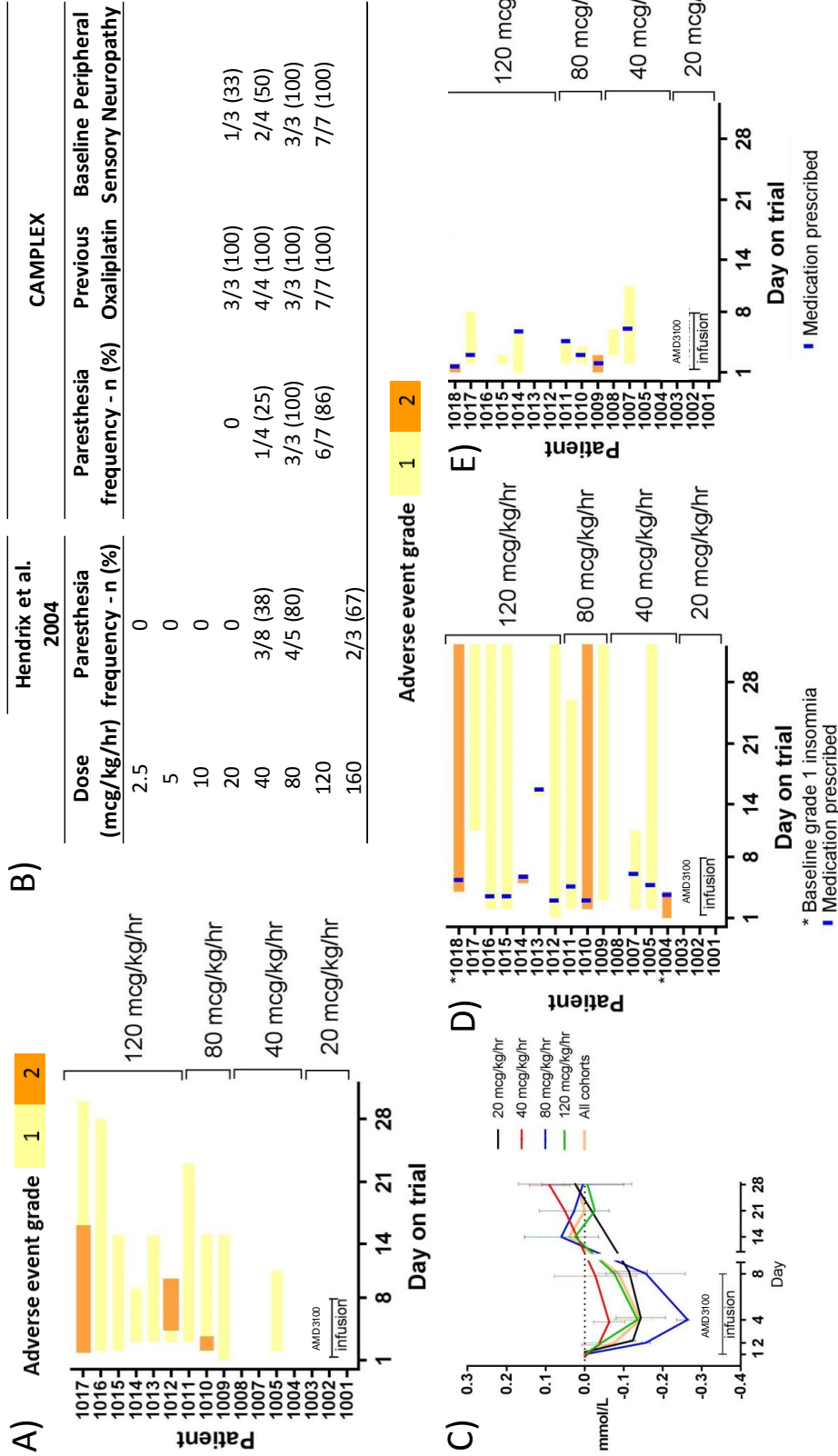


Figure 2 Select AMD3100-related adverse events. A) Paresthesia onset and resolution on the CAMPLEX trial by patient and dose cohort. **B)** Comparison of paresthesia in CAMPLEX and the only other known study with continuous IV infusion of AMD3100, Hendrix et al. 2004. **C)** Plasma calcium concentrations on study. The absolute change from baseline is displayed. **D)** Insomnia onset and resolution on the CAMPLEX trial by patient and dose cohort. **E)** Diarrhea onset and resolution on the CAMPLEX trial by patient and dose cohort.

Hendrix et al.[58] previously identified the potential for cardiac arrhythmias with continuous IV AMD3100 infusion. As matter of precaution, patients on the CAMPLEX trial were monitored by cardiac telemetry until the anticipated concentration at steady state was achieved, and then transitioned to Holter monitoring for the remaining infusion. Telemetry was used for the first 48hr, but it was extended to 72hr based on emerging pharmacokinetic data (discussed below). Patients 1001 and 1002 had a brief, asymptomatic, run of supraventricular tachycardia (SVT) that terminated spontaneously (Table 3). This may be within the normal physiologic limits, although a baseline 24hr-Holter monitor recording did not show any runs of SVT. Patient 1014 had an increase in supraventricular ectopic beats while on infusion that were asymptomatic. Of note, this patient had a markedly elevated 168hr AMD3100 concentration of 9360 ng/ml and was likely due to acute kidney injury, associated with AMD3100-related grade 1 diarrhea and grade 2 nausea. Finally, patient 1017 had a brief run of non-sustained ventricular tachycardia that was also asymptomatic. No cardiac AE required drug interruption, and all resolved without sequelae.

Table 3 Cardiac adverse events on infusion

Dose cohort (mcg/kg/hr)	Patient ID	Adverse event	Grade	Relation to AMD3100	Action	Outcome of adverse event
20	1001	Supraventricular tachycardia	1	Definitely related	None	Recovered
20	1002	Supraventricular tachycardia	1	Unlikely to be related	None	Recovered
120	1014	Supraventricular ectopic beats	1	Probably related	None	Recovered
120	1017	Non-sustained ventricular tachycardia	1	Possibly related	None	Recovered

6.2.2. Dose limiting toxicities

There were no DLTs at the 20, 40 and 80 µg/kg/hr doses, but 2 patients had DLTs at the 120µg/kg/hr dose (Table 4). Patient 1014 had a vasovagal reaction (grade 3) in the context of pain shortly after the Day 8 biopsy. Although pain is the most likely cause of the vasovagal reaction, AMD3100 has been associated with vasovagal reactions. Therefore, the vasovagal reaction was deemed to be possibly related to AMD3100 and, consequently, a DLT. Patient 1018 developed severe abdominal pain (grade 3), hypotension (grade 3), and a vasovagal reaction (grade 3) on day 2 of the infusion. Symptoms entirely

resolved back to baseline within 24hr after discontinuing the drug, pain control, and IV fluids. The patient had peritoneal disease, grade 1 abdominal pain at baseline not requiring analgesia, and a history of irritable bowel syndrome.

Two patients were also withdrawn prior to completing a 7-day continuous IV infusion of AMD3100, but neither for reasons deemed related to AMD3100. Patient 1007 (40µg/kg/hr) was withdrawn on day 7 due to a new biliary obstruction from porta hepatis bulky lymphadenopathy. Patient 1013 (120µg/kg/hr) developed duodenal obstruction on day 5 related to the primary PDAC.

Table 4 Drug interruption or discontinuation due to adverse events

Dose cohort (mcg/kg/hr)	Patient ID	Day of discontinuation or interruption	Adverse event	Relation to AMD3100	Action	Outcome of adverse event
40	1007	7	Biliary tract obstruction and infection	Unlikely to be related	Discontinued	Recovered
120	1013	5	Duodenal obstruction	Unlikely to be related	Discontinued	Recovered
120	1014	8	Vasovagal reaction*	Possibly related	Discontinued	Recovered
120	1018	2	Vasovagal reaction, hypotension, abdominal pain*	Possibly related	Discontinued	Recovered

* DLT

6.3. Pharmacokinetics

6.3.1. Target plasma AMD3100 concentrations achieved at 80 µg/kg/hr

Of the 17 patients that received any AMD3100 in the dose escalation phase, 15 contributed to estimates of the C_{ss} , CL, and 13 to AUC_{0-168} . All patients in the 80 and 120 µg/kg/hr dose cohorts achieved a C_{ss} above the target 2µg/ml (Table 5). AMD3100 displayed linear pharmacokinetics: CL was dose independent ($r^2=0.09$, $p=ns$); C_{ss} increased linearly with dose ($r^2=0.74$, $p<0.0001$); and AUC_{0-168} increased linearly with dose ($r^2=0.88$, $p<0.0001$).

Table 5 AMD3100 pharmacokinetic parameter estimates.

Dose cohort (mcg/kg/hr)	Patients	C _{ss} (ng/ml)	AUC ₀₋₁₆₈ (ng*h/ml)	Cl (L/hr)	T _{1/2} (hr)
20	3	738 (707-707)	90783 (90433-91150)	2.26 (2.10-2.48)	9.7 (8.4-11.7)
40	4*	1182 (698--1490)	158070 (94553-200208)	2.80 (2.19-3.10)	7 (4.1-8.8)
80	3	2310 (2170-2420)	308510 (277748-347704)	2.60 (2.20-3.03)	8.1 (6.4-9.2)
120	7†	3774 (2640-5490)	472620 (364320-698880)	2.55 (1.46-3.27)	8.1 (5.2-11.7)

Mean (range)

* Patient 1007 withdrawn at day 7, no AUC₀₋₁₆₈† Patient 1013 withdrawn at day 5, no AUC₀₋₁₆₈. Patients 1014 and 1018 withdrawn at day 8 and 2, respectively, excluded.

6.3.2. AMD3100 terminal T_{1/2} may be longer than previously identified

The time to steady state is a function of the terminal half-life (T_{1/2})[86]. The first in man clinical trial with AMD3100 by 15 min IV injection determined the terminal T_{1/2} to be 3.6hr [59]. The time to steady state by continuous IV infusion is approximately 3 to 5 half-lives [86] and, therefore, C_{ss} should have been achieved by 24hr in our trial. However, visual inspection of the plasma AMD3100 concentration curves for each patient showed increasing concentrations beyond 24hr, reaching apparent steady state by 72hr in nearly all patients (Figure 3A). In fact, patients reached a mean of 71% and 94% by 24hr and 72hr, respectively, of concentrations at 168hr.

The pharmacokinetic sampling schedule was designed to evaluate the C_{ss}, and is not optimal to determine the terminal T_{1/2}. The terminal T_{1/2} can nonetheless be estimated from the available data, with certain assumptions, using the following formula[86]:

$$t_{1/2} = \frac{0.693 \cdot Vd}{CL} = \frac{\ln(2)}{k_e} = \frac{0.693}{k_e}$$

One approach is to assume a one compartment pharmacokinetic model. The elimination rate constant (K_e) can be estimated by non-linear regression with a one phase decay curve. By this approach, the mean T_{1/2} is 15.3hr. However, the T_{1/2} 95% confidence intervals for individual patients were wide (Figure 3B), and a curve could not be fitted adequately to the data for some patients. A second approach is to estimate the T_{1/2} by using the previously calculated Cl and

volume of distribution ($V_d=0.34L/kg$) from the first in man trial of AMD3100[59]. $T_{1/2}$ was similar across dose cohorts (Table 5), with a mean of 8.1hr (range 4.1 - 11.7hr), and dose independent ($r^2=0.02$, $p=ns$).

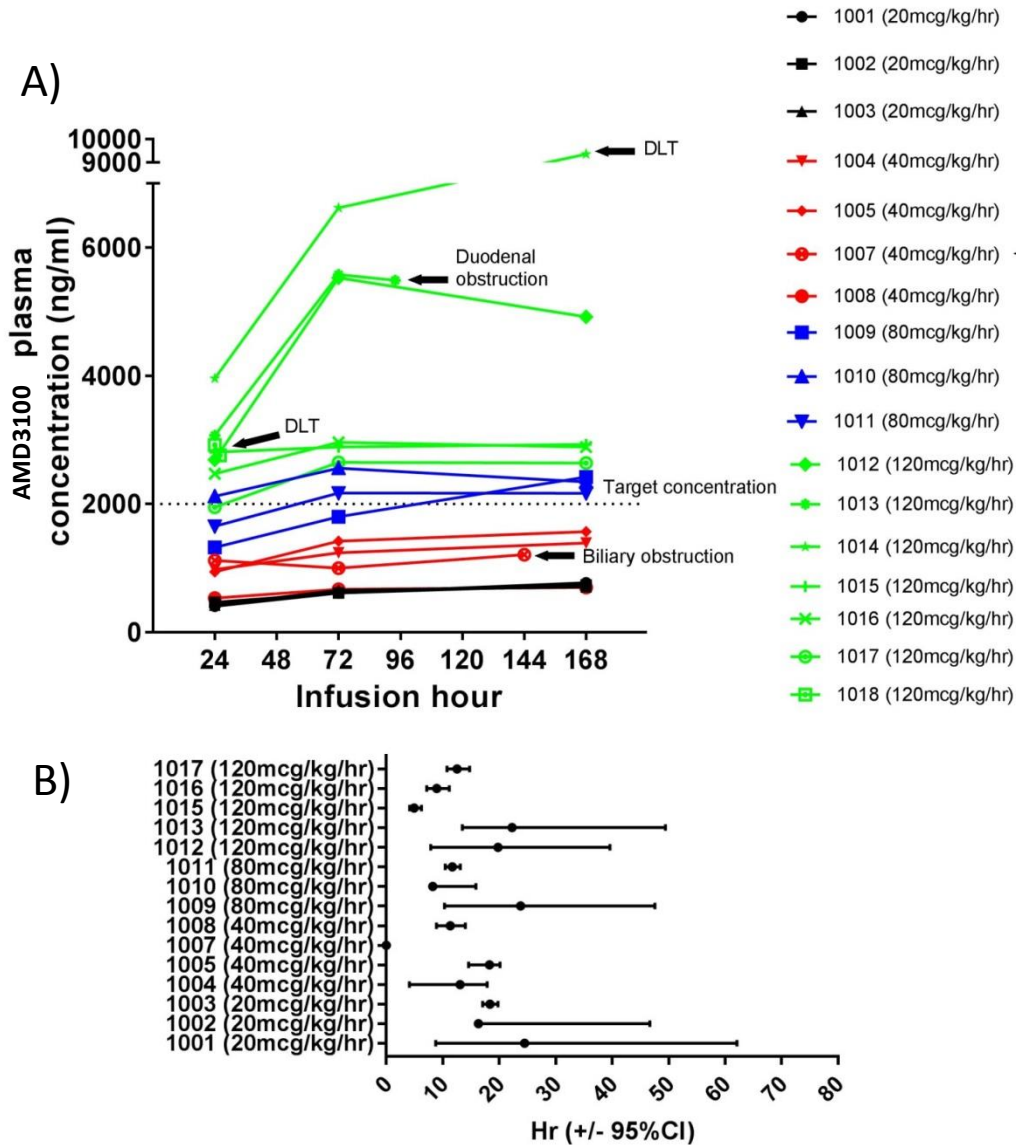


Figure 3 Individual patient pharmacokinetic profiles **A)** Plasma AMD3100 concentration profiles for every patient that received any duration of continuous IV AMD3100 infusion. **B)** Every patient AMD3100 concentration values was fitted to a one-phase decay model to estimate K_e and subsequently $T_{1/2}$. Fitting was inadequate and resulted in wide confidence intervals for $T_{1/2}$ by this method. Dose limiting toxicity (DLT).

To investigate the $T_{1/2}$ further, the protocol was amended and additional PK samples collected at follow-up day 13-17 for patients 1017 onwards, which is

approximately 1 week after discontinuing the infusion. Plasma AMD3100 were 91 and 88 ng/ml in patients 1017 and 1018, respectively, at 168hr after infusion discontinuation, suggesting a terminal $T_{1/2} \approx 33$ hr. Both patients had normal renal function. Additional PK data from the dose expansion phase will confirm and refine these estimates.

6.3.3. AMD3100 clearance correlates with renal function, but not with measures of body composition

Weight-based dosing of AMD3100 is currently used in clinical practice for hematopoietic stem cell mobilization (240µg/kg S/C daily for 4 days), and has been used in other clinical trials investigating continuous infusion of AMD3100 [58, 115]. In CAMPLEX, AMD3100 was also dosed based on patient weight. Interestingly, in the dose escalation phase, no correlation was found between AMD3100 clearance and various indirect measures of body composition (Figure 4). CL did not correlate with albumin or C-reactive protein (CRP), the latter being a surrogate for the basophilic drug binding protein α 1-acid glycoprotein. AMD3100 CL did correlate with renal function (Figure 4, Table 6). However, renal function only accounted for 33% of the AMD3100 CL variance ($r^2=0.33$).

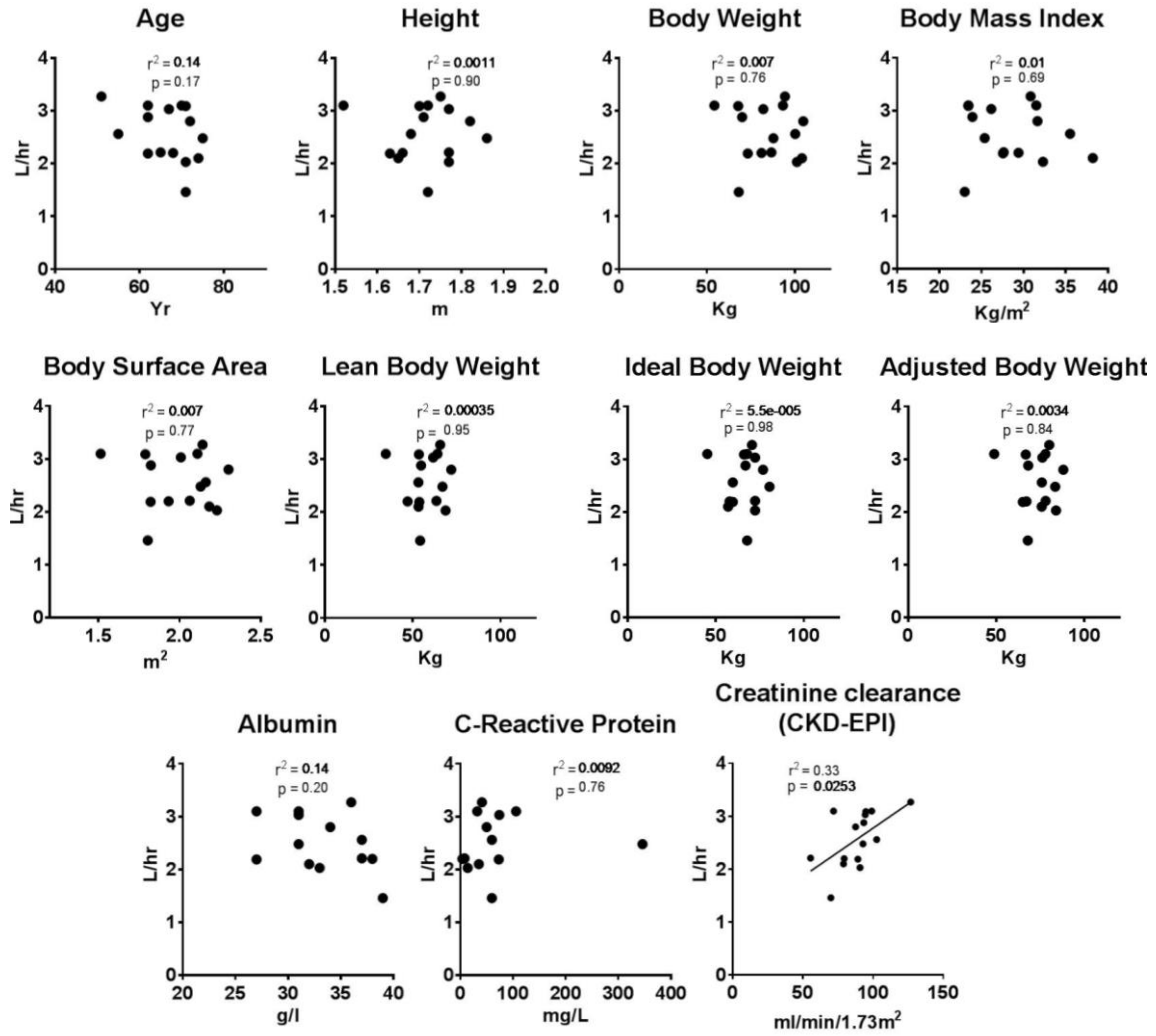


Figure 4 AMD3100 clearance correlations with indirect measures of body composition, plasma binding proteins, and renal function.

Table 6 AMD3100 pharmacokinetic parameter estimates according to renal function (CKD-EPI).

Renal function (ml/min/1.73m ²)	Cl _{cr} (ml/min/1.73 m ²)	Cl (L/hr)	Cl (ml/min/kg)	Cl (L/hr/kg)	T _{1/2} (hr)
All patients N=15	88.5 ± 16	2.57 ± 0.5 (1.46-3.27)	0.53 ± 0.16 (0.33-0.95)	0.031 ± 0.009 (0.020-0.057)	8.1 ± 2.2 (4.1-11.7)
Normal (>90) N= 8	99.4 ± 11.0	2.81 ± 0.38 (2.03-3.27)	0.55 ± 0.13 (0.33-0.76)	0.033 ± 0.007 (0.020-0.045)	7.5 ± 2.0 (5.2-11.7)
Mild reduction (60-89) N= 6	79.5 ± 7.2	2.31 ± 0.52 (1.46-3.1)	0.50 ± 0.21 (0.34-0.95)	0.030 ± 0.012 (0.020-0.057)	8.7 ± 2.4 (4.1-11.7)
Moderate reduction (45-59) N= 1	55.4	2.21	0.43	0.025	9.2
Mean ± SD (range)					

6.4. AMD3100 mobilizes white blood cell subsets into the peripheral circulation

WBC mobilization is a known pharmacodynamic effect of AMD3100 administered by single dose S/C injection [59, 60] or continuous IV infusion [58]. AMD3100 is currently licensed in combination with G-CSF to mobilize CD34+ cells into the peripheral circulation for harvesting for autologous stem cell transplantation [62, 63]. We therefore measured WBC subsets on standard clinical CBC assay and CD34+ counts in the peripheral circulation as a pharmacodynamic readout of CXCR4 inhibition in CAMPLEX.

As expected, CD34+, monocytes, lymphocytes, neutrophils, basophils and eosinophils were maximally increased in the peripheral circulation by 24hr across all cohorts, and maintained throughout the infusion (Figure 5). WBC subsets largely returned to baseline by day 28. Interestingly, WBC mobilization could still be appreciated on day 14 and, to a less extent, on day 21 (WBC counts were only measured on day 14 and 21 starting with cohort 80µg/kg/hr).

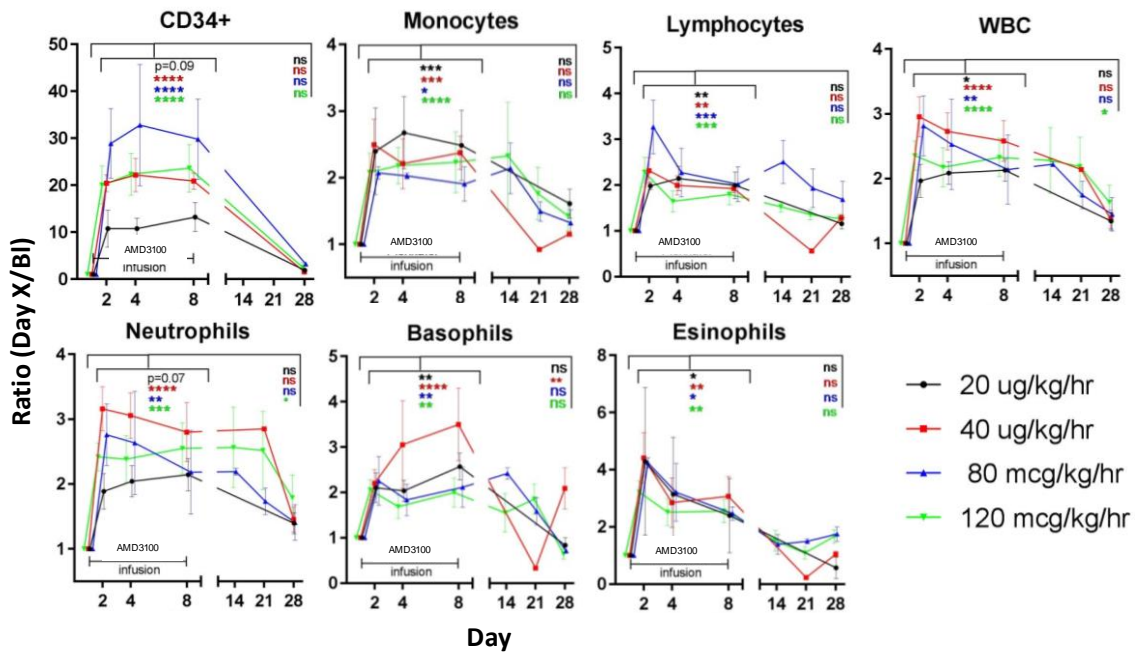


Figure 5 AMD3100 mobilizes WBC subsets into the peripheral circulation. All WBC subsets are mobilized into the peripheral circulation early and maintained throughout the AMD3100 infusion. Day 14 and 21 WBC were measured starting with cohort 80mcg/kg/hr. Two-way ANOVA comparison of mean on infusion (day 2/4/8) and Day 28 vs day 1, Dunnett's multiple comparison test (mean +/- SEM). WBC subset counts were normalized to baseline values.

Mobilization of WBC subsets was robust in most patients at all time-points during the infusion. WBC subsets measured on CBC were generally >1.5-2 fold increased, when compared to baseline (Figure 6A). CD34+ mobilisation was variable between patients, but generally >10 fold compared to baseline (CD34+ fold change: mean 21, range 6-59; cells/ μ l mean 23, range 7-63) (Figure 6B). There was no correlation between mean CD34+ counts or fold change on infusion with age ($p=0.57$ and $p=0.63$, respectively) or months of previous chemotherapy ($p=0.35$ and $p=0.79$, respectively) in this small sample. Patient 1013 displayed relatively poor mobilization across many counts on CBC, but CD34+ cells were clearly mobilized. Patient 1013 had PDAC, was previously treated with 2 lines of chemotherapy, and discontinued infusion on day 5 due to a new duodenal obstruction.

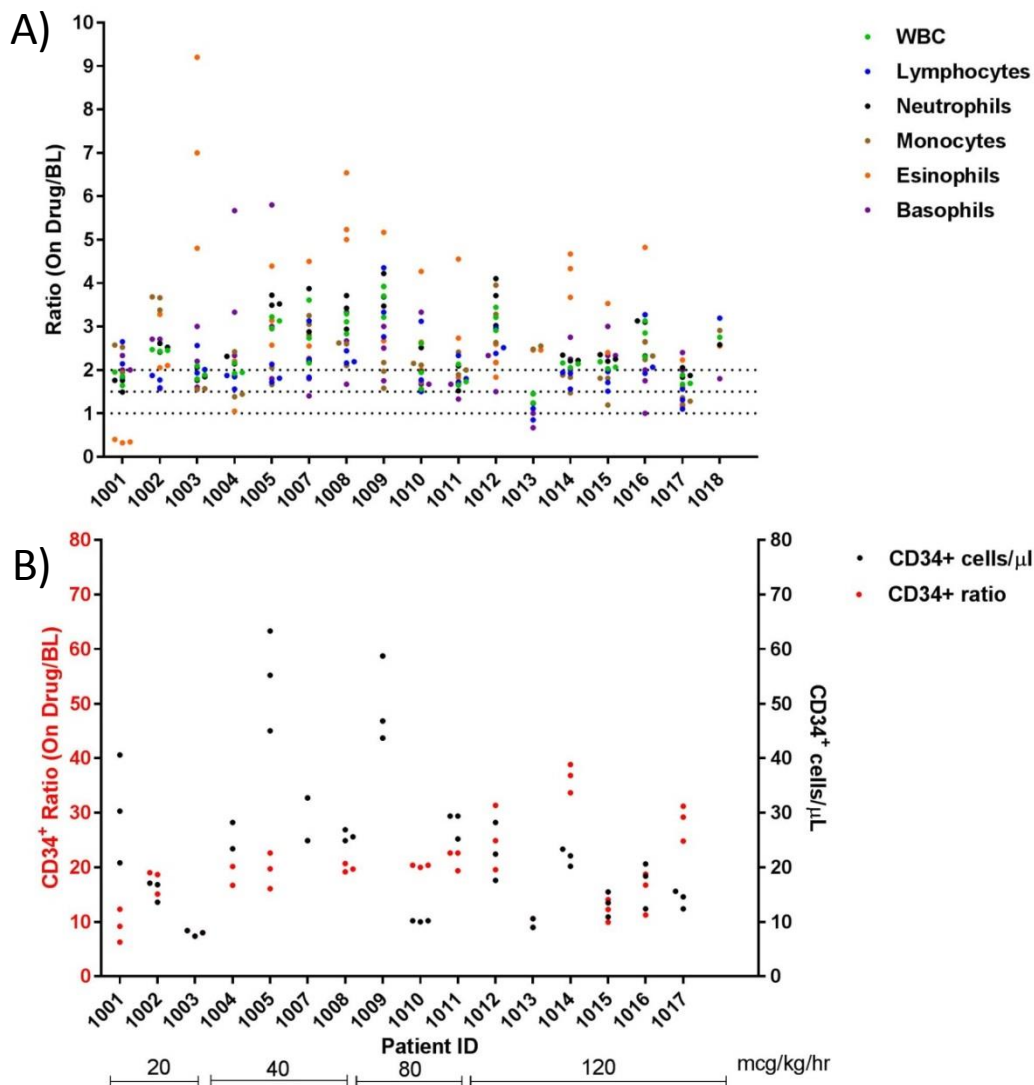


Figure 6 WBC subset mobilization by patient while on AMD3100 infusion. WBC subsets determined by full blood count A) and CD34+ cells B). Counts were measured on day 2, 4 and 8 of the infusion. Patients 1007, 1013 and 1018 discontinued on day 7, 4, and 2 of the infusion. WBC subset counts were normalized to baseline values.

Pharmacodynamic modelling showed near maximal mobilization of all subsets in the lowest dose cohort (20 μ g/kg/hr) (Figure 7). The half-maximal effect (EC_{50}) is estimated to occur at a dose below 20 μ g/kg/hr for all WBC subsets, albeit with large confidence intervals. The plateau (maximum effect [EC_{max}]) for all subsets was consistently around 2.5 fold over baseline, except for CD34+ counts at 28 fold. Similar results were obtained when modelling by actual dose administered and C_{ss} .

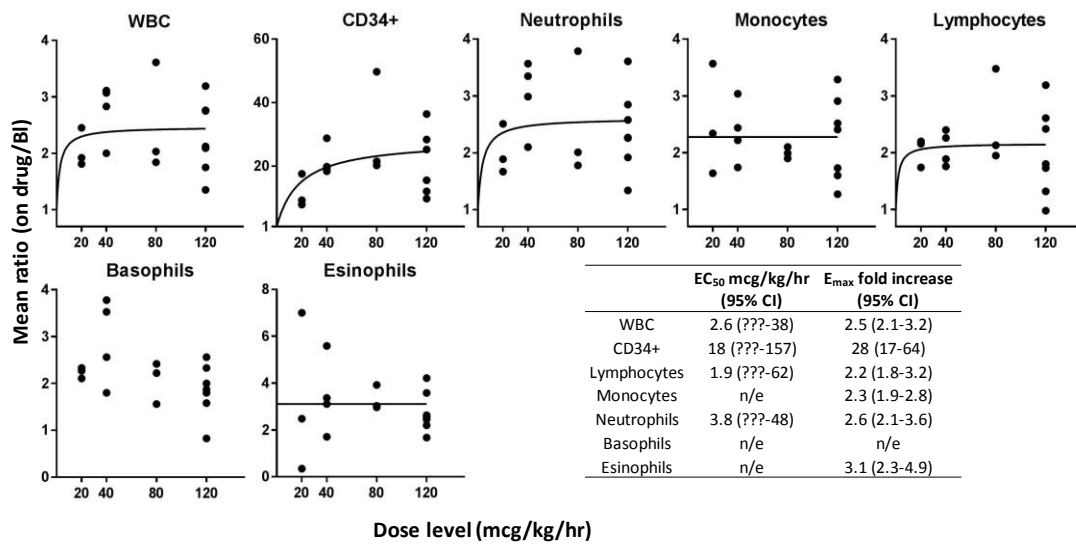
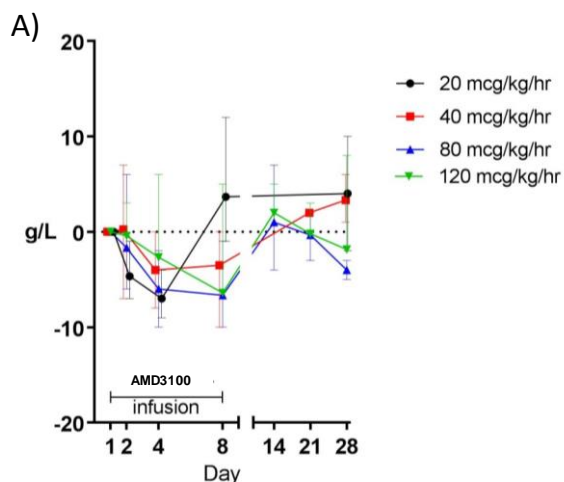


Figure 7 Pharmacodynamic modelling of WBC mobilization into the peripheral circulation. WBC subset mobilization is near maximal at the lowest dose administered 20mcg/kg/hr. For every WBC subset, the plateau of fold change (maximum effect [E_{max}]) and dose (mcg/kg/hr) at which the half-maximal effect is estimated to occur (EC₅₀) was calculated, if possible.

Hemoglobin concentrations appeared to drop slightly (mean change on Day 8: -3.7 g/L, range -13/+10 g/L) in all dose cohorts while receiving the infusion (Figure 8A). Hemoglobin recovered by day 14 in all cohorts, despite WBC subsets showing persistent mobilization at day 14 (Figure 5). There was no significant correlation between the actual dose received and the magnitude of change at day 8 (p=0.11). The blood sampling schedule may have contributed to the slight drop in haemoglobin while on study (Figure 8B).



B)

CAM-PLEX - Blood sampling	Screening	Infusion (days)								13-17	20-24	28	56
Sample Type		1	2	3	4	5	6	7	8				
Clinical bloods	10.3	4.7	10.3		7.3					10.3	7.3	10.3	7.3
Research bloods	59.5	0	59.5	0	34.5	0	0	0	42.5	9	0	16.5	9
Total (ml)	69.8	4.7	69.8	0	41.8	0	0	0	52.8	16.3	7.3	26.8	16.3
Cumulative total (ml)	69.8	74.5	144.3	144.3	186.1	186.1	186.1	186.1	238.9	255.2	262.5	289.3	305.6

Figure 8 Hemoglobin changes on study. A) Hemoglobin concentration changes by dose cohort (mean +/-range). The absolute hemoglobin change from baseline is displayed. B) Blood sampling schedule.

6.5. Discussion

AMD3100 was overall well tolerated up to a dose of 80 µg/kg/hr. All patients in this dose cohort achieved a C_{ss} above 2µg/ml. Therefore, 80µg/kg/hr would be considered to be the RP2D, as pre-defined in the protocol. The most common AMD3100-related AEs of paraesthesiae and gastrointestinal symptoms were also described in a previous study with continuous infusion, although not insomnia[58], which was common in our study. These AMD3100 related AEs were mostly grade 1-2 with a 7-day infusion.

The mechanism of the neurological toxicities is unclear. A general receptor activity screen identified moderate or strong binding affinity of AMD3100 to a number of different receptors mostly located in the central and peripheral systems. This had not been investigated further because AMD3100 displays poor central nervous system (CNS) penetration[116], an established safety record,

and rapid CL following daily s/c injection for the mobilization of CD34+ cells. However, continuous IV infusion, especially over prolonged periods, could result in drug accumulation in the CNS and engagement of the receptors identified in this screen may explain some of the neurological toxicities seen in this study. Lastly, CXCR4 is important in neurological development[117], is widely expressed in the central nervous system, and activation has been reported to modulate neuronal activity through multiple pathways, including voltage-dependent channels and neurotransmitter release[118]. Therefore, AMD3100 target engagement of CXCR4 receptor may also help explain the observed toxicities but remains unexplored.

The clinical symptoms of paresthesiae are similar to the acute neurotoxicity seen with oxaliplatin, namely relatively rapid onset and resolution, and relation to touching cold items. Oxaliplatin acute neurotoxicity is thought to be related to chelation of intracellular calcium and alteration of voltage-gated sodium channels[114]. The 2 cyclam rings of AMD3100 can chelate metal ions (Cu^{2+} , Zn^{2+} , Ni^{2+}), which increases affinity for the CXCR4 receptor [119, 120]. It is unknown whether AMD3100 may also chelate calcium and lead to a similar acute neurotoxicity mechanism to oxaliplatin. Plasma calcium concentration did decrease in all cohorts but it is unknown how this might relate to intracellular calcium. The treatment course is too short to evaluate if any chronic sensory neuropathy characteristic of cisplatin and oxaliplatin [121] might develop with prolonged or repeated administration of AMD3100. This chronic sensory neuropathy is cumulative and dose-limiting, and thought to be related to DNA damage and subsequent induction of apoptosis of nerves in the dorsal root ganglion [122]. AMD3100 did not demonstrate genotoxicity [116] and, therefore, chronic sensory neuropathy is less likely.

Sleep disorders are commonly reported in patients with cancer [123] and cancer treatment or their side effects contribute to the aggravation of insomnia[124]. Admission to the Clinical Research Facility for the AMD3100

infusion may have contributed to insomnia [125]. However, the prolonged duration after discharge suggests at least some contribution from AMD3100.

With respect to dose limiting toxicities, the vasovagal reactions are consistent with previously reported experience with AMD3100[116]. This is perhaps not surprising given AMD3100 may directly act on the nervous system and vasovagal reactions are thought to be neurally mediated[126], although the mechanism is unclear. It is tempting to speculate that AMD3100 might modulate nociception or physiologic reactions to pain. Both patients with DLTs had significant abdominal pain that likely contributed to the vasovagal reactions. For 1014, it was abdominal pain following the repeat biopsy on Day 8. Patient 1018 experienced grade 3 abdominal pain on Day 2 of the infusion in the context of peritoneal metastases (though not requiring analgesia at baseline) and a history of irritable bowel syndrome. However, limited pre-clinical work suggests that that AMD3100 may have analgesic properties in models of bone cancer pain[127] and neuropathic pain[128].

The safety profile of single agent AMD3100 suggests it could be combined with checkpoint inhibitors targeting PD-(L)1 or CTLA-4 given little overlapping toxicities. However, particular attention should be paid to differentiating gastrointestinal symptoms, in particular diarrhea, related to AMD3100 and the more serious colitis from checkpoint inhibitor treatment. The latter tends to present after 6-8 weeks of treatment (24), whereas AMD3100 related diarrhea starts within a few days of starting the infusion and resolves promptly on drug discontinuation or administration of anti-motility agents.

We anticipated achieving the target C_{ss} by 24hr with a 120 $\mu\text{g}/\text{kg}/\text{hr}$ dose. This prediction was based on the pharmacokinetic data from 2 clinical trials. In the first in man clinical trial by Hendrix et al. [59], AMD3100 was given by 15 min IV injection to healthy volunteers and the terminal $T_{1/2}$ was determined to be 3.6hr. The time to steady state by continuous IV infusion is approximately 3 to 5

half-lives [86] and, therefore, we anticipated C_{ss} would be achieved by 24hr in CAMPLEX. In another clinical trial by Hendrix et al. [58], patients with HIV received a continuous IV infusion of AMD3100 over 10 days. The 80 and 160 $\mu\text{g}/\text{kg}/\text{hr}$ cohorts achieved mean C_{ss} of 1.8 $\mu\text{g}/\text{ml}$ (range 1.5-2.7) and 3.3 $\mu\text{g}/\text{ml}$ (range 2.9-4.1), respectively. We anticipated a 120 $\mu\text{g}/\text{kg}/\text{hr}$ dose would be needed to achieve the target 2 $\mu\text{g}/\text{ml}$ in >80% of patients. However, in the dose escalation phase of CAMPLEX, all patients achieved a C_{ss} above 2 $\mu\text{g}/\text{ml}$ by the 80 $\mu\text{g}/\text{kg}/\text{hr}$ dose, and near C_{ss} was achieved around 72hr in most patients.

To discuss possible reasons for achieving the target C_{ss} at a lower dose than expected, it is important to state that the only factors that control C_{ss} are dose and CL. Comparing the pharmacokinetic data from CAMPLEX and Hendrix et al. [58] (Figure 9), the mean C_{ss} in every cohort was similar but consistently higher in CAMPLEX (only mean and ranges were available in the Hendrix et al. paper), and conversely for CL. AMD3100 is primarily excreted unchanged in the urine (71% by 24hr post dose) in patients with normal renal function [130]. In a study administering a single 240 $\mu\text{g}/\text{kg}$ S/C dose to patients with varying renal impairment [130], AMD3100 CL decreased and exposure increased with renal impairment. In CAMPLEX, 7 of 15 patients that contributed to CL estimates had mild or moderate renal impairment. While Hendrix et al. [58] did not report renal function, patients in CAMPLEX with normal renal function had a lower AMD3100 CL compared to those in Hendrix et al. (Table 6, Figure 9). Thus, renal function does not fully explain the differences in CL and C_{ss} between these studies.

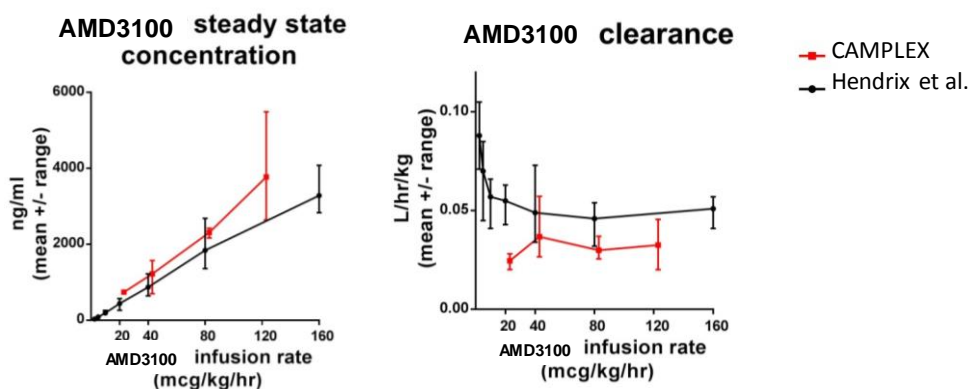


Figure 9 Comparison of C_{ss} and AMD3100 clearance from CAMPLEX and Hendrix et al (mean +/- range).

AMD3100 is bound to human plasma proteins up to 58% [116] and a strong base due to the basic nitrogens of each bicyclam ring. Changes in protein binding can affect liver and renal clearance of a drug, depending on the drug's extraction ratio in these organs. The major plasma binding proteins are albumin and alpha 1-acid glycoprotein [86]. The latter is an acute phase protein, correlates with CRP [131], and is important for binding of basic drugs [132]. However, there was no correlation between albumin or CRP and AMD3100 CL. Additional data from the expansion cohort will help clarify if any correlation exists, although 58% protein binding is not particularly high.

AMD3100 does not appear to be metabolised *in vivo*. AMD3100 was not found to be metabolized in experiments with human liver microsomes and primary hepatocytes, suggesting a low potential for CYP450 dependent drug interactions[116], a common issue in patients with HIV on anti-retroviral therapy [133]. Additionally, nonparent radiolabelled components previously identified as metabolites in rat [59] and dog studies were confirmed as Cu²⁺ complexes with AMD3100 [116]. However, a small proportion (5-10%) of AMD3100 was found to be excreted in faeces in animal studies [116], suggesting AMD3100 undergoes some biliary excretion. It is possible that differences in AMD3100 biliary excretion in patients with cancer or HIV could explain the relatively small differences in C_{ss} and CL between CAMPLEX and Hendrix et al. [58], but a mechanism is not clear.

To discuss possible reasons for achieving a C_{ss} later than expected, it is important to state that the time to steady state is only a function of the terminal half-life (T_{1/2})[86]. The initial pharmacokinetic sampling schedule in CAMPLEX was designed to evaluate the C_{ss}, and was not optimal to assess the terminal T_{1/2}. The detection of AMD3100 at 168hr after infusion discontinuation suggests a much longer terminal T_{1/2} of ≈33hr than the 3.6hr observed in the first in man study[59]. In that study, the reported CL and terminal T_{1/2} were based on a two-compartment model, though a three-compartment model fit marginally better. Importantly, the sampling schedule covered a 24hr period. To adequately

characterize a terminal $T_{1/2}$, sampling needs to cover at least 3 times the expected terminal $T_{1/2}$ [134]. Furthermore, AMD3100 was below the level of detection of their assay for much of the elimination phase of the lower dose cohorts. Given the limitation in assay sensitivity and sampling schedule, there was insufficient data to adequately assess the third compartment and likely determinant of the terminal $T_{1/2}$. For the same reasons, the second compartment may have also been inadequately evaluated.

The data from CAMPLEX and Hendrix et al [59] would suggest a 3 compartment model (Figure 10A) to explain the observed pharmacokinetic data. The thickness of the arrows represents the speed of the processes of distribution and elimination. On injection of a bolus IV dose, AMD3100 begins to be eliminated, but also redistributes to the peripheral compartments V_2 and V_3 . Equilibration between V_1 and V_2 occurs relatively quickly and is marked by the transition from the α to β phase (Figure 10B) of the plasma concentration-time curve. V_3 is only apparent once k_{31} becomes the rate limiting step for K_{10} , which is represented by the transition from the β to γ phase. Hendrix et al.[59] mostly captured the 2 compartment model composed of V_1 and V_2 , or α and β phases.

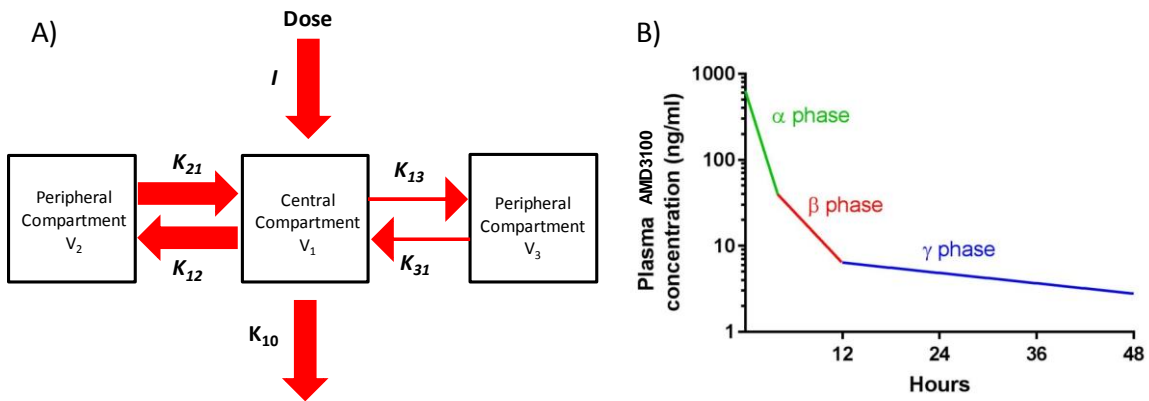


Figure 10 Proposed compartmental pharmacokinetic model. A) 3 compartment model, with a rapid equilibration between the central compartment and peripheral compartment V_2 , and slower equilibration with peripheral compartment V_3 . The thickness of the arrows represents the speed of the processes of distribution and elimination. B) Semi-logarithmic concentration-time plot of AMD3100 elimination following a single IV bolus dose.

In the context of intermittent doses of a drug, the terminal $T_{1/2}$ controls accumulation if more than 50% of drug is eliminated during the terminal phase [134]. This is not the case for AMD3100, and it is therefore not clinically relevant to the current approved use of AMD3100 as daily S/C injections with G-CSF for the mobilization of CD34+ cells. However, it is relevant to continuous IV infusions of AMD3100. Firstly, C_{ss} will only be achieved once all compartments are saturated (ie V1, V2 and V3). In the context of CAMPLEX, it was relevant because patients required cardiac telemetry until C_{ss} was achieved, and the protocol was amended to extend cardiac telemetry from 48hr to 72hr. Secondly, and more importantly, pharmacodynamically relevant concentrations of AMD3100 are present 1 week post infusion discontinuation, demonstrated by the persistence of WBC mobilization (Figure 5). This is consistent with Hendrix et al. [59] who reported a nearly 2 fold WBC mobilization with a C_{max} of around 100ng/ml. It is unknown how this might relate to potential anti-tumour activity.

The $T_{1/2}$ values in Tables 5 and 6 were calculated with the volume of distribution from Hendrix et al. [59], which would have captured mostly V1+V2 (Figure 10). This is also inadequate in that the same V_d was applied to every patient. However, the mean $T_{1/2}$ of 8.1hr (range 4.1 -11.7hr) obtained using this method is similar to that reported in the HIV study [58], namely 8.6hr (range 8.1-11.1). This is because a non-compartmental analysis was performed on a sampling schedule over a 24hr period after infusion discontinuation, and would be inadequate to capture a late terminal $T_{1/2}$.

Many drugs, particularly those used in the treatment of cancer, are dosed based on weight or, more commonly, by body surface area (BSA). The underlying assumption is that the CL of a drug is proportional to measures of body composition. Therefore, to achieve a target C_{ss} , which is only dependent on dose and CL, a drug is dosed based on weight or BSA. AMD3100 is currently dosed at 240 μ g/kg in clinical practice for the mobilization of CD34+ cells. In CAMPLEX however, we found no evidence of a correlation between CL and any

measure of body composition. Only renal function correlated with AMD3100 CL, as expected, albeit weakly ($R^2=0.33$). This raises the question whether AMD3100 could be considered for flat dosing in future clinical trials using a continuous IV infusion. Flat dosing would have the advantage of simplifying drug supply and preparation. However, additional patient data is required to develop a population pharmacokinetic model and confirm this finding.

WBC mobilization in the peripheral circulation is a robust pharmacodynamic readout of CXCR4 inhibition by AMD3100 in patients previously treated with chemotherapy. Most patients had sustained mobilization of all WBC subsets for the duration of the infusion and CD34⁺ counts showed the largest increases, over 10 fold in most patients. Due to the near maximal mobilization of WBC subsets by the lowest dose in this trial, pharmacodynamic modelling yielded poor estimates of the EC₅₀. Nonetheless, the EC₅₀ of WBC mobilization in this study (2.6 µg/kg/hr) is consistent with Hendrix et al. (11.6µg/kg/hr)[58]. However, WBC E_{max} is somewhat lower at 2.5 (2.1-3.2) vs 3.4 (2.9-3.9). Furthermore, the mean CD34⁺ count of 23 cells/µl is lower than the mean of 40 cells/µl achieved by a single AMD3100 dose of 240µg/kg in healthy volunteers[60]. The number of previous chemotherapy cycles is a known risk factor for poor mobilization of CD34⁺ cells to G-CSF[135]. Although we did not find a correlation between CD34⁺ mobilization and length of previous chemotherapy, this is a limited sample size and the exact number of cycles received was not captured. Therefore, the most likely explanation for the somewhat blunted WBC mobilization in this trial remains the extensive previous treatment with chemotherapy.

The relatively frequent blood sampling schedule may have contributed to a slight drop in haemoglobin while on the infusion. Every 100ml of phlebotomy is associated with a 7.0g/l decrease in haemoglobin [136] and patients had 239ml of whole blood taken over a 7 day period. Furthermore, hemoglobin concentrations recovered within 7 days of drug discontinuation, despite

detectable pharmacodynamic effect on WBC subsets mobilization. Lastly, anemia has not been previously reported in Hendrix et al.[58].

An important question facing the field of immunotherapy is how the host might influence response to immunotherapy [137]. A number of factors have been identified for further study, including the microbiome[138, 139] and stress hormones such as cortisol [140]. A peripheral absolute lymphocyte count (ALC) below the LLN was an exclusion criterion in this trial, which excluded 50% and 33% of otherwise eligible patients with PDAC and CRC, respectively. A low ALC is a common finding in patients with cancer and is often related to previous anti-cancer treatments [141–143]. A significant proportion of treatment naïve patient present with lymphopenia for unclear reasons [141, 144], including up to 40% of patients with PDAC[145–147]. Interestingly, in patients treated with ipilimumab, on treatment increase of ALC is associated with improved overall survival, but not baseline ALC [148–152]. Similarly, in patients treated with PD-1 inhibitor pembrolizumab, low baseline ALC is not associated with worse survival[153]. However, the high baseline *relative* lymphocyte count is associated with improved survival with pembrolizumab[153] and ipilimumab[152]. Other peripheral counts (such as relative eosinophil counts, absolute monocyte counts...) were also associated with outcomes but not necessarily common to these agents. These data are interesting, may be agent or class specific, and require further validation for use as stratification or inclusion criteria in immunotherapy trials.

In conclusion, the RP2D was identified as 80 µg/kg/hr. This dose was overall well tolerated, could be readily combined with checkpoint inhibitors and achieved relevant plasma concentrations at steady state. The pharmacokinetic data is consistent with previous reports, although the potential identification of a longer terminal $T_{1/2}$ requires additional data from the dose expansion cohort to confidently describe this. This is not clinically relevant to the current approved use of AMD3100 as daily S/C injections for CD34⁺ cell mobilization. However, it

does offer an explanation for the persistence of WBC mobilization and AEs after discontinuation of a prolonged continuous IV infusion. It is also unknown whether this could be relevant to anti-tumour activity. WBC subset mobilization, particularly CD34⁺ counts, is a robust pharmacodynamic readout of CXCR4 inhibition that could be further explored in later stage trials as a marker of successful drug delivery, and in correlations with anti-tumour effect. Finally, flat dosing of AMD3100 should be explored if AMD3100 is further developed as a continuous IV infusion in cancer.

7. CAMPLEX CLINICAL TRIAL: AMD3100 MAY INCREASE T CELL INFILTRATION AND TURNOVER IN A SUBSET OF PATIENTS

7.1. Clinical outcome endpoints (secondary and exploratory) following a 7 day AMD3100 continuous intravenous infusion

The secondary objective of CAMPLEX was to explore the objective clinical impact of a 7 day AMD3100 infusion. This was evaluated by CT scans at baseline and 14 days (+/- 2) after the infusion, ¹⁸FDG-PET/CT scans at baseline and within 1 day of infusion completion, tumour markers, and survival status.

16 patients were evaluable for tumour response by RECIST 1.1 [84]. Of these 12 patients (75%) achieved stable disease and 4 patients (25%) had progressive disease (PD) at assessment on day ~21. (Figure 1A). Patient 1006 was withdrawn on Day 1 due a new biliary obstruction, and did not receive any AMD3100 infusion.

Eleven patients were evaluable for metabolic tumour response by PERCIST 1.0 [85], in which the target lesion with the highest SUL_{peak} is compared between scans (Figure 1B). In this case, the biopsied lesion was excluded from analysis due to the uncertain effect of a biopsy on the metabolic uptake of a metastasis. Of patients with PD by RECIST 1.1, 1005 and 1015 also had evidence of progressive metabolic disease (PMD). Patient 1011 did not undergo ¹⁸FDG-PET/CT scan. The acquisition of PET data for 1003 did not meet PERCIST 1.0 technical specifications for direct comparison of metabolic uptake values. However, the clinical report showed progression on ¹⁸FDG-PET/CT with increase in the size of many lesions, including a liver metastasis (30 to 47mm, +56%). For patient 1002, similar technical issues precluded direct comparison, but the clinical report also showed progression of many lesions, including a pelvic mass (28 to 40 mm, +43%). On informal review of 1002 CT scans and RECIST

1.1 report, much of the non-target disease had increased in size, including the pelvic mass, but it is a matter of judgement whether this is unequivocal non-target PD. Interestingly, patient 1008 had a 22% decrease in SUL_{peak} (2.68 to 2.1), although not meeting the minimum requirements for a partial metabolic response (PMR) per PERCIST 1.0 (decrease by >30% and >0.8 SUL_{peak}). Furthermore, the target lesion was part of extensive omental caking, which can be difficult to accurately measure. An exploratory analysis of the SUL_{peak} on the biopsied metastasis or sum of up 5 target lesion SUL_{peak} did not suggest different outcomes.

Tumour marker changes were consistent with the radiologic assessments, generally increasing at Day 28 (Figure 1D). Patient 1007 (CRC) had an apparent 47% decrease in CEA by day 8. However, CEA was only 30 ng/ml on Day 1, despite fairly extensive liver and lung metastases. The CT scan at day 28 (RECIST 1.1) was stable and survival duration was 3.0 months. RECIST 1.1 assessment was SD at day 28. Patient 1001 did not have an elevated CEA at baseline.

7 patients (41%) had worsening ECOG performance status within 2 weeks of discontinuing the infusion (Figure 1C). Six of these patients had evidence of at least some tumour progression, including 2 with RECIST 1.1 PD. The median overall survival was 5.4 months (Figure 1E), and 4 patients received additional chemotherapy after CAMPLEX.

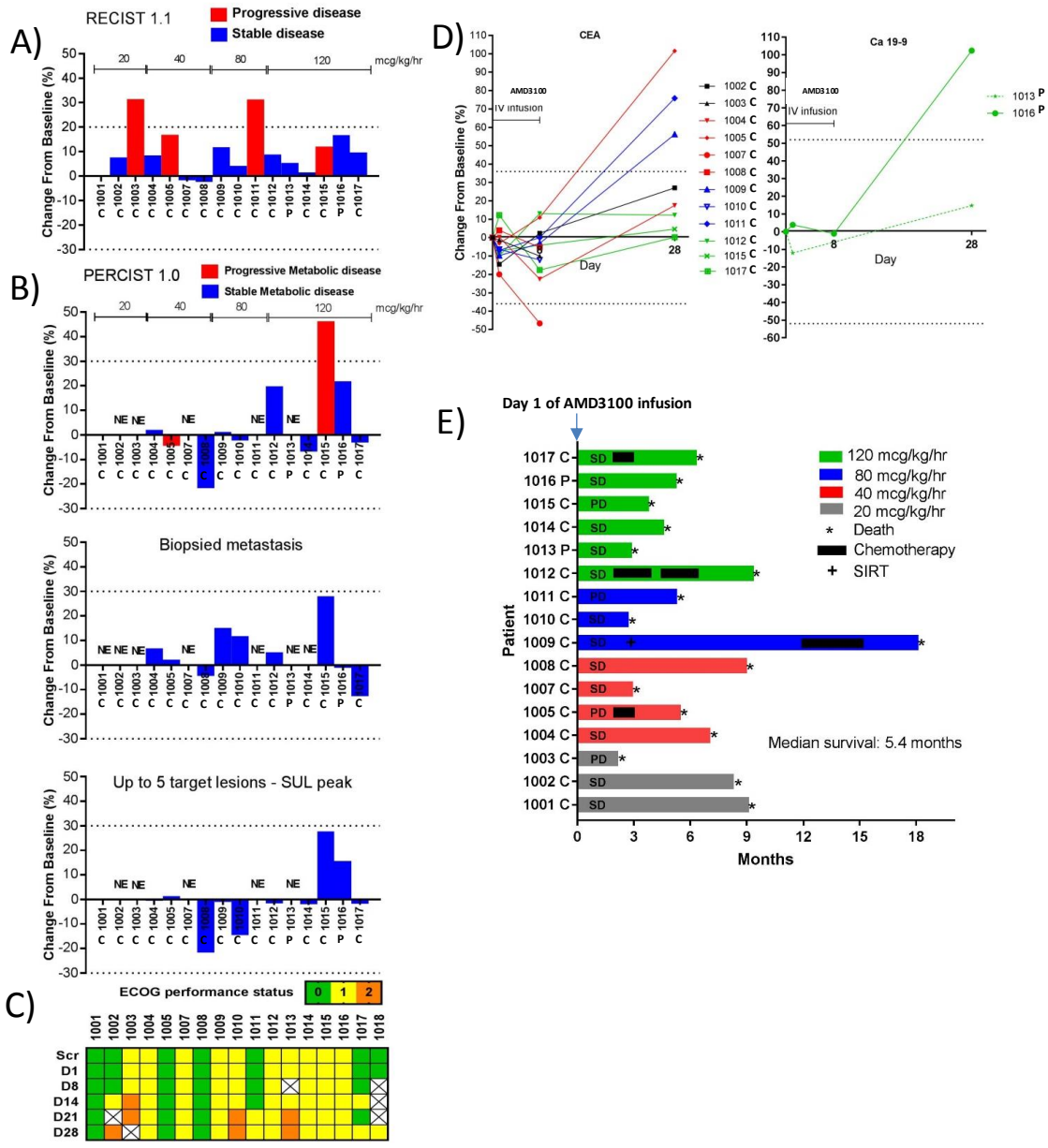


Figure 1 Clinical evaluation of perixafor anti-tumour activity in the dose escalation phase of CAMPLEX A) Tumour response by RECIST 1.1 assessment of CT scans performed at baseline and 14 days (+/- 2) after the infusion. B) Metabolic tumour response by ¹⁸F FDG-PET/CT scans performed at baseline and within 1 day of infusion completion. The first panel indicates assessment according to PERCIST 1.0, and the others are exploratory analyses: the % change in the SUL_{max} of the biopsied metastasis, and the % change in the sum of SUL_{peak} of up to 5 metastases. Patients 1007, 1011, 1013 did not have Day8 PET/CT scans. The acquisition of PET data for 1002 and 1003 did not meet PERCIST 1.0 technical specifications for direct comparison of metabolic uptake values. The biopsied metastasis of 1001 did not meet minimum SUL_{peak} value at baseline for comparison. C) The ECOG performance status of patients while on CAMPLEX. D) CEA and Ca 19-9 tumour marker changes on study. Dotted lines represent thresholds for significant changes in tumour marker levels. E) Swimmer plot with additional therapy received after CAMPLEX, and survival. Not evaluable (NE), Pancreatic adenocarcinoma (P), Colorectal adenocarcinoma (C), progressive disease (PD), stable disease (SD), selective internal radiation therapy (SIRT).

7.2. Paired biopsies for pharmacodynamic analysis from CAMPLEX dose escalation phase

The CAMPLEX protocol specified paired biopsies at baseline and within +/- 4hr of infusion completion on Day 8 of the same metastatic lesion. We successfully obtained baseline biopsies in 19 patients, of which 17 commenced the AMD3100 infusion (Figure 2). Day 8 biopsies were not obtained in 5 patients due to the following reasons: 3 patients were withdrawn before the end of the infusion, patient 1016 started therapeutic anticoagulation for an incidental pulmonary embolism found on screening CT, and patient 1009 poorly tolerated the baseline biopsy. Upon review of H&E from the 12 paired biopsies, no cancer could be identified in either biopsy in patient 1001, while the day 8 biopsy from patient 1005 contained focal nodular hyperplasia and no cancer. Therefore, 10 pairs of biopsies are analysable for pharmacodynamic readout, all from patients with CRC. However, many contained extensive necrosis, a characteristic feature of CRC, with limited viable cancer in some biopsies. Lastly, patient 1008 had a mucinous adenocarcinoma, with extensive mucin and little interspersed cancer cells.

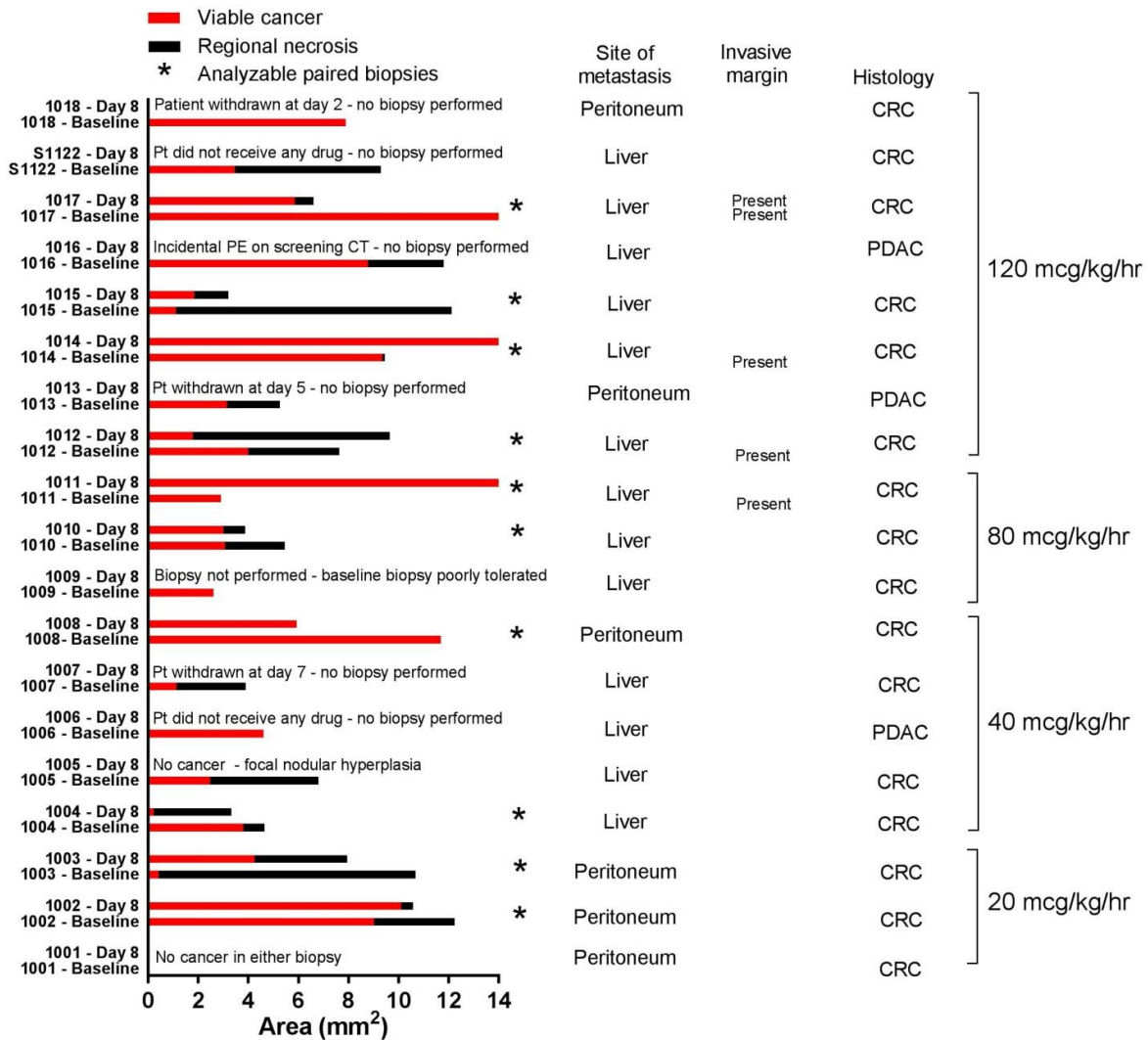


Figure 2 Summary of biopsies from CAMPLEX dose escalation phase

7.3. CXCR4 expression in tumour is a pharmacodynamic effect of AMD3100

To determine whether tissue CXCR4 expression changed after AMD3100 administration in human tumours, the same anti-CXCR4 antibody (UMB2 clone) as used on murine tissue was validated on human tonsil tissue. Strong and weak membranous staining pattern was observed in a proportion of larger activated germinal centre cells of tonsil tissue, probably representing centroblasts and

centrocytes (B cells) within the dark zone (DZ) and light zone (LZ), respectively (Figure 3). Many smaller lymphoid cells within germinal centres, the mantle zone and T-cell zone displayed perinuclear-dot staining (possibly the Golgi apparatus) without associated membranous staining. These cells would be expected to have membrane CXCR4 expression, but this may be below the detection threshold of CXCR4 IHC. The staining pattern on human tissue is similar to that observed in mouse tissue (see Chapter 5), and consistent with mouse data showing that centroblasts undergo CXCR4 dependent chemotaxis to the dark zone in response to CXCL12 producing reticular cells in the DZ [95]. A similar staining pattern was also reported by others on human tonsil tissue [102]. Therefore, these results validate the anti-CXCR4 antibody (UMB2) for IHC use on human tissue. For the purpose of image analysis, only membranous CXCR4 staining defined a CXCR4+ cell.

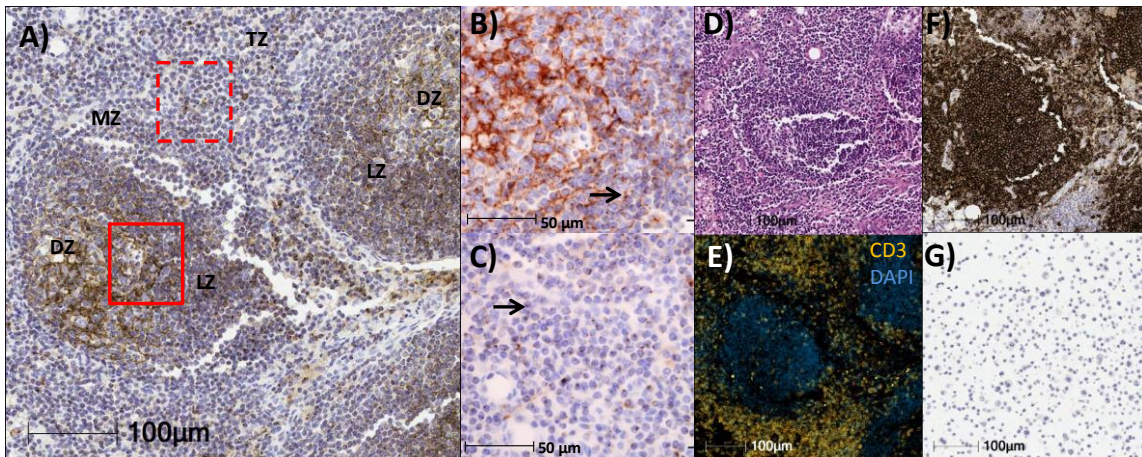


Figure 3 CXCR4 expression in a human tonsil tissue. **A)** A proportion of larger activated germinal centre cells display strong and weak CXCR4 membranous staining probably representing centroblasts and centrocytes within the dark zone (DZ) and light zone (LZ), respectively. **B)** Higher magnification of the solid red box in A) also demonstrates the presence of a perinuclear dot-like CXCR4 staining (arrow), possibly the Golgi apparatus, in the smaller lymphoid cells. **C)** Higher magnification of the dotted red box overlapping the mantle zone (MZ) and T-cell zone (TZ) in A) shows only perinuclear-dot CXCR4 staining (arrow). **D), E), and F)** are H&E, CD3 IF (T cell marker) and CD20 IHC (B cell marker) on serial sections of the lymphoid follicle in A), respectively. **G)** CXCR4 IHC on a FFPE cell block of the AsPC-1 cell line negative for CXCR4 expression by RNAseq.

CXCR4 protein expression was examined by IHC in tumour biopsies from CAMPLEX. The %CXCR4+ cells increased in all day 8 biopsies compared to baseline ($p < 0.0001$) by a median fold of 5.7 (range 2.9-106.8) (Figure 4). There

was no correlation between the fold change and dose cohort ($r=-0.23$, $p=0.51$), plasma AMD3100 concentration at day 8 ($r=-0.25$, $p=0.51$), or actual dose received ($r=-0.30$, $p=0.40$). Pathologist review suggested that, at baseline, most of the CXCR4+ cells are endothelial cells. Areas with high infiltration with CD3+ cells showed no membranous CXCR4 staining, but a faint perinuclear dot-like CXCR4 staining could be discerned. In day 8 biopsies, strong membranous CXCR4+ staining was apparent in regions with high CD3+ infiltration. In the opinion of the pathologist, the membranous staining CXCR4+ cells are a mixture of immune cells, possibly B cells, macrophages, and T cells. Cancer cells are CXCR4 negative in all samples.

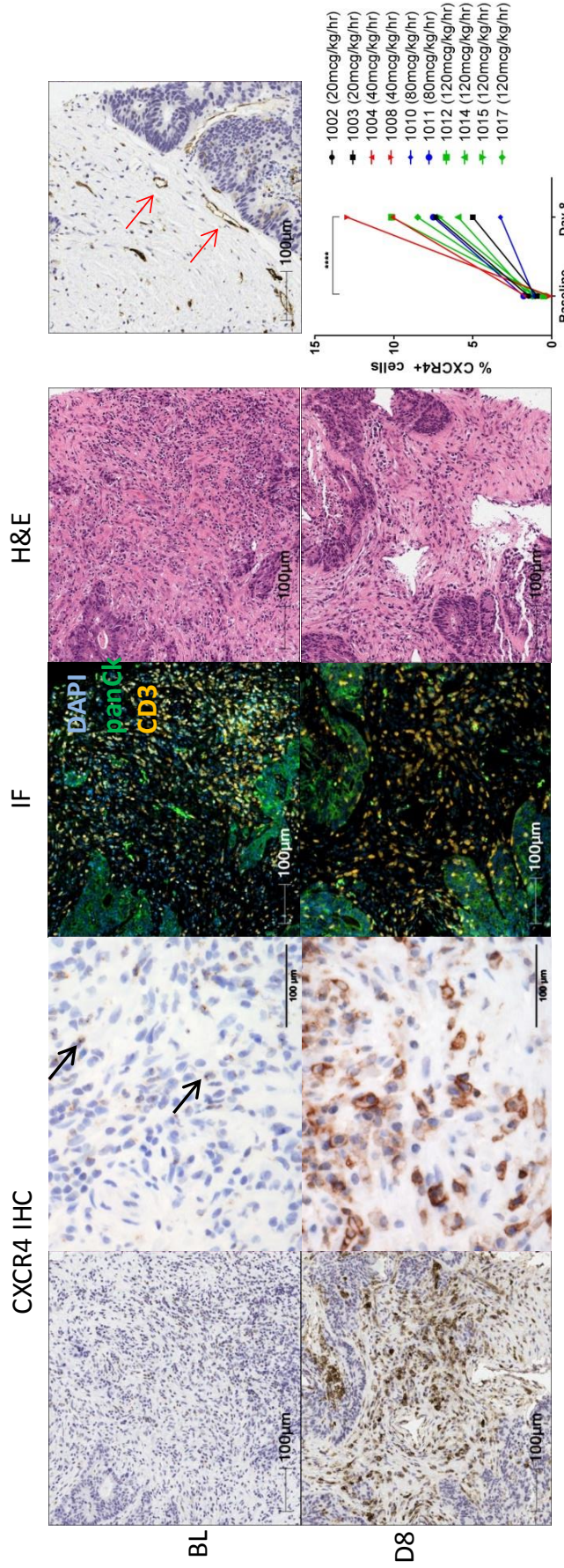


Figure 4 Plerixafor increases CXCR4 expression in the tumour Serial sections of baseline and day 8 tumour biopsies were stained for CXCR4 protein by IHC, CD3 cells by immunofluorescence (IF), and H&E. Representative images from patient 1002 are shown. CXCR4+ cells on baseline (BL) biopsy are predominantly endothelial cells (red arrows), although faint perineurial dot-like CXCR4 staining (black arrows) can be observed in areas with high CD3+ cell infiltration. In day 8 (D8) biopsies, CXCR4+ cells appear to be a mixture of immune cells, such as B cells, macrophages, and T cells. Cancer cells are CXCR4 negative in all samples. CXCR4 + cells were quantified across whole tumour sections (excluding areas of necrosis) using Halo image software. Only membranous CXCR4 staining defined a CXCR4+ cell. Stats: paired T-Test, **** $p < 0.0001$

7.4. AMD3100 increased TILs in a subset of patients and a change in T cell repertoire

7.4.1. Image analysis algorithm validation and immunofluorescence variability

TILs were quantified using two triple-IF panels, containing antibodies against panCK, CXCL12 and either CD3 or CD8, on whole tumour sections. As discussed in Chapter 3, the calibration of algorithms proved challenging due to significant variation in IF signal intensity between slides. An algorithm was designed for each slide, and the correlations between manual counts and algorithm counts of objects of interest in small areas of each slide are summarized in Figure 5A.

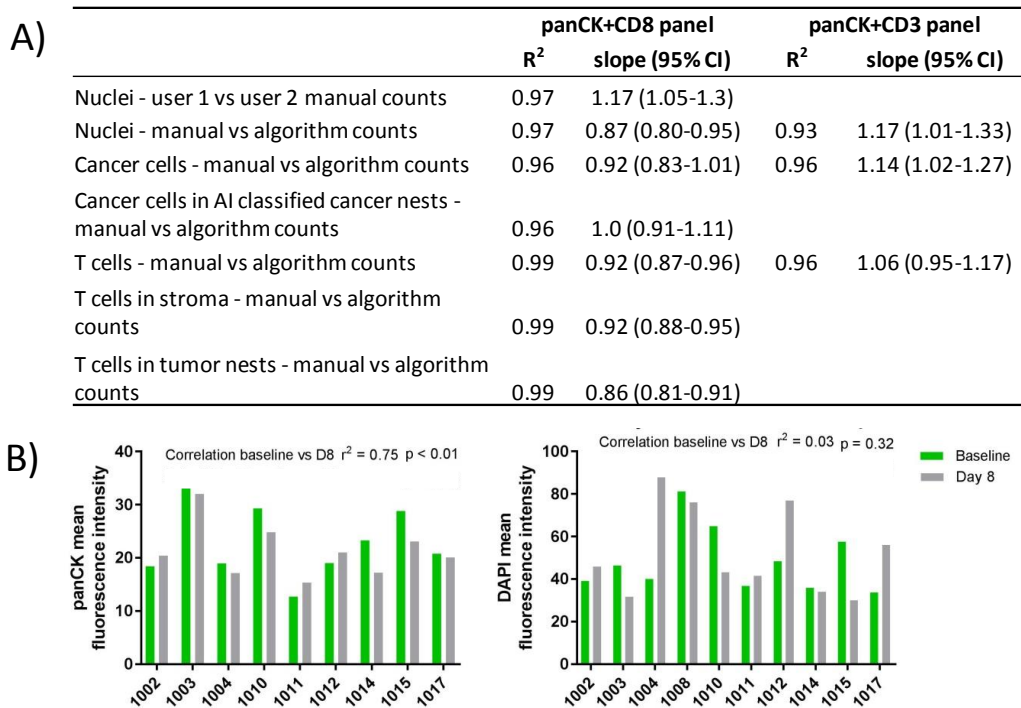


Figure 5 Immunofluorescence algorithm validation and variability **A)** Image analysis algorithms for each slide and immunofluorescence panel were validated with manual counts on small areas identified to contain at least 50-100 objects of interest, from every biopsy. **B)** The mean fluorescence intensity of the pan-cytokeratin stain (panCK) in cancer cell objects and DAPI of nuclei objects was compared in panel panCK+CD3. All slides stained with a given panel were scanned in a single batch with the same microscope settings. Stats: paired t-test, Pearson correlation. Artificial Intelligence (AI) random forest algorithm.

The two IF panels were scanned at different microscope settings, precluding direct comparison of serial sections. Nonetheless, the mean fluorescence intensity correlation between serial sections was strong for panCK ($r^2=0.73$, $p<0.0001$), and only moderate for DAPI ($r^2=0.37$, $p=0.004$). However, all slides for a given panel were stained and scanned using the same conditions. There was a strong correlation in panCK mean fluorescence of cancer cells between baseline and day 8 biopsies ($r^2=0.75$, $p<0.01$), but differences exist between patients (Figure 5B). This suggests intrinsic biological differences in cytokeratin expression between patient tumours that are maintained over time. On the other hand, there was no correlation for DAPI between baseline and day 8 ($r^2=0.03$, $p=0.32$). It is not possible to differentiate whether these differences are due to patient specific AMD3100 effects or variation in pre-analytic factors. The correlation of panCK fluorescence intensity between baseline and day 8 would suggest the latter, but somehow specific to DAPI. The image analysis algorithms were not able to overcome this variability in panCK and DAPI mean fluorescence intensity and therefore required individualization. This illustrates one of the difficulties in scaling IF image analysis.

7.4.2. AMD3100 increased TILs in a subset of patients

TIL analysis is primarily descriptive because there are no known criteria to define a biologically significant change in TILs, or a clinical correlate. Patients 1003, 1004, 1008, 1011, 1012, 1014, 1015, and 1017 demonstrated an increase in either CD3+ (8/11 patients, 73%) or CD8+ density (6/11 patients, 55%) quantified across whole tumour sections (Figure 6A). Unlike CXCR4 protein expression, there was no systematic pharmacodynamic effect of AMD3100 on CD3+ and CD8+ cell infiltration (Wilcoxon matched-pairs signed rank test, $p=0.23$ and $p=0.65$, respectively).

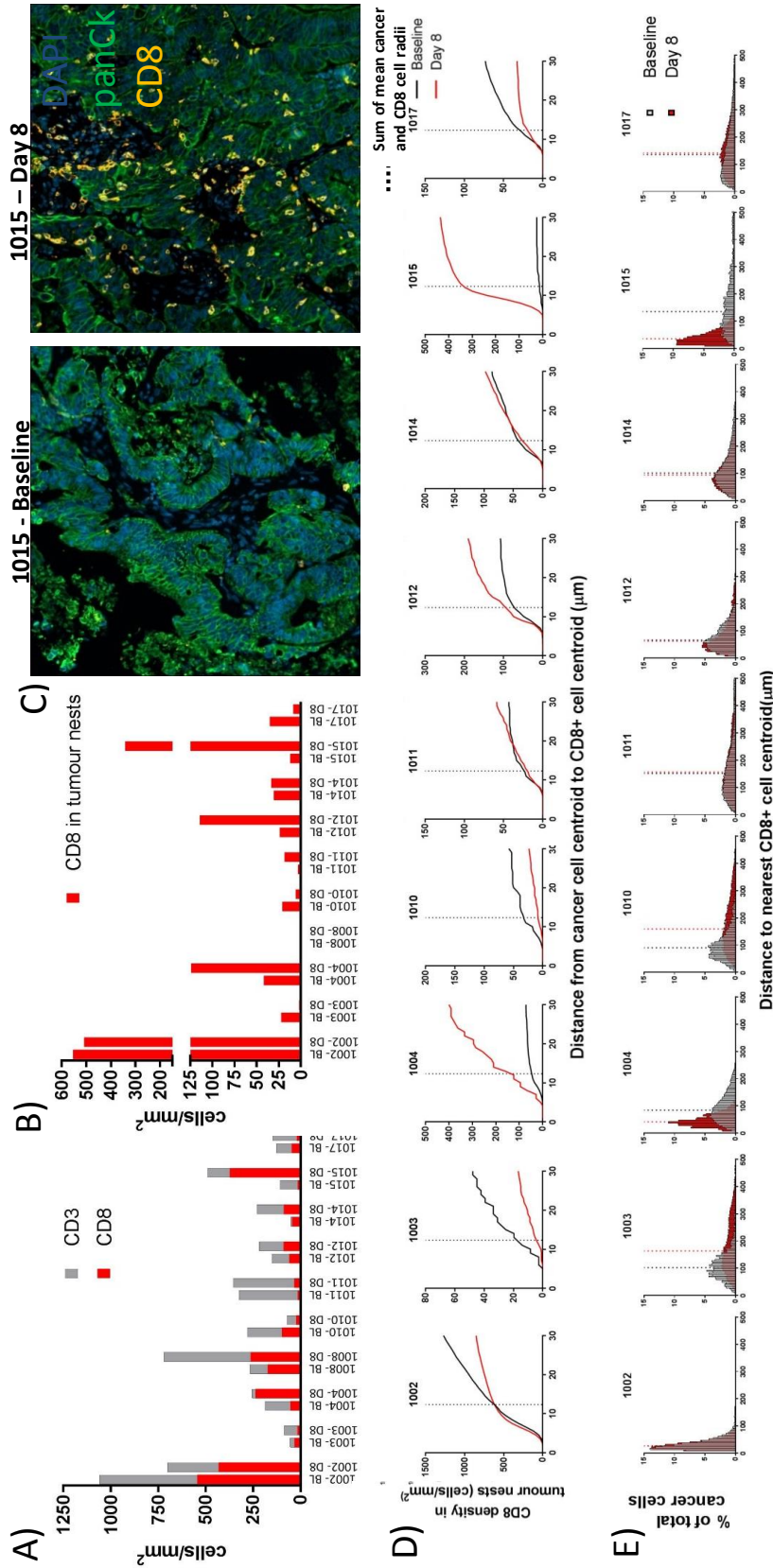


Figure 6 Plerixafor may increase tumour infiltrating lymphocytes in a subset of patients **A**) Density of CD3+ and CD8+ cells across whole tumour biopsy sections at baseline (BL) and after a 7 day plerixafor infusion (D8). The density values are displayed superimposed. **B**) Density of CD8+ cells within tumour nests. A CD8+ cell was classified as being within a tumour nest if at least touching a tumour nest. Tumours nests were identified using a machine learning algorithm in Halo image analysis software (see Chapter 2, Figure 6). **C**) Immunofluorescence image of areas with subjectively highest CD8+ cell density at baseline and Day 8 in patient 1015. For **D**) and **E**), individual cancer cells were identified on the basis of panCK staining around a nucleus defined by DAPI staining. The distance between a cancer cell centroid and the nearest CD8+ cell centroid was determined. **D**) The cumulative CD8+ cell count by distance from cancer cells was divided by the tumour nest area determined by the machine learning algorithm (Figure 6D). The dotted line represents the sum of the mean cancer and CD8+ cell radii. **E**) The percentage of cancer cells at a given distance from the nearest CD8+ cell was determined. The dotted line is the median distance.

In a compartmental tumour analysis, tumours nests were identified using a machine learning algorithm in Halo image analysis software (see Chapter 3, Figure 6). A CD8+ cell was classified as being within a tumour nest if at least touching a tumour nest. In patients where an increase in either CD3+ or CD8+ density had been identified across whole tumour sections, 1004, 1012 and 1015 (3/10 patients, 30%) (Figure 6B/C) had an increase in CD8+ density within tumour nests, but no appreciable increase was identified in patients 1011 and 1014. However, there was no systematic pharmacodynamic effect of AMD3100 on CD8+ cell infiltration in tumour nests (Wilcoxon matched-pairs signed rank test, $p=0.46$). The biopsy from 1008 was not amenable to a compartmental analysis because of very sparse cancer cells and extensive mucin (Figure 7).

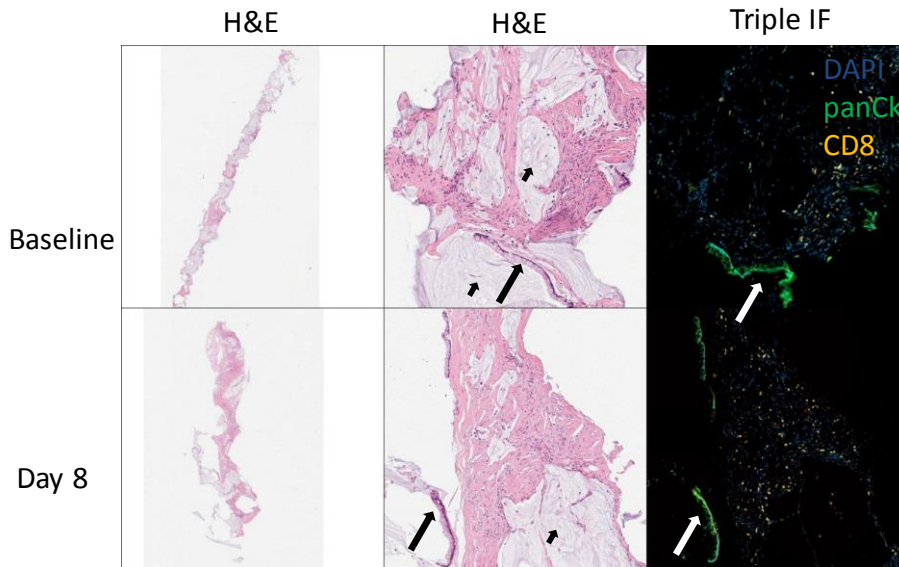


Figure 7 Biopsies from patient 1008 are not amenable to a compartmental analysis of tumour infiltrating lymphocytes. Patient 1008 had a mucinous adenocarcinoma of the colon, with abundant mucin (short arrows), limited cancer cells nests with distorted architecture (long arrows).

In a sensitivity analysis, individual cancer cells were identified on the basis of panCK staining around a nucleus defined by DAPI staining. The distance between a cancer cell centroid and the nearest CD8+ cell centroid was determined. These data were analysed in two ways.

Firstly, the cumulative CD8+ cell count by distance from cancer cells was divided by the tumour nest area determined by the machine learning algorithm (Figure 6D). The dotted line represents the sum of the mean cancer and CD8+ cell radii. The intersection of the dotted line with the solid lines should approximate the CD8+ density in tumour nests determined using the machine learning algorithm. Indeed, the data from Figure 6B and D are consistent. Again, patients 1011 and 1014 had no increase of CD8+ cells within tumour nests, suggesting that the increase in CD8+ cells observed in Figure 6A are located in the stroma, away from cancer cell nests.

Secondly, the percentage of cancer cells at a given distance from the nearest CD8+ cell was determined (Figure 6E). A peak at a smaller distance illustrates that a larger proportion of cancer cells have a CD8+ cell in close proximity. Significant new peaks were observed in patients 1004 and 1015, and a possible change in patient 1012. Patient 1002 had a heavily infiltrated tumour at baseline and the pattern did not change on day 8

The compartmental analysis addresses the hypothesis that the biologically relevant CD8+ cells are in close proximity to cancer cells. However, there was a strong correlation between the density of CD8+ in tumour nests and across the whole tumour sections ($r^2=0.95$, $p<0.0001$).

7.4.3. AMD3100 may induce significant T cell turnover in the tumour

To investigate the changes in T cell infiltration further, next generation sequencing of the T-cell receptor β -chain complementarity determining regions (CDR3s) (TCRseq) was performed (Adaptive Biotechnologies) on the snap frozen biopsies. There was poor correlation between the T cell fraction determined by IF (CD3+ cells/all cells in whole tumour sections) and TCRseq ($r^2=0.24$, $p=0.04$), but consistent with a recent report in primary PDAC that found a correlation between T cell fraction and CD8+ infiltration ($r^2=0.28$, $p=0.03$), but not CD4+ infiltration [154]. There was, however, significant discrepancy in the

direction of change of the T cell fraction between baseline and day 8 in some patients, most notably for patients 1002, 1008, and 1012 (Figure 8A and Figure 6A). The TCRseq analysis suggested that patients 1002, 1004, 1014, and 1015 had increases in T cell fraction on Day 8 compared to baseline, but there was no consistent pharmacodynamic effect across the population (paired t-test, $p=0.67$).

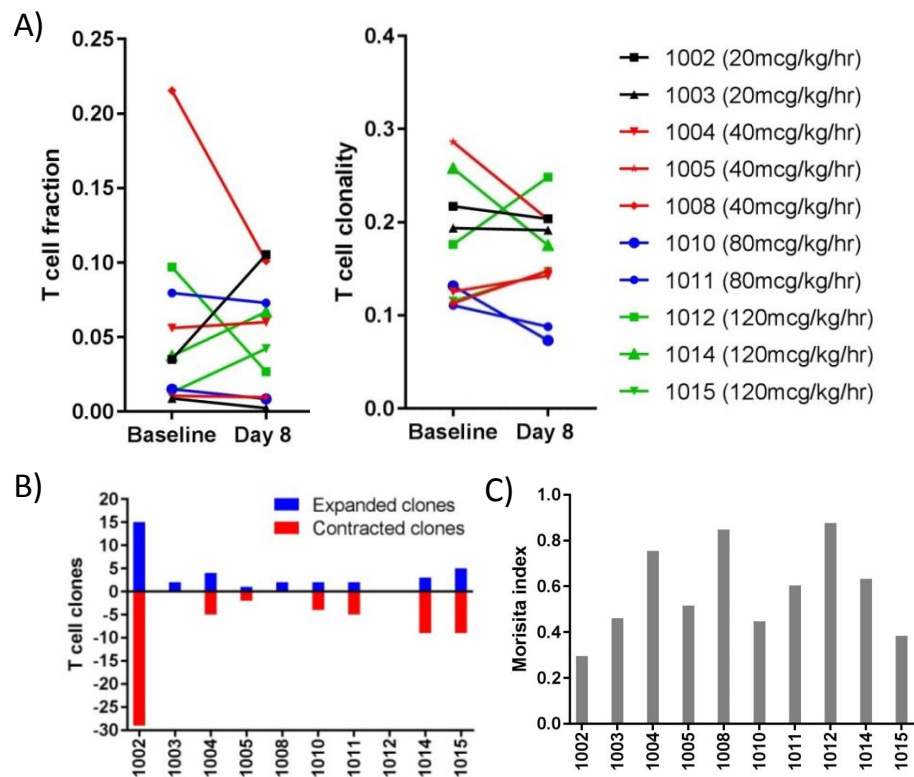


Figure 8 Deep-sequencing of the T-cell receptor β -chain complementarity determining regions **A)** T cell fraction of all nucleated cells and T cell clonality in snap frozen biopsies at baseline and Day 8 from the CAMPLEX dose escalation phase. **B)** Expanded and contracted T cell clones. **C)** The Morisita Index (MI) compares TCR rearrangements and template counts between baseline and day 8 biopsies. A lower MI value indicates a higher repertoire turnover.

TCR clonality (0 to 1) is a measure of population skewing, where high clonality indicates biased expansion of individual T cell clones and implies the presence of a specific immune response to tumour antigens. In patients with melanoma treated with anti-PD-1, high TCR clonality in baseline biopsies is associated with clinical responses [79]. Unlike CXCR4 protein expression, there was no consistent change in clonality on day 8 biopsies (Figure 8B, paired t-test $p=0.53$). There was no correlation between clonality and T cell fraction determined by TCRseq at either baseline ($p=0.31$) or day 8 ($p=0.88$). However,

patients 1004, 1008, 1012 and 1015 had increases in clonality at Day 8, all of whom had clear increases in CD3 or CD8 cell density by IF (Figure 6A). There was no systematic expansion or contraction of T cell clones (Figure 8B, paired t-test $p=0.10$).

The Morisita Index (MI) compares TCR rearrangement and template counts between 2 samples, where a value of 1 indicates that the same T cell clones are present at the same proportions in the 2 samples. In CAMPLEX, the MI ranged from 0.30 to 0.89 (mean = 0.58), suggesting a high TCR repertoire turnover (Figure 8C). Patients 1004, 1008, 1012, and 1014 had the highest MI.

To explore possible explanations for the variability in T cell count estimates between TCRseq and IF, the heterogeneity of TIL spatial distribution was assessed. TCRseq was performed on flash frozen biopsies, whereas IF analysis on FFPE biopsies (Figure 9A). Importantly, the former were quartered and DNA extracted from only 1 fragment for analysis, whereas IF analysis was performed on a longitudinal section of an FFPE biopsy (excluding tissue within 500 μ m of the invasive margin, when present). Patients 1002 and 1008 were significantly discrepant in changes between baseline and day 8 of CD3 density by IF and T cell fraction by TCRseq (Figures 6A and 8A). CD3 infiltration was highly heterogeneous by IF, appearing gradient-like in 1002 baseline, and patchy in 1008 baseline (Figure 9B). It is unknown if such heterogeneity would be maintained across the smaller “y” axis. If it did, however, it is conceivable how a single small fragment may not be representative of the entire biopsy, and therefore an important source of variability.

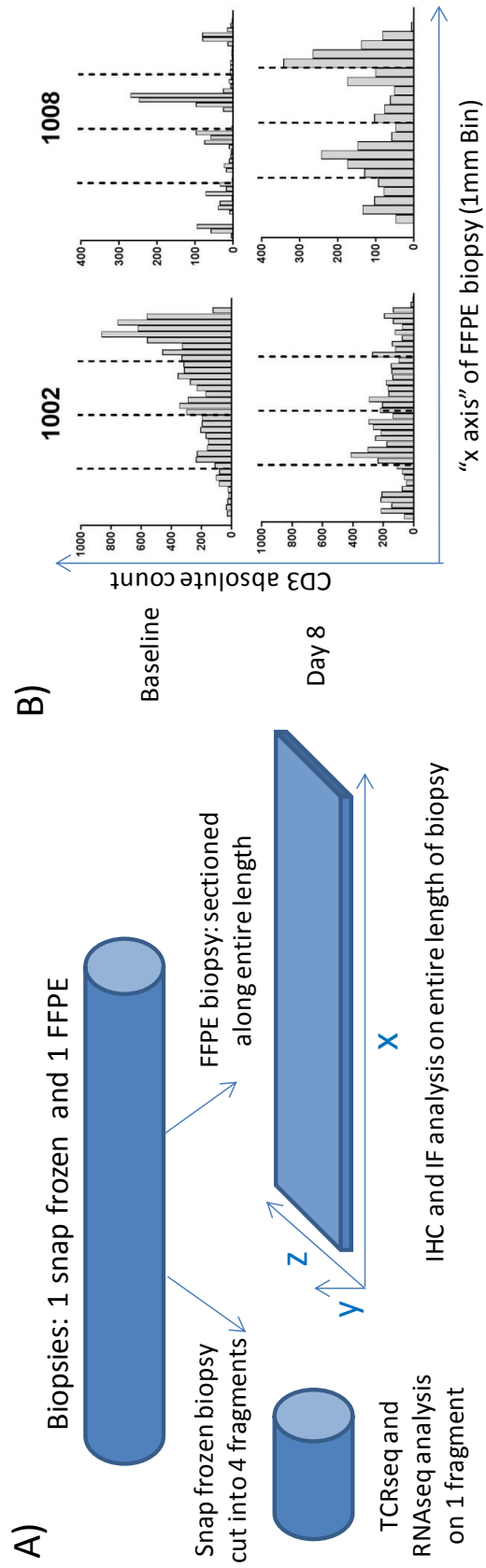


Figure 9 Sources of variability between TCRseq and Immunofluorescence analyses A) 2 biopsies were obtained from each patient at baseline and day 8, and processed by snap freezing and formalin fixation paraffin embedding (FFPE). The snap frozen biopsy was quartered and 1 fragment was submitted for TCRseq analysis. The FFPE biopsy was cut longitudinally, and analyzed by immunohistochemistry (IHC) and immunofluorescence (IF) staining . B) Absolute CD3 counts along the "x axis" of the FFPE biopsy from A) were binned into 1mm intervals. The dotted lines display hypothetical locations for quartering of biopsies. Patients 1002 and 1008 were very discrepant in changes between baseline and day 8 of CD3 density by IF and T cell fraction by TCRseq.

7.5. CXCL12 expression is variable between patients and does not correlate with the number of TILs

To investigate the relationship between intratumoural CXCL12 expression and the number of TILs, CXCL12 expression was assessed by IF staining of tumour sections. As previously reported [32], there was strong CXCL12 staining of cancer cells, defined as pan-CK positive, in a positive control primary PDAC. Furthermore, a number of panCK⁻CXCL12⁺ cells could be identified in the stroma surrounding cancer cell nests (Figure 10A). These panCK⁻CXCL12⁺ cells were not further defined but, based on published data [32], they may be FAP⁺ stromal cells and the source of the CXCL12 found on the cancer cells. A similar observation was made in baseline biopsies from patients on the CAMPLEX trial.

Cancer cells represented the largest proportion of all cells positive for CXCL12, except in patient 1008 (Figure 10B). The percentage of cancer cells positive for CXCL12 varied widely between patients (Figure 10C). However, there was strong correlation between baseline and Day 8 biopsies in the percentage of cancer cells positive for CXCL12 ($r^2=0.71$, $p<0.01$), and no significant change between the time points (paired t-test, $p=0.82$). This suggests intrinsic differences in CXCL12 expression between patient tumours are maintained over time, and despite AMD3100 administration. There was no correlation between CD8⁺ cell density and the percentage of cancer cells positive for CXCL12 (Figure 10D) in these patients.

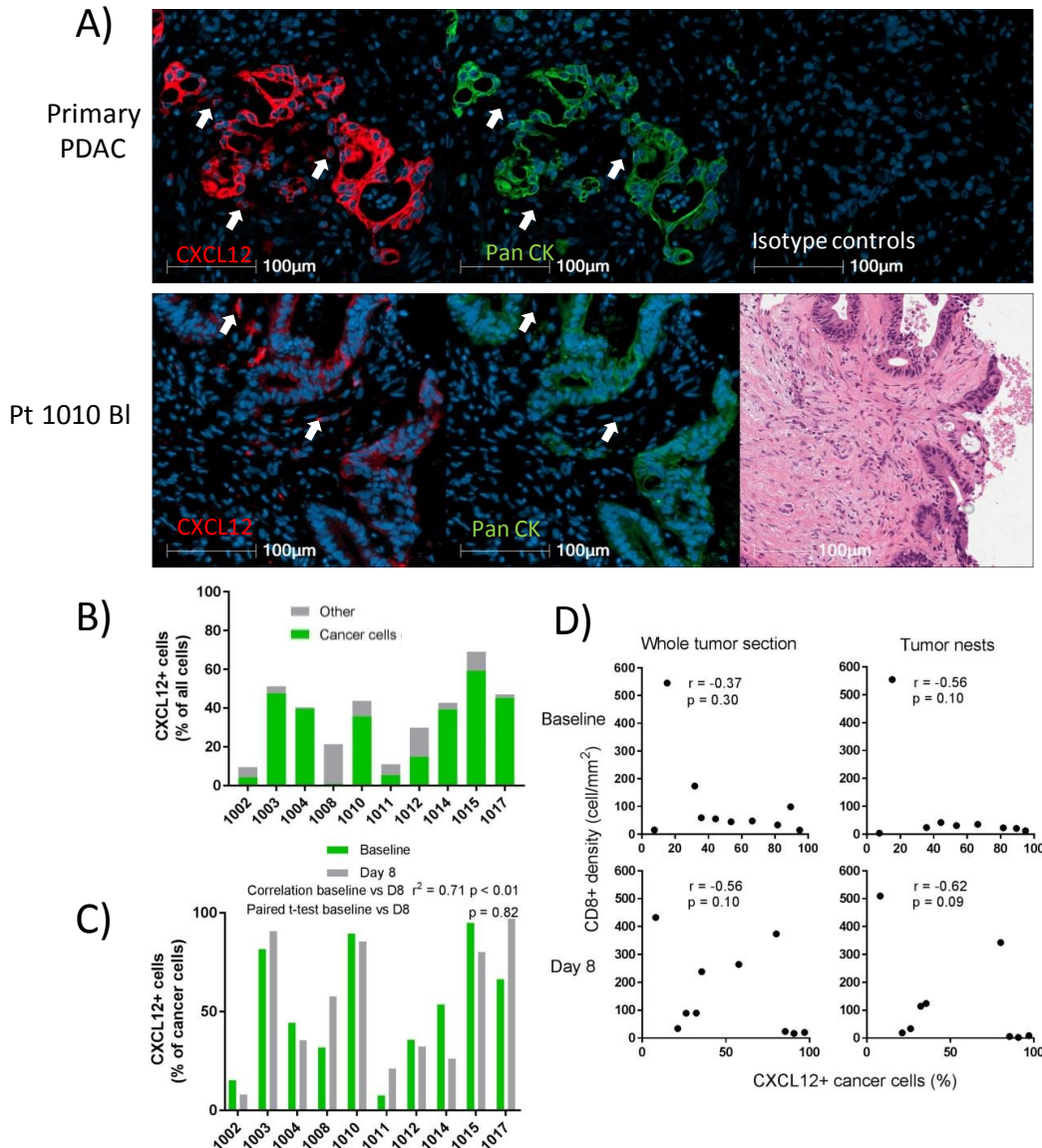


Figure 10 CXCL12 expression is variable between patients with CRC but does not correlate with TILs **A)** Dual CXCL12 and panCK immunofluorescent staining of a primary PDAC and baseline biopsy from patient 1010. White arrows indicate panCK⁻CXCL12⁺ cells, located in the stroma surrounding cancer cell nests. **B)** The percentage of CXCL12+ cancer cells (panCK⁺CXCL12⁺) and other CXCL12+ cells (panCK⁻CXCL12⁺) from all cells identified across whole tumour sections from biopsies at baseline was determined. The values are displayed stacked. **C)** The percentage of CXCL12+ cancer cells (panCK⁺CXCL12⁺/panCK⁺ cells) across whole tumour sections from biopsies at baseline and Day 8 was determined. **D)** The CD8+ cell density across whole tumour sections or within tumour nests was correlated with the percentage of CXCL12+ cancer cells at baseline and on day 8. Stats: paired t-test, Pearson correlation.

7.6.Changes in cancer and immune cell PD-L1 expression following AMD3100 infusion

To investigate for evidence of adaptive immune resistance to AMD3100 infusion, PD-L1 expression was assessed by IHC on baseline and day 8 biopsies. Quantification was performed by a pathologist (Figure 11A). Cancer cells were mostly negative for PD-L1 expression at baseline, even in patient 1002 who had significant baseline CD8 cell infiltration (Figure 6). The low expression of PD-L1 in CRC metastases is consistent with the literature [155]. In patients with clear increases in either CD3+ or CD8+ density on day 8 (1004, 1008, 1012, 1014, 1015), there were no clear increases in cancer cell PD-L1 expression at day 8.

PD-L1 expression on immune cells has been proposed as a biomarker for response to the anti-PD-L1 agent atezolizumab [156]. In addition to marked CD8+ infiltration at day 8, patient 1015 had an increase in PD-L1 expression in cells located in the stroma and consistent with immune cells (Figure 11A and B). Similar magnitude changes in immune cell PD-L1 expression, but in the opposite direction, were observed in patients 1002 and 1011.

A)

Dose cohort (mcg/kg/hr)	Patient ID	Baseline biopsy		Day 8 biopsy	
		% PD-L1+ tumour cells	% area with PD-L1+ immune cells	% PD-L1+ tumour cells	% area with PD-L1+ immune cells
20	1002	<1%	5%	<1%	<1%
	1003	0%	0%	0%	0%
40	1004	0%	0%	0%	0%
	1008	0%	<1%	0%	<1%
80	1010	0%	<1%	0%	0%
	1011	0%	5%	0%	<1%
120	1012	0%	<1%	<1%	0%
	1014	<1%	0%	0%	<1%
	1015	0%	0%	0%	1 to 5%
	1017	<1%	<1%	<1%	0%

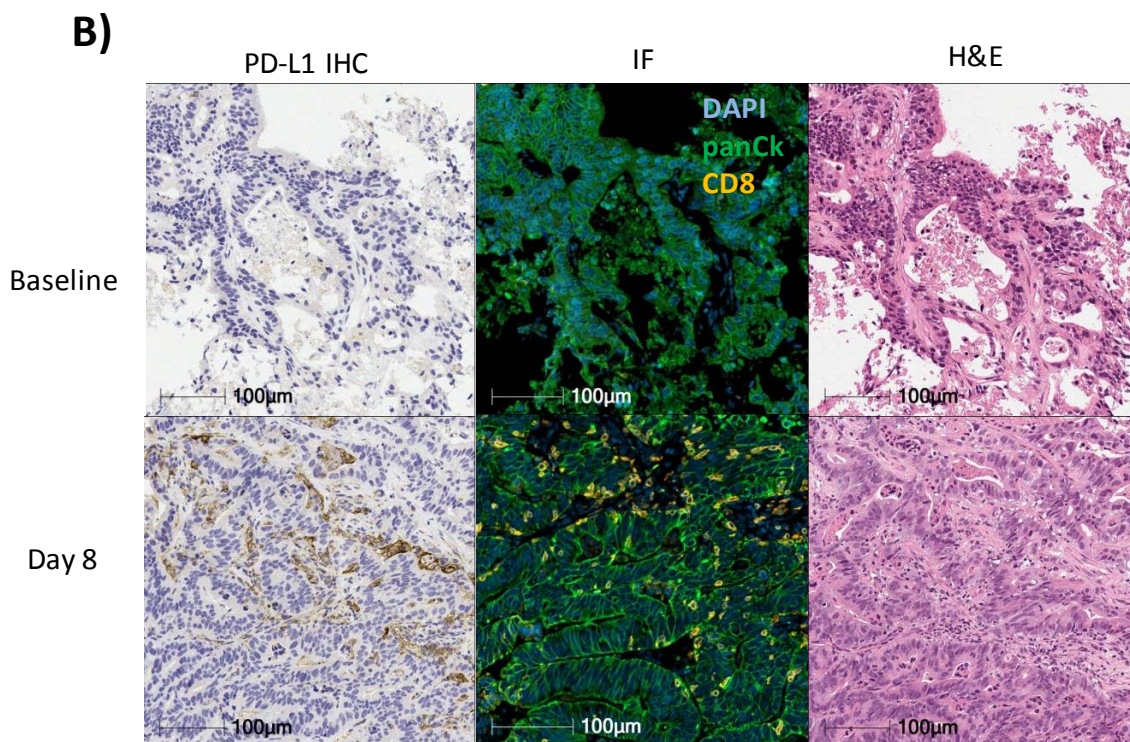


Figure 11 PD-L1 expression **A)** PD-L1 IHC of baseline and Day 8 biopsies from the dose escalation phase was quantified by a pathologist . **B)** Patient 1015 baseline and day 8 representative images of serial sections stained for PD-L1 by IHC, CD8+ infiltration by immunofluorescence (IF), and H&E.

7.7. Discussion

The CAMPLEX clinical trial was designed to assess the safety and tolerability of administering a 7 day IV infusion of AMD3100 to patients with advanced cancer. The short duration of the study was unlikely to reveal clinical anti-cancer activity and there was no definite evidence of anti-tumour activity by

traditional clinical assessment tools, such as tumour measurement by RECIST 1.1, metabolic assessment by ^{18}F FDG-PET/CT, and tumour markers. However, the paired biopsies before and after the infusion provide some evidence that AMD3100 may induce favourable immune-related changes in a subset of patients. In the absence of a systematic effect of AMD3100 on intra-tumoural pharmacodynamic markers assessed thus far (other than %CXCR4+ cells), assessing individual patients based on a combination of factors may provide insight on AMD3100 anti-tumour effects.

The “cancer immunogram” has been proposed as a tool to visualize the state of cancer-immune system interactions by evaluating biomarkers in seven parameters: absence of checkpoints (PD-L1), immune cell infiltration, general immune status (lymphocyte count), tumour foreignness (mutational load), tumour sensitivity to immune effectors (IFN- γ sensitivity, MHC expression), absence of inhibitory tumour metabolism (glucose utilization), and absence of soluble inhibitors (IL-6)[157]. The “cancer immunogram” is a theoretical framework to help understand the complexity of immune anti-tumour responses, and may help personalized immunotherapy. The current study has only assessed some of these markers, and it is thus beyond the scope of the current data to provide a complete “cancer immunogram” for each patient before and after the AMD3100 infusion. Furthermore, in the context of drug development, it may be important to also add radiological and clinical evaluations into the “cancer immunogram”. It is unclear, however, how best to integrate the various biomarkers into a comprehensive picture. Therefore, the effort to evaluate the effects of AMD3100 across a variety of modalities is mainly descriptive and exploratory. A summary of all radiological, tumour markers, histologic and TCRseq data is provided in Figure 12. Potentially favourable, unfavourable and indeterminate changes between baseline and post-infusion assessments are coloured green, red and yellow, respectively, and discussed below.

Dose (mcg/kg/hr)	Patient	Clinical		CT scan		¹⁸ F-DG-PET/CT scan			Histology					TCRseq			
		Survival (months)	ECOG worsening on study	RECIST % Change	PERCIST % Change	Biopsied to metastasis % SUL _{peak} change	Sum of up to 5 target lesions % SUL _{peak} change	Tumour marker (day 8) % Change	CXCR4 IHC Absolute %CXCR4+ cell increase (fold)	CD3+ density in entire biopsy cell/mm ² change (fold)	CD8+ density in entire biopsy cell/mm ² change (fold)	CD8+ density in tumour nests cell/mm ² change (fold)	% PD-L1+ tumour cells	% PD-L1+ immune cells	T cell fraction Absolute change (fold)	T cell clonality Absolute change (fold)	Morisa Index
20	1003	2.2	Yes	31.4	-2.32	11.81	-14.48	-10	4.1 (5.4)	33 (1.6)	-16 (0.5)	-20 (0.1)	0%	0%	-0.6 (0.3)	-0.002 (0.9)	0.46
80	1010	2.7	Yes	4.2				-12	2.1 (2.9)	-208 (0.3)	-75 (0.2)	-15 (0.3)	0%	0%	-0.7 (0.5)	-0.058 (0.6)	0.45
120	1013	2.9	Yes	5.4													
40	1007	3	No	-1.8				-47									
120	1015	3.8	No	12.1	46.31	28.11	27.76	-4	6.1 (7.0)	382 (4.5)	359 (25.6)	330 (28.1)	0%	1 to 5%	2.9 (3.3)	0.032 (1.3)	0.38
120	1014	4.6	No	1.53	-6.83		-1.89		4.5 (4.2)	179 (4.4)	44 (2.0)	2.9 (1.1)	0%	<1%	2.9 (1.8)	-0.083 (0.7)	0.63
80	1011	5.3	Yes	31.3				0	5.7 (4.2)	31 (1.1)	19 (2.2)	15 (5.3)	0%	<1%	-0.7 (0.9)	-0.023 (0.8)	0.6
120	1016	5.3	No	16.7	21.91	0.14	15.65	-1									
40	1005	5.5	No	16.9	-4.35	2.22	1.39	11									
120	1017	6.3	Yes	9.7	-3.04	-12.7	-1.79	-18	7.4 (8.0)	20 (1.2)	-27 (0.4)	-26 (0.2)	<1%	0%			
40	1004	7	No	8.5	2.12	6.84	-0.5	-23	8.4 (6.1)	68 (1.4)	183 (4.3)	82.2 (3.0)	0%	0%	0.4 (1.1)	0.017 (1.1)	0.76
20	1002	8.3	Yes	7.6				2.4	5.9 (5.0)	-357 (0.7)	-113 (0.8)	-45 (0.9)	<1%	<1%	7.0 (3.0)	-0.014 (0.9)	0.3
40	1008	9	No	-2.4	-21.64	-4.35	-21.64	-5	12.8 (106.8)	453 (2.7)	91 (1.5)		0%	<1%	-11.4 (0.5)	0.035 (1.3)	0.85
20	1001	9.1	No	0	-0.28		-0.28										
120	1012	9.4	No	8.8	19.83	5.26	-1.59	13	9.6 (20.1)	66 (1.4)	30 (1.5)	90.4 (4.8)	<1%	0%	-7.0 (0.3)	0.072 (1.4)	0.88
80	1009	18.1	No	11.8	1.23	15.15	-0.98	-3									

Figure 12 Heatmap summary of all radiological, tumour markers, histologic and TCRseq data. Potentially favourable, unfavourable and indeterminate changes between baseline and post-infusion assessments are coloured green, red and yellow, respectively. Patients are ordered according to survival length

Tumour measurements by RECIST 1.1 did not provide any convincing evidence of anti-tumour activity. However, response based assessments are typically performed after at least 8 weeks of anti-cancer therapy, or 2 cycles, and therefore it is difficult to contextualize the RECIST 1.1 measurements in this trial. Furthermore, unusual patterns of tumour response have been observed with immunotherapy treatment. Pseudoprogression describes a clinical scenario where progressive disease is declared based on RECIST 1.1 (new target lesions, unequivocal progression of non-target lesions, or increase in the sum of measures of target lesions), but continued follow-up demonstrates stabilization or regression of these same lesions. Pseudoprogression is typically seen in a patient that is clinically stable or improved, and occurs in less than 5% of patients treated with anti-PD-(L)1 agents [98, 99]. 2 of 4 patients (1005 and 1015) with RECIST 1.1 PD did not have worsening of ECOG performance status or new cancer related symptoms, but no further imaging was obtained. Tumour measurement with the modified RECIST 1.1 for immune-based therapeutics, termed iRECIST[158], may help identify pseudoprogression in patients administered AMD3100. iRECIST requires a second imaging study between 4 and 8 weeks after first evidence of PD to confirm PD.

Conversely, the phenomenon of hyperprogression refers to the observation that some patients experience apparent rapid disease acceleration within a few weeks of initiating anti-PD-1/L1 therapy [159–161]. 41% of patients in CAMPLEX had deterioration of ECOG performance status while on study, including 2 of 4 patients with RECIST 1.1 PD (1003 and 1011). Quantifying tumour growth kinetics prior to therapy initiation would be essential to detect growth acceleration on CAMPLEX, but previous CT scans were not collected as part of the protocol. The clinical deterioration of a substantial proportion of patients on CAMPLEX may simply be a reflection of the natural history of this patient population. Indeed, the median OS was 5.4 months and is consistent with the placebo control group (median OS 5.3 months) of the RECURSE study[9],

which tested TAS-102 in a population similar to CAMPLEX. For the purposes of Figure 12, favourable and unfavourable survival was dichotomized, according to the median, and ordered according to overall survival.

For the purposes of Figure 12 and RECIST 1.1, favourable and unfavourable changes are defined as decreases or increases in the sum of target lesions, respectively, regardless if assessments met standard RECIST 1.1 definitions for response, progression or stability of disease. To account for possible pseudoprogression, RECIST 1.1 increases in patients without a clinically significant increase in cancer related symptoms during the study, as defined by worsening ECOG performance status, were deemed indeterminate, and unfavourable if ECOG worsened.

The interpretation of the ^{18}F FDG-PET/CT data is challenging. There are only limited studies examining metabolic tumour response by ^{18}F FDG-PET/CT to immunotherapy, and none as early as 1 week. A case series of 10 melanoma patients treated with anti-PD-1 agents reported that all 3 patients with PMR at 2 weeks had a complete metabolic response (CMR) at 12 weeks by PERCIST [162]. On the other hand, of 17 melanoma patients treated with ipilimumab, 4 of 5 patients with clinical benefit (2 PR and 1 CR at ≥ 4 months by RECIST 1.1, and 1 SD for ≥ 6 months) had at least a 15.5% *increase* in SUL_{peak} by PERCIST at 21-28 days after therapy initiation. Importantly, these patients had SD by RECIST 1.1 at 21-28 days [163]. The other patient with CR at ≥ 4 months by RECIST 1.1 had PR and PMR at 21-28 days. In another study with 22 patients with melanoma treated with ipilimumab, the only 2 patients with PMR at the end of four cycles had PMD after 2 cycles[164]. Others have suggested that reactive lymph node uptake in the drainage basin of metastases and diffuse splenic uptake may be early markers of eventual response to anti-CTLA4 agents[165]. Therefore, depending on the class of IO agent, clinical benefit may be preferentially, but not exclusively, associated with either PMR or PMD on early ^{18}F FDG-PET/CT. Furthermore, determining the relevance of small changes in

SUL_{peak} is challenging because the test/re-test variability of ¹⁸F-DG-PET/CT ranges between 10 and 40%, which is why PERCIST 1.0 recommends a 30% change for significance, and up to 65% in some disease such as lymphoma [85]. Correlation with longer term clinical outcome is critical to determine what early ¹⁸F-DG-PET/CT pattern might be associated with clinical benefit with AMD3100.

For the purposes of Figure 12, favourable and unfavourable changes are defined as decreases or increases in SUL_{peak}, respectively, regardless if assessments met standard clinical definitions for response, progression or stability of disease. To account for possible favourable effects of PMD on early ¹⁸F-DG-PET/CT assessment, increases in patients without a clinically significant increase in cancer related symptoms during the study, as defined by worsening ECOG performance status, were deemed indeterminate, and unfavourable if ECOG worsened.

Consistent with the pre-clinical data (see Chapter 5), CXCR4 protein expression is an intra-tumoural pharmacodynamic readout of AMD3100 target engagement in humans. As discussed in detail in Chapter 5, the increase in %CXCR4+ cells within tumour likely mostly reflects changes in surface expression of CXCR4 receptor. In baseline biopsies, areas with high infiltration with CD3+ cells showed no membranous CXCR4 staining, but a faint perinuclear dot-like CXCR4 staining could be discerned (possibly the Golgi apparatus or an internal storage of CXCR4 protein). These cells would be expected to have membrane CXCR4 expression, but this may be below the detection threshold of CXCR4 IHC. In day 8 biopsies, strong membranous CXCR4+ staining was apparent in regions with high CD3+ infiltration. However, it remains possible that the increase in %CXCR4+ cells in all tissues reflects infiltration of a different immune cell population expressing high surface CXCR4 protein. For the purposes of Figure 12, all patients exhibited evidence of increased %CXCR4+ on day 8 biopsies and therefore all were deemed to have favourable changes.

The histologic TIL infiltration analysis is a key exploratory pharmacodynamic assessment in the CAMPLEX trial. The published pre-clinical data in the KPC model suggests large increases in CD3+ cell infiltration in tumour nests with AMD3100 treatment [32]. TILs have been extensively studied as a baseline predictive markers for response to anti-PD-(L)1 therapy, as well as an on-treatment pharmacodynamic effect associated with response [79, 166, 167]. On treatment biopsies, often performed more than 3 weeks after beginning therapy, show a several fold increase in CD3+ or CD8+ cell density is associated with clinical responses [166, 167]. However, there are no known criteria to define a biologically significant change or target TIL density, while also taking into consideration the sampling variability. Large absolute and fold increases in CD3+ and CD8+ cell densities are strongly suggestive of a favourable effect of AMD3100, and were observed in patients 1004, 1008, 1012 and 1015. However, the biological relevance of the following situations remains unclear: small absolute but large fold increases in CD8+ cell density in tumour nests (patient 1011); relatively large absolute/fold CD3+ cell density increases across an entire biopsy but small absolute/fold CD8+ cell density increase in tumour nests (patient 1014); increase in CD3+ density but decrease in CD8+ density (patients 1003, 1017); or relatively large absolute but small fold decreases in CD3+ and CD8+ densities in the context of heavy baseline TIL infiltration (patient 1002). For the exploratory purposes of Figure 12, any increase in CD3+ or CD8+ cell was deemed favourable.

The compartmental analysis of CD8+ density in tumour nests vs entire section attempts to address the hypothesis that the biologically relevant CD8+ cells are in close proximity to cancer cells. This type of analysis requires multiplexed immunohistochemistry or fluorescence to identify CD8+ cells and cancer cells, and complex and labour intensive image analysis. In this limited sample of 10 biopsies, there was a strong correlation between the density of CD8+ in tumour nests and across the whole tumour sections ($r^2=0.95$, $p<0.0001$). Furthermore, the direction of change in CD8+ density in tumour nests and across

whole tumour sections was concordant in all patients (Figure 12). This suggests that a simple CD8+ count without compartmental analysis is a good surrogate marker of CD8+ within tumour nests.

A recent paper by Riaz et al.[167] showed that previous therapy may influence the TIL pharmacodynamic readout. Melanoma patients treated with nivolumab that showed clinical responses had increased CD3+ cell infiltration and T cell clonality on treatment, but only in immunotherapy naïve patients. On the other hand, patients previously treated with ipilimumab that achieved a clinical response with nivolumab did not show increased CD3+ cell infiltration or clonality, but rather an increased richness of T cell clones (number of unique T cell clones). However, whether ipilimumab pre-treated or not, all patients showing clinical responses had increases in the RNA-based cytolytic score, indicative of T cell activation. The authors concluded that nivolumab therapy facilitates selective intra-tumoural expansion of tumour-reactive clones in immunotherapy naïve patient, whereas nivolumab relieves exhaustion of previously expanded T cells following ipilimumab. For CAMPLEX, therefore, it will be worthwhile to analyze samples for evidence of T cell activation and RNAseq analyses are ongoing.

The Riaz et al.[167] paper also highlighted the importance of a qualitative assessment of the T cell infiltrate by TCRseq. Increases in TCR clonality on treatment are associated with clinical responses in melanoma patient treated with nivolumab, but not in patients previously treated with anti-CTLA-4[167]. In patients with resected PDAC, a lower TCR clonality is associated with long term survival, although the overlap is marked[168]. Therefore, further research is needed to clarify how to interpret TCR clonality, and this will likely be context specific to disease and treatment. No patients in CAMPLEX were previously treated with ipilimumab or any other immunotherapeutic agent. For the purposes of Figure 12, an increase in TCR clonality was deemed favourable. All patients with large absolute and fold increases in CD3+ and CD8+ cell densities (patients 1004, 1008, 1012 and 1015) also had increases in TCR clonality.

The MI of TCR rearrangements suggested a high TCR repertoire turnover between baseline and day 8 biopsies in CAMPLEX. No control data are available from untreated, serially sampled tumours over a short period to contextualize this data. Unpublished data from Adaptive Biotechnologies suggests that the MI was above 0.8 across PBMC samples collected from 3 healthy volunteers over a year. However, a recent study by Reuben et al.[169] examining intra-tumoural heterogeneity in 11 resected primary non-small cell lung cancers found MI ranged between 0.48 and 0.98 in randomly sampled areas of a given tumour (mean =0.80, which was estimated from a graph). The range (0.30 to 0.89) and mean (0.58) in CAMPLEX appears lower. Based on the Reuben et al paper, a proportion of the MI is likely due to sampling variability. Any additional differences could be explained by either an AMD3100 effect or a natural turnover of T cells in tumour over time. However, the study by Reuben et al. [169] also found that patients without recurrences had a higher MI. For the purposes of Figure 12, a MI above the mean was deemed favourable. Patients 1004, 1008, and 1012 had the highest MI. The heterogeneity described by Reuben et al.[169] would also justify analysing the other fragments from the snap frozen biopsies and may help explain the discrepancy between T cell fractions estimated by TCRseq and IF (Figure 9).

The expression of PD-L1 by cancer cells can be constitutive or induced by IFN- γ as a mechanism to evade immune attack [170]. PD-L1 IHC was performed on CAMPLEX samples to evaluate for upregulation of PD-L1 as a surrogate marker for an immune response. Additionally, a higher expression of PD-L1 is associated with a higher likelihood of a clinical response to anti-PD-(L)1 therapy, although it is an imperfect marker [171]. Nonetheless, increased expression would further support a combination study of AMD3100 with an anti-PD-(L)1 agent. No CAMPLEX patients demonstrated significant upregulation of PD-L1 expression on cancer cells. PD-L1 expression on immune cells has also been proposed as a biomarker for response to the anti-PD-L1 agent atezolizumab

[156]. For the purposes of figure 12, PD-L1 expression of >1% on either cancer cells or immune cells was deemed favourable, while expression <1% indeterminate.

In summary, patient 1008 had the clearest evidence of favourable changes to AMD3100, with decreasing trends in tumour metabolic activity by ¹⁸F-DG-PET/CT, tumour size by CT, and a large absolute increase in TILs and T cell clonality. Patients 1004, 1012, 1014, and 1015 also showed quite consistent evidence of favourable changes to AMD3100 with relatively large increases in TILs, T cell clonality, but tumours progressed to varying extents by CT and ¹⁸F-DG-PET/CT (except 1014). An element of pseudoprogression cannot be ruled-out. Additionally, patient 1015 had an increase in PD-L1 expression on immune cells, suggesting possible new sensitivity to anti-PD-(L)1 agents [156]. Patient 1007 showed a 47% decrease in CEA tumour marker but was withdrawn at day 7 due to a new biliary obstruction related to porta hepatis bulky lymphadenopathy. Repeat biopsy was not obtained. It is possible that the slight increase in lymphadenopathy to cause the biliary obstruction was in fact reactive, akin to what had been described with ipilimumab [165]. Patients 1001 and 1005 are difficult to evaluate without analyses of biopsies. All other patients had clinical deterioration during the study (1002, 1003, 1010, 1011, 1013, 1017), but this may not be inconsistent with potentially favourable changes on histology. However, the favourable changes in TILs were overall modest, and all showed decreases in T cell clonality. There was no clear correlation between individual patient survival and any of the variables noted in Figure 12.

8. CONCLUSION

The conclusions from Chapter 5, 6 and 7 will now be discussed to identify the future directions for research on the role of AMD3100 in immunotherapy. Chapters 5 evaluated the pharmacodynamic effects of AMD3100 in the KPC mouse model of PDAC, Chapter 6 evaluated the safety and pharmacokinetics of AMD3100 administered to patients with CRC and PDAC in the CAMPLEX clinical trial, and Chapter 7 evaluated the pharmacodynamics of AMD3100 on the tumour microenvironment of these patients.

The dose of AMD3100 is an important consideration for future clinical studies. In Chapter 6, the RP2D was identified as 80 µg/kg/hr because it was overall well tolerated and achieved the target plasma concentrations at steady state of 2 µg/ml. However, there was a lack of dose response in any of the pharmacodynamic markers evaluated across all cohorts, including CD34+/WBC mobilization in the peripheral circulation and CXCR4+ protein expression in the tumour microenvironment. Patients with favourable immunological changes could be found in every dose cohort, except at the lowest dose of 20 µg/kg/hr (Chapter 7, Figure 12). Even in this cohort, CD34+/WBC mobilization and CXCR4 protein expression were near maximal. Furthermore, a higher dose of AMD3100 (200 µg/hr) in the KPC model (Chapter 5) did not improve anti-tumour activity compared to the 45 µg/hr dose that established the target plasma concentrations of 2 µg/ml in the Feig et al. paper [32]. Taken together, the pharmacodynamic data suggests that the 20 or 40 µg/kg/hr may be adequate for future clinical trials. These doses had very little drug related AEs and none of the patients administered the 20 µg/kg/hr dose developed diarrhea, which is a potential overlapping toxicity with PD-(L)1 agents. Finally, flat dosing of AMD3100 should be explored if AMD3100 is further developed as a continuous IV infusion in cancer.

The anti-tumour pharmacodynamic effects of AMD3100 remain to be better characterized and would help identify the mechanism of action.

The striking accumulation of F4/80+ cells in the KPC experiments (Chapter 5) warrants additional investigation to characterize the M1/M2 polarization of these cells. Macrophage depletion experiments may help determine if F4/80+ cell have any causal link to the anti-tumour effects of AMD3100. Additionally, the myeloid compartment remains to be investigated in the CAMPLEX samples. RNAseq analyses and additional histologic assessments are ongoing.

The increase in TILs observed in a subset of patients on the CAMPLEX trial is consistent with the pre-clinical data from the Feig et al.[32] paper. It is unclear why a similar increase in TILs was not observed in the KPC experiments in Chapter 5. As discussed, the quantification methodology may have been insensitive, and a quantification of TILs within tumour nests may be required. However, in the CAMPLEX trial, there was a strong correlation between CD8+ cell quantification across whole tumour sections and within tumour nests. Additional detailed image analysis is required to characterize the AMD3100 effect on TIL infiltration in the KPC model. Nonetheless, the increase in TILs in a subset of patients suggests sensitivity to a combination treatment with an anti-PD-(L)1 agent.

In conclusion, the experiments in the KPC mice and in the CAMPLEX clinical trial support the notion that AMD3100 favourably modulates the tumour microenvironment. It can be safely administered to patients, and should be considered for further clinical development in combination with an anti-PD-(L)1 agent.

9. ACKNOWLEDGMENTS

I would like to thank my wife Kasia for supporting my decision to go through this PhD, and being there for me every day. The journey to becoming an academic physician is filled with challenges and sacrifices that are shared and lived by one's partner. We always made it work, and are stronger for it.

Thank you to Duncan Jodrell for mentoring me over the last few years, and providing a positive learning environment amidst all the challenges I faced over the last 3 years.

I had relatively limited laboratory experience and I am greatly indebted to certain members of the lab for their help and support. In particular, Lukasz Magiera provided regular insightful conversation and technical expertise to help me through my experiments. Fran Richards regularly met with me to discuss ongoing experiments, and kindly reviewed my first year report, and thesis. Aarthi Gopinathan was always ready to listen and provide constructive feedback on my work. Claire Connell taught me some key skills early in my PhD. Finally, James Thaventhiran occasionally provided helpful comments.

Thank you to Doug Fearon for the critical appraisal of my work.

My work involved a fair amount of clinical work and I would like to acknowledge the clinical team. It was a pleasure to work in clinic with Simon Pacey, Richard Baird, and, in particular, Bristi Basu. Bristi provided an environment that supported independent practice, but with advice readily available when needed. I would also like to thank the nurses in the Early Phase Clinical Trial Unit, and the Clinical Research Facility.

10.ABBREVIATIONS

Abbreviation	Term	Abbreviation	Term
AE	Adverse event	LLOQ	lower limit of quantification
ALC	Absolute lymphocyte count	LM	Lukasz Magiera, scientist
AML	acute myeloid leukemia	LZ	light zone
CBC	Complete blood cell	MDSC	Myeloid-derived suppressor cell
CC3	Cleaved Caspase-3	MHRA	Medicine and healthcare regulatory authority
CL	Clearance	MI	Morisita Index
C _{max}	Maximum plasma concentration	panCK	pan-cytokeratin
CMR	complete metabolic response	PC	LSL-Trp53R172H/+;Pdx1-Cre mice
CNS	central nervous system	pCR	Pathologic complete response
CRC	Colorectal cancer	PD	Progressive disease
CRP	C-reactive protein	PDAC	Pancreatic adenocarcinoma
C _{ss}	Concentration at steady state	PD-1	Programmed cell death protein 1
CTA	Clinical Trial Authorisation	PD-L1	Programmed death-ligand 1
CTCAE	Common Terminology Criteria for Adverse Events	PERCIST	PET Response Criteria in Solid Tumours
CXCL12	chemokine ligand 12	PMR	partial metabolic response
DLT	dose-limiting toxicity	QC	Quality control
DZ	dark zone	RB	Rebecca Brais, consultant pathologist
EC ₅₀	half-maximal effect	RECIST	Response Evaluation Criteria in Solid Tumours
ECOG	Eastern Cooperative Oncology Group	ROI	region of interest
FFPE	formalin-fixed, paraffin-embedded	RP2D	recommended phase 2 dose
GCP	Good Clinical Practice	S/C	subcutaneous
G-CSF	Granulocyte colony stimulating factor	SUL	standardized uptake value lean
IF	immunofluorescence	SVT	supraventricular tachycardia
IHC	immunohistochemistry	TAM	Tumour associated macrophage
Ke	elimination rate constant	TIL	Tumour infiltrating lymphocyte
KPC	LSL-KrasG12D/+;LSL-Trp53R172H/+;Pdx1-Cre mice	TMA	Tissue microarray
LLN	Lower limit of normal	Vd	volume of distribut
		WBC	White blood cell

11. REFERENCES

1. Malvezzi M, Carioli G, Bertuccio P et al. European cancer mortality predictions for the year 2018 with focus on colorectal cancer. *Ann. Oncol.* 2018; 29(4):1016–1022.
2. Gordon-Dseagu VL, Devesa SS, Goggins M, Stolzenberg-Solomon R. Pancreatic cancer incidence trends: evidence from the Surveillance, Epidemiology and End Results (SEER) population-based data. *Int. J. Epidemiol.* 2018; 47(2):427–439.
3. Oettle H, Neuhaus P, Hochhaus A, et al. Adjuvant chemotherapy with gemcitabine and long-term outcomes among patients with resected pancreatic cancer: The conko-001 randomized trial. *JAMA* 2013; 310(14):1473–1481.
4. Conroy T, Hammel P, Hebbar M et al. Unicancer GI PRODIGE 24/CCTG PA.6 trial: A multicenter international randomized phase III trial of adjuvant mFOLFIRINOX versus gemcitabine (gem) in patients with resected pancreatic ductal adenocarcinomas. *J. Clin. Oncol.* 2018; 36(18_suppl):LBA4001-LBA4001.
5. Neoptolemos JP, Palmer DH, Ghaneh P et al. Comparison of adjuvant gemcitabine and capecitabine with gemcitabine monotherapy in patients with resected pancreatic cancer (ESPAC-4): a multicentre, open-label, randomised, phase 3 trial. *Lancet* 2017; 389(10073):1011–1024.
6. Conroy T, Desseigne F, Ychou M et al. FOLFIRINOX versus Gemcitabine for Metastatic Pancreatic Cancer. *N. Engl. J. Med.* 2011; 364(19):1817–1825.
7. Von Hoff DD, Ervin T, Arena FP et al. Increased Survival in Pancreatic Cancer with nab-Paclitaxel plus Gemcitabine. *N. Engl. J. Med.* 2013; 369(18):1691–1703.
8. AP V, Niedzwiecki D, Lenz H, et al. Effect of first-line chemotherapy combined with cetuximab or bevacizumab on overall survival in patients

- with kras wild-type advanced or metastatic colorectal cancer: A randomized clinical trial. *JAMA* 2017; 317(23):2392–2401.
9. Mayer RJ, Van Cutsem E, Falcone A et al. Randomized Trial of TAS-102 for Refractory Metastatic Colorectal Cancer. *N. Engl. J. Med.* 2015; 372(20):1909–1919.
 10. Hodi FS, O'Day SJ, McDermott DF et al. Improved Survival with Ipilimumab in Patients with Metastatic Melanoma. *N. Engl. J. Med.* 2010; 363(8):711–723.
 11. Borghaei H, Paz-Ares L, Horn L et al. Nivolumab versus Docetaxel in Advanced Nonsquamous Non–Small-Cell Lung Cancer. *N. Engl. J. Med.* 2015; 373(17):1627–1639.
 12. Motzer RJ, Escudier B, McDermott DF et al. Nivolumab versus Everolimus in Advanced Renal-Cell Carcinoma. *N. Engl. J. Med.* 2015; 373(19):1803–1813.
 13. Bellmunt J, de Wit R, Vaughn DJ et al. Pembrolizumab as Second-Line Therapy for Advanced Urothelial Carcinoma. *N. Engl. J. Med.* 2017; 376(11):1015–1026.
 14. Chen R, Zinzani PL, Fanale MA et al. Phase II Study of the Efficacy and Safety of Pembrolizumab for Relapsed/Refractory Classic Hodgkin Lymphoma. *J. Clin. Oncol.* 2017; 35(19):2125–2132.
 15. Ferris RL, Blumenschein G, Fayette J et al. Nivolumab for Recurrent Squamous-Cell Carcinoma of the Head and Neck. *N. Engl. J. Med.* 2016; 375(19):1856–1867.
 16. Le DT, Uram JN, Wang H et al. PD-1 Blockade in Tumors with Mismatch-Repair Deficiency. *N. Engl. J. Med.* 2015; 372(26):2509–2520.
 17. Brahmer JR, Tykodi SS, Chow LQ et al. Safety and activity of anti-PD-L1 antibody in patients with advanced cancer. *N. Engl. J. Med.* 2012; 366(26):2455–2465.
 18. Royal RE, Levy C, Turner K et al. Phase 2 Trial of Single Agent Ipilimumab (Anti-CTLA-4) for Locally Advanced or Metastatic Pancreatic Adenocarcinoma. *J. Immunother.* 2010.

19. Topalian SL, Hodi FS, Brahmer JR et al. Safety, Activity, and Immune Correlates of Anti-PD-1 Antibody in Cancer. *N. Engl. J. Med.* 2012; 366(26):2443–2454.
20. Chung KY, Gore I, Fong L et al. Phase II Study of the Anti-Cytotoxic T-Lymphocyte-Associated Antigen 4 Monoclonal Antibody, Tremelimumab, in Patients With Refractory Metastatic Colorectal Cancer. *J. Clin. Oncol.* 2010; 28(21):3485–3490.
21. Overman MJ, Lonardi S, Wong KYM et al. Durable Clinical Benefit With Nivolumab Plus Ipilimumab in DNA Mismatch Repair-Deficient/Microsatellite Instability-High Metastatic Colorectal Cancer. *J. Clin. Oncol.* 2018; 36(8):773–779.
22. Bonneville R, Krook MA, Kautto EA et al. Landscape of Microsatellite Instability Across 39 Cancer Types. *JCO Precis. Oncol.* 2017; (1):1–15.
23. Koopman M, Kortman GAM, Mekenkamp L et al. Deficient mismatch repair system in patients with sporadic advanced colorectal cancer. *Br. J. Cancer* 2009; 100:266.
24. Hu ZI, Shia J, Stadler ZK et al. Evaluating Mismatch Repair Deficiency in Pancreatic Adenocarcinoma: Challenges and Recommendations. *Clin. Cancer Res.* 2018; 24(6):1326 LP-1336.
25. Macherla S, Laks S, Naqash RA et al. Emerging Role of Immune Checkpoint Blockade in Pancreatic Cancer. *Int. J. Mol. Sci.* 2018. doi:10.3390/ijms19113505.
26. Zhu Y, Knolhoff BL, Meyer MA et al. CSF1/CSF1R blockade reprograms tumor-infiltrating macrophages and improves response to T-cell checkpoint immunotherapy in pancreatic cancer models. *Cancer Res.* 2014; 74(18):5057–5069.
27. Highfill SL, Cui Y, Giles AJ et al. Disruption of CXCR2-mediated MDSC tumor trafficking enhances anti-PD1 efficacy. *Sci. Transl. Med.* 2014. doi:10.1126/scitranslmed.3007974.
28. Beatty GL, Chiorean EG, Fishman MP et al. CD40 Agnsts Alter Tumor Stroma and Show Efficacy Against Pancreatic Carcinoma in Mice and

- Humans. *Science* (80-.). 2011; 331(May):1612–1616.
29. Gunderson AJ, Kaneda MM, Tsujikawa T et al. Bruton tyrosine kinase–Dependent immune cell cross-talk drives pancreas cancer. *Cancer Discov.* 2016; 6(3):270–285.
 30. Sanford DE, Belt BA, Panni RZ et al. Inflammatory monocyte mobilization decreases patient survival in pancreatic cancer: A role for targeting the CCL2/CCR2 axis. *Clin. Cancer Res.* 2013; 19(13):3404–3415.
 31. Jiang H, Hegde S, Knolhoff BL et al. Targeting focal adhesion kinase renders pancreatic cancers responsive to checkpoint immunotherapy. *Nat. Med.* 2016; 22(8):851–860.
 32. Feig C, Jones JO, Kraman M et al. Targeting CXCL12 from FAP-expressing carcinoma-associated fibroblasts synergizes with anti – PD-L1 immunotherapy in pancreatic cancer. *Proc Natl Acad Sci U S A* 2013; 110(50):20212–20217.
 33. Herbein G, Mahlknecht U, Batliwalla F et al. Apoptosis of CD8+ T cells is mediated by macrophages through interaction of HIV gp120 with chemokine receptor CXCR4. *Nature* 1998; 395:189.
 34. Poznansky MC, Olszak IT, Foxall R et al. Active movement of T cells away from a chemokine. *Nat. Med.* 2000; 6(5):543–548.
 35. Chen T, Yuan J, Duncanson S et al. Alginate Encapsulant Incorporating CXCL12 Supports Long-Term Allo- and Xenoislet Transplantation Without Systemic Immune Suppression. *Am. J. Transplant.* 2015; 15(3):618–627.
 36. Tang D, Kang R, Cheh C-W et al. HMGB1 release and redox regulates autophagy and apoptosis in cancer cells. *Oncogene* 2010; 29:5299.
 37. Schiraldi M, Raucci A, Muñoz LM et al. HMGB1 promotes recruitment of inflammatory cells to damaged tissues by forming a complex with CXCL12 and signaling via CXCR4. *J. Exp. Med.* 2012; 209(3):551–563.
 38. Liang JJ, Zhu S, Bruggeman R et al. High levels of expression of human stromal cell-derived factor-1 are associated with worse prognosis in patients with stage II pancreatic ductal adenocarcinoma. *Cancer Epidemiol Biomarkers Prev* 2010; 19(10):2598–2604.

39. Akishima-Fukasawa Y, Nakanishi Y, Ino Y et al. Prognostic significance of CXCL12 expression in patients with colorectal carcinoma. *Am. J. Clin. Pathol.* 2009; 132(2):202–210.
40. Balkwill F. Cancer and the chemokine network. *Nat. Rev. Cancer* 2004; 4:540.
41. Oberlin E, Amara A, Bachelier F et al. The CXC chemokine SDF-1 is the ligand for LESTR/fusin and prevents infection by T-cell-line-adapted HIV-1. *Nature* 1996; 382:833.
42. Hoffmann F, Müller W, Schütz D et al. Rapid Uptake and Degradation of CXCL12 Depend on CXCR7 Carboxyl-terminal Serine/Threonine Residues. *J. Biol. Chem.* 2012; 287(34):28362–28377.
43. Busillo JM, Benovic JL. Regulation of CXCR4 signaling. *Biochim. Biophys. Acta - Biomembr.* 2007; 1768(4):952–963.
44. Bleul CC, Farzan M, Choe H et al. The lymphocyte chemoattractant SDF-1 is a ligand for LESTR/fusin and blocks HIV-1 entry. *Nature* 1996; 382:829.
45. Sugiyama T, Kohara H, Noda M, Nagasawa T. Maintenance of the Hematopoietic Stem Cell Pool by CXCL12-CXCR4 Chemokine Signaling in Bone Marrow Stromal Cell Niches. *Immunity* 2006; 25(6):977–988.
46. Bleul CC, Wu L, Hoxie JA et al. The HIV coreceptors CXCR4 and CCR5 are differentially expressed and regulated on human T lymphocytes. *Proc. Natl. Acad. Sci.* 1997; 94(5):1925–1930.
47. Zabel BA, Agace WW, Campbell JJ et al. Human G Protein–Coupled Receptor Gpr-9-6/Cc Chemokine Receptor 9 Is Selectively Expressed on Intestinal Homing T Lymphocytes, Mucosal Lymphocytes, and Thymocytes and Is Required for Thymus-Expressed Chemokine–Mediated Chemotaxis. *J. Exp. Med.* 1999; 190(9):1241 LP-1256.
48. Nagasawa T, Hirota S, Tachibana K et al. Defects of B-cell lymphopoiesis and bone-marrow myelopoiesis in mice lacking the CXC chemokine PBSF/SDF-1. *Nature* 1996; 382:635.
49. Ma Q, Jones D, Borghesani PR et al. Impaired B-lymphopoiesis, myelopoiesis, and derailed cerebellar neuron migration in CXCR4- and

- SDF-1-deficient mice. *Proc. Natl. Acad. Sci.* 1998; 95(16):9448 LP-9453.
50. Hernandez PA, Gorlin RJ, Lukens JN et al. Mutations in the chemokine receptor gene CXCR4 are associated with WHIM syndrome, a combined immunodeficiency disease. *Nat. Genet.* 2003; 34:70.
 51. Signoret N, Oldridge J, Pelchen-Matthews A et al. Phorbol esters and SDF-1 induce rapid endocytosis and down modulation of the chemokine receptor CXCR4. *J. Cell Biol.* 1997; 139(3):651–664.
 52. Tarasova NI, Stauber RH, Michejda CJ. Spontaneous and ligand-induced trafficking of CXC-chemokine receptor 4. *J. Biol. Chem.* 1998; 273(26):15883–15886.
 53. Marchese A, Benovic JL. Agonist-promoted Ubiquitination of the G Protein-coupled Receptor CXCR4 Mediates Lysosomal Sorting. *J. Biol. Chem.* 2001; 276(49):45509–45512.
 54. Hatse S, Princen K, Gerlach L-O et al. Mutation of Asp¹⁷¹ and Asp²⁶² of the Chemokine Receptor CXCR4 Impairs Its Coreceptor Function for Human Immunodeficiency Virus-1 Entry and Abrogates the Antagonistic Activity of AMD3100. *Mol. Pharmacol.* 2001; 60(1):164 LP-173.
 55. Sigrid H, Katrien P, Gary B et al. Chemokine receptor inhibition by AMD3100 is strictly confined to CXCR4. *FEBS Lett.* 2002; 527(1–3):255–262.
 56. Fricker SP, Anastassov V, Cox J et al. Characterization of the molecular pharmacology of AMD3100: A specific antagonist of the G-protein coupled chemokine receptor, CXCR4. *Biochem. Pharmacol.* 2006; 72(5):588–596.
 57. De Clercq E. The bicyclam AMD3100 story. *Nat. Rev. Drug Discov.* 2003; 2(7):581–587.
 58. Hendrix CW, Collier AC, Lederman MM et al. A selective CXCR4 receptor inhibitor, in HIV-1 infection. *J. Acquir. Immune Defic. Syndr.* 2004; 37(2):1253–1262.
 59. Hendrix CW, Flexner C, MacFarland RT et al. Pharmacokinetics and safety of AMD-3100, a novel antagonist of the CXCR-4 chemokine receptor, in

- human volunteers. *Antimicrob. Agents Chemother.* 2000; 44(6):1667–73.
60. Liles WC, Broxmeyer HE, Rodger E et al. Mobilization of hematopoietic progenitor cells in healthy volunteers by AMD3100, a CXCR4 antagonist. *Blood* 2003; 102(8):2728–2730.
 61. Flomenberg N, Comenzo RL, Badel K, Calandra G. Plerixafor (Mozobil®) Alone to Mobilize Hematopoietic Stem Cells from Multiple Myeloma Patients for Autologous Transplantation. *Biol. Blood Marrow Transplant.* 2010; 16(5):695–700.
 62. Micallef IN, Stiff PJ, DiPersio JF et al. Successful Stem Cell Remobilization Using Plerixafor (Mozobil) Plus Granulocyte Colony-Stimulating Factor in Patients with Non-Hodgkin Lymphoma: Results from the Plerixafor NHL Phase 3 Study Rescue Protocol. *Biol. Blood Marrow Transplant.* 2009. doi:10.1016/j.bbmt.2009.08.005.
 63. DiPersio J, Stadtmauer E, Nademanee A et al. Plerixafor and G-CSF versus placebo and G-CSF to mobilize hematopoietic stem cells for autologous stem cell transplantation in patients with multiple myeloma. *Blood* 2009. doi:10.1182/blood-2008-08-174946.
 64. DiPersio JF, Micallef IN, Stiff PJ et al. Phase III prospective randomized double-blind placebo-controlled trial of plerixafor plus granulocyte colony-stimulating factor compared with placebo plus granulocyte colony-stimulating factor for autologous stem-cell mobilization and transplantation for . *J. Clin. Oncol.* 2009; 27(28):4767–4773.
 65. Hübel K, Liles WC, Broxmeyer HE et al. Leukocytosis and Mobilization of CD34+ Hematopoietic Progenitor Cells by AMD3100, a CXCR4 Antagonist. *Support. Cancer Ther.* 2004. doi:10.3816/SCT.2004.n.008.
 66. Popple A, Durrant LG, Spendlove I et al. The chemokine, CXCL12, is an independent predictor of poor survival in ovarian cancer. *Br. J. Cancer* 2012; 106(7):1306–1313.
 67. Naito Y, Saito K, Shiiba K et al. CD8 + T Cells Infiltrated within Cancer Cell Nests as a Prognostic Factor in Human Colorectal Cancer Advances in Brief CD8 + T Cells Infiltrated within Cancer Cell Nests as a Prognostic

- Factor in Human Colorectal Cancer. 1998:3491–3494.
68. Zhang L, Conejo-Garcia JR, Katsaros D et al. Intratumoral T Cells, Recurrence, and Survival in Epithelial Ovarian Cancer. *N. Engl. J. Med.* 2003; 348(3):203–213.
 69. Kim EJ, Sahai V, Abel E V. et al. Pilot clinical trial of hedgehog pathway inhibitor GDC-0449 (vismodegib) in combination with gemcitabine in patients with metastatic pancreatic adenocarcinoma. *Clin. Cancer Res.* 2014; 20(23):5937–5945.
 70. Olive KP, Jacobetz MA, Davidson CJ et al. Inhibition of Hedgehog Signaling Enhances Delivery of Chemotherapy in a Mouse Model of Pancreatic Cancer. *Science (80-.).* 2009; 324(5933):1457 LP-1461.
 71. Catenacci DVT, Junttila MR, Karrison T et al. Randomized Phase Ib/II Study of Gemcitabine Plus Placebo or Vismodegib, a Hedgehog Pathway Inhibitor, in Patients With Metastatic Pancreatic Cancer. *J. Clin. Oncol.* 2015; 33(36):4284–4292.
 72. Fukunaga A, Miyamoto M, Cho Y et al. CD8+ Tumor-Infiltrating Lymphocytes Together with CD4+ Tumor-Infiltrating Lymphocytes and Dendritic Cells Improve the Prognosis of Patients with Pancreatic Adenocarcinoma. *Pancreas* 2004; 28(1):26–31.
 73. Ene-Obong A, Clear AJ, Watt J et al. Activated pancreatic stellate cells sequester CD8+T cells to reduce their infiltration of the juxtatumoral compartment of pancreatic ductal adenocarcinoma. *Gastroenterology* 2013; 145(5):1121–1132.
 74. Pagès F, Berger A, Camus M et al. Effector Memory T Cells, Early Metastasis, and Survival in Colorectal Cancer. *N. Engl. J. Med.* 2005; 353(25):2654–2666.
 75. Galon J, Costes A, Sanchez-Cabo F et al. Type, density, and location of immune cells within human colorectal tumors predict clinical outcome. *Science (80-.).* 2006; 313(5795):1960–1964.
 76. Mlecnik B, Tosolini M, Kirilovsky A et al. Histopathologic-based prognostic factors of colorectal cancers are associated with the state of the local

- immune reaction. *J. Clin. Oncol.* 2011; 29(6):610–618.
77. Halama N, Michel S, Kloor M et al. Localization and density of immune cells in the invasive margin of human colorectal cancer liver metastases are prognostic for response to chemotherapy. *Cancer Res.* 2011; 71(17):5670–5677.
 78. Denkert C, Loibl S, Noske A et al. Tumor-associated lymphocytes as an independent predictor of response to neoadjuvant chemotherapy in breast cancer. *J. Clin. Oncol.* 2010; 28(1):105–113.
 79. Tumei PC, Harview CL, Yearley JH et al. PD-1 blockade induces responses by inhibiting adaptive immune resistance. *Nature* 2014; 515(7528):568–571.
 80. Mahmoud SMA, Paish EC, Powe DG et al. Tumor-infiltrating CD8+ lymphocytes predict clinical outcome in breast cancer. *J. Clin. Oncol.* 2011; 29(15):1949–1955.
 81. Pagès F, Kirilovsky A, Mlecnik B et al. In situ cytotoxic and memory T cells predict outcome in patients with early-stage colorectal cancer. *J. Clin. Oncol.* 2009; 27(35):5944–5951.
 82. Fridman WH, Pagès F, Sauts-Fridman C, Galon J. The immune contexture in human tumours: Impact on clinical outcome. *Nat. Rev. Cancer* 2012; 12(4):298–306.
 83. Galon J, Mlecnik B, Bindea G et al. Towards the introduction of the “Immunoscore” in the classification of malignant tumours. *J. Pathol.* 2014; 232(2):199–209.
 84. Eisenhauer EA, Therasse P, Bogaerts J et al. New response evaluation criteria in solid tumours: Revised RECIST guideline (version 1.1). *Eur. J. Cancer* 2009; 45(2):228–247.
 85. Wahl RL, Jacene H, Kasamon Y, Lodge MA. From RECIST to PERCIST: Evolving Considerations for PET Response Criteria in Solid Tumors. *J. Nucl. Med.* 2009; 50(Suppl_1):122S–150S.
 86. Rowland M, Tozer TN. *Clinical pharmacokinetics and pharmacodynamics*, 4th edition. Baltimore, MD, USA: Lippincott Williams & Wilkins, 2011.

87. Hingorani SR, Wang L, Multani AS et al. Trp53R172H and KrasG12D cooperate to promote chromosomal instability and widely metastatic pancreatic ductal adenocarcinoma in mice. *Cancer Cell* 2005; 7(5):469–483.
88. Dako/Agilent. PD-L1 IHC 22C3 pharmDx interpretation manual, 2016.
89. Roche. VENTANA PD-L1 (SP142) Assay Interpretation Guide for Urothelial Carcinoma, 2016.
90. Robins HS, Campregher P V, Srivastava SK et al. Comprehensive assessment of T-cell receptor β -chain diversity in $\alpha\beta$ T cells. *Blood* 2009; 114(19):4099 LP-4107.
91. Six A, Mariotti-Ferrandiz E, Chaara W et al. The Past, Present, and Future of Immune Repertoire Biology – The Rise of Next-Generation Repertoire Analysis. *Front. Immunol.* 2013; 4:413.
92. Heng TSP, Painter MW, Consortium TIGP et al. The Immunological Genome Project: networks of gene expression in immune cells. *Nat. Immunol.* 2008; 9:1091.
93. Uy GL, Rettig MP, Motabi IH et al. A phase 1/2 study of chemosensitization with the CXCR4 antagonist plerixafor in relapsed or refractory acute myeloid leukemia. *Blood* 2012; 119(17):3917–3924.
94. Allen CDC, Ansel KM, Low C et al. Germinal center dark and light zone organization is mediated by CXCR4 and CXCR5. *Nat. Immunol.* 2004; 5(9):943–952.
95. Rodda LB, Bannard O, Ludewig B et al. Phenotypic and Morphological Properties of Germinal Center Dark Zone *Cxcl12* -Expressing Reticular Cells. *J. Immunol.* 2015; 195(10):4781–4791.
96. Hiraoka N, Ino Y, Yamazaki-Itoh R. Tertiary Lymphoid Organs in Cancer Tissues. *Front. Immunol.* 2016; 7:244.
97. Liu Q, Li Z, Gao JL et al. CXCR4 antagonist AMD3100 redistributes leukocytes from primary immune organs to secondary immune organs, lung, and blood in mice. *Eur. J. Immunol.* 2015; 45(6):1855–1867.
98. Kazandjian D, Keegan P, Suzman DL et al. Characterization of outcomes

- in patients with metastatic non-small cell lung cancer treated with programmed cell death protein 1 inhibitors past RECIST version 1.1–defined disease progression in clinical trials. *Semin. Oncol.* 2017; 44(1):3–7.
99. Beaver JA, Hazarika M, Mulkey F et al. Patients with melanoma treated with an anti-PD-1 antibody beyond RECIST progression: A US Food and Drug Administration pooled analysis. *Lancet Oncol.* 2018; 19(2):229–239.
 100. Zhang W, Navenot J, Haribabu B et al. A Point Mutation That Confers Constitutive Activity to CXCR4 Reveals That T140 Is an Inverse Agonist and That AMD3100 and ALX40-4C Are Weak Partial Agonists *. 2002; 277(27):24515–24521.
 101. Kobayashi N, Takata H, Yokota S, Takiguchi M. Down-regulation of CXCR4 expression on human CD8+ T cells during peripheral differentiation. *Eur. J. Immunol.* 2004; 34(12):3370–8.
 102. Förster R, Kremmer E, Schubel a et al. Intracellular and surface expression of the HIV-1 coreceptor CXCR4/fusin on various leukocyte subsets: rapid internalization and recycling upon activation. *J. Immunol.* 1998; 160(3):1522–1531.
 103. Herbst RS, Soria JC, Kowanetz M et al. Predictive correlates of response to the anti-PD-L1 antibody MPDL3280A in cancer patients. *Nature* 2014; 515(7528):563–567.
 104. Hirsch S, Austyn JM, Gordon S. Expression of the macrophage-specific antigen F4/80 during differentiation of mouse bone marrow cells in culture. *J. Exp. Med.* 1981; 154(3):713–725.
 105. Austyn JM, Gordon S. F4-80, a Monoclonal-Antibody Directed Specifically against the Mouse Macrophage. *Eur. J. Immunol.* 1981; 11(10):805–815.
 106. Francke A, Herold J, Weinert S et al. Generation of mature murine monocytes from heterogeneous bone marrow and description of their properties. *J. Histochem. Cytochem.* 2011; 59(9):813–825.
 107. McDermott DH, Liu Q, Ulrick J et al. The CXCR4 antagonist plerixafor corrects panleukopenia in patients with WHIM syndrome. *Blood* 2011;

- 118(18):4957 LP-4962.
108. Mantovani A, Marchesi F, Malesci A et al. Tumour-associated macrophages as treatment targets in oncology. *Nat. Rev. Clin. Oncol.* 2017; 14(7):399–416.
 109. Chatterjee M, Von Ungern-Sternberg SNI, Seizer P et al. Platelet-derived CXCL12 regulates monocyte function, survival, differentiation into macrophages and foam cells through differential involvement of CXCR4-CXCR7. *Cell Death Dis.* 2015; 6(11):1–16.
 110. Sánchez-Martín L, Estecha A, Samaniego R et al. The chemokine CXCL12 regulates monocyte-macrophage differentiation and RUNX3 expression. *Blood* 2011; 117(1):88–97.
 111. Italiani P, Boraschi D. From monocytes to M1/M2 macrophages: Phenotypical vs. functional differentiation. *Front. Immunol.* 2014; 5(OCT):1–22.
 112. Burris HA, Moore MJ, Andersen J et al. Improvements in survival and clinical benefit with gemcitabine as first-line therapy for patients with advanced pancreas cancer: a randomized trial. *J. Clin. Oncol.* 1997; 15(6):2403–2413.
 113. Hanna RN, Cekic C, Sag D et al. Patrolling monocytes control tumor metastasis to the lung. *Science (80-.)*. 2015; 350(6263):985 LP-990.
 114. Grolleau F, Gamelin L, Boisdron-Celle M et al. A Possible Explanation for a Neurotoxic Effect of the Anticancer Agent Oxaliplatin on Neuronal Voltage-Gated Sodium Channels. *J. Neurophysiol.* 2001.
 115. Plerixafor After Radiation Therapy and Temozolomide in Treating Patients With Newly Diagnosed High Grade Glioma. [<http://clinicaltrials.gov/show/NCT01977677>].
 116. Investigator's Brochure Plerixafor, 18th edition. Genzyme Corporation, 2015.
 117. Zou Y-R, Kottmann AH, Kuroda M et al. Function of the chemokine receptor CXCR4 in haematopoiesis and in cerebellar development. *Nature* 1998; 393(6685):595–599.

118. Guyon A. CXCL12 chemokine and its receptors as major players in the interactions between immune and nervous systems. *Front. Cell. Neurosci.* 2014; 8(March):1–10.
119. Gerlach LO, Jakobsen JS, Jensen KP et al. Metal ion enhanced binding of AMD3100 to Asp262 in the CXCR4 receptor. *Biochemistry* 2003; 42(3):710–717.
120. Rosenkilde MM, Gerlach LO, Jakobsen JS et al. Molecular mechanism of AMD3100 antagonism in the CXCR4 receptor: Transfer of binding site to the CXCR3 receptor. *J. Biol. Chem.* 2004; 279(4):3033–3041.
121. Pachman DR, Qin R, Seisler DK et al. Clinical course of oxaliplatin-induced neuropathy: Results from the randomized phase III trial N08CB (Alliance). *J. Clin. Oncol.* 2015; 33(30):3416–3422.
122. Gill JS, Windebank a J. Cisplatin-induced apoptosis in rat dorsal root ganglion neurons is associated with attempted entry into the cell cycle. *J. Clin. Invest.* 1998; 101(12):2842–2850.
123. Wilmot JP. Cancer-Related Fatigue and Sleep Disorders. *Cancer* 2007; 12(suppl 1):35–42.
124. Savard J, Ivers H, Savard MH, Morin CM. Cancer treatments and their side effects are associated with aggravation of insomnia: Results of a longitudinal study. *Cancer* 2015; 121(10):1703–1711.
125. Venkateshiah SB, Collop NA. Sleep and Sleep Disorders in the Hospital. *Chest* 2018; 141(5):1337–1345.
126. Mosqueda-Garcia R, Furlan R, MD JT, Fernandez-Violante R. The Elusive Pathophysiology of Neurally Mediated Syncope. *Circulation* 2000; 102(23):2898 LP-2906.
127. Shen W, Hu XM, Liu YN et al. CXCL12 in astrocytes contributes to bone cancer pain through CXCR4-mediated neuronal sensitization and glial activation in rat spinal cord. *J. Neuroinflammation* 2014; 11(1):1–14.
128. Luo X, Tai WL, Sun L et al. Crosstalk between astrocytic CXCL12 and microglial CXCR4 contributes to the development of neuropathic pain. *Mol. Pain* 2016; 12:1–15.

129. Naidoo J, Page DB, Li BT et al. Toxicities of the anti-PD-1 and anti-PD-L1 immune checkpoint antibodies. *Ann. Oncol.* 2015; 26(12):2375–2391.
130. MacFarland R, Hard ML, Scarborough R et al. A Pharmacokinetic Study of Plerixafor in Subjects with Varying Degrees of Renal Impairment. *Biol. Blood Marrow Transplant.* 2010; 16(1):95–101.
131. Schultz DR, Arnold PI. Properties of four acute phase proteins: C-reactive protein, serum amyloid a protein, α 1-acid glycoprotein, and fibrinogen. *Semin. Arthritis Rheum.* 1990; 20(3):129–147.
132. Huang Z, Ung T. Effect of alpha-1-acid glycoprotein binding on pharmacokinetics and pharmacodynamics. *Curr. Drug Metab.* 2013. doi:10.2174/1389200211314020011.
133. Hughes CA, Tseng A, Cooper R. Managing drug interactions in HIV-infected adults with comorbid illness. *CMAJ* 2015. doi:10.1503/cmaj.131626.
134. Toutain PL, Bousquet-Mélou A. Plasma terminal half-life. *J. Vet. Pharmacol. Ther.* 2004; 27(6):427–439.
135. Wuchter P, Ran D, Bruckner T et al. Poor Mobilization of Hematopoietic Stem Cells-Definitions, Incidence, Risk Factors, and Impact on Outcome of Autologous Transplantation. *Biol. Blood Marrow Transplant.* 2010; 16(4):490–499.
136. Thavendiranathan P, Bagai A, Ebidia A et al. Do blood tests cause anemia in hospitalized patients? The effect of diagnostic phlebotomy on hemoglobin and hematocrit levels. *J. Gen. Intern. Med.* 2005. doi:10.1111/j.1525-1497.2005.0094.x.
137. Chen DS, Mellman I. Elements of cancer immunity and the cancer-immune set point. *Nature* 2017; 541(7637):321–330.
138. Sivan A, Corrales L, Hubert N et al. Commensal Bifidobacterium promotes antitumor immunity and facilitates anti-PD-L1 efficacy. *Science (80-.).* 2015; 350(6264):1084–1089.
139. Marie Vétizou, 1, 2, 3 Jonathan M. Pitt, 1, 2, 3 Romain Daillère, 1, 2, 3 Patricia Lepage, 4 Nadine Waldschmitt, 5 Caroline Flament, 1, 2, 6 Sylvie

- Rusakiewicz, 1, 2, 6 Bertrand Routy, 1, 2, 3, 6 Maria P. Roberti, 1, 2, 6
Connie P. M. Duong, 1, 2, 6 Vichn 5* Laurence Zitvogel. Anticancer
immunotherapy by CTLA-4 blockade relies on the gutmicrobiota. *Science*
(80-). 2015; 350(6264):1079–1083.
140. Flint TR, Janowitz T, Connell CM et al. Tumor-Induced IL-6 Reprograms
Host Metabolism to Suppress Anti-tumor Immunity. *Cell Metab.* 2016;
24(5):672–684.
141. Grossman S, Ellsworth S, Campian J et al. Survival in Patients With
Severe Lymphopenia Following Treatment With Radiation and
Chemotherapy for Newly Diagnosed Solid Tumors. *J. Natl. Compr. Cancer
Netw.* 2015; 13(10):1225–31.
142. Balmanoukian A, Ye X, Herman J et al. The association between
treatment-related lymphopenia and survival in newly diagnosed patients
with resected adenocarcinoma of the pancreas. *Cancer Invest.* 2012;
30(8):571–576.
143. Raben M, Walach N, Galili U, Schlesinger M. The effect of radiation
therapy on lymphocyte subpopulations in cancer patients. *Cancer* 1976;
37(3):1417–1421.
144. Ray-Coquard I, Cropet C, Van Glabbeke M et al. Lymphopenia as a
prognostic factor for overall survival in advanced carcinomas, sarcomas,
and lymphomas. *Cancer Res.* 2009; 69(13):5383–5391.
145. Fogar P, Sperti C, Basso D et al. Decreased total lymphocyte counts in
pancreatic cancer: an index of adverse outcome. *Pancreas* 2006;
32(1):22–8.
146. An X, Ding P-R, Li Y-H et al. Elevated neutrophil to lymphocyte ratio
predicts survival in advanced pancreatic cancer. *Biomarkers* 2010;
15(6):516–522.
147. Clark EJ, Connor S, Taylor MA et al. Preoperative lymphocyte count as a
prognostic factor in resected pancreatic ductal adenocarcinoma. *Hpb* 2007;
9(6):456–460.
148. Delyon J, Mateus C, Lefeuvre D et al. Experience in daily practice with

- ipilimumab for the treatment of patients with metastatic melanoma: A nearly increase in lymphocyte and eosinophil counts is associated with improved survival. *Ann. Oncol.* 2013; 24(6):1697–1703.
149. Postow MA, Chasalow SD, Yuan J et al. Pharmacodynamic effect of ipilimumab on absolute lymphocyte count (ALC) and association with overall survival in patients with advanced melanoma. *J. Clin. Oncol.* 2013; 31(15_suppl):9052.
 150. Ku GY, Yuan J, Page DB et al. Single-institution experience with ipilimumab in advanced melanoma patients in the compassionate use setting lymphocyte count after 2 doses correlates with survival. *Cancer* 2010; 116(7):1767–1775.
 151. Martens A, Wistuba-Hamprecht K, Yuan J et al. Increases in absolute lymphocytes and circulating CD4+ and CD8+ T cells are associated with positive clinical outcome of melanoma patients treated with ipilimumab. *Clin. Cancer Res.* 2016; 22(19):1–23.
 152. Martens A, Wistuba-Hamprecht K, Foppen MG et al. Baseline peripheral blood biomarkers associated with clinical outcome of advanced melanoma patients treated with ipilimumab. *Clin. Cancer Res.* 2016; 22(12):2908–2918.
 153. Weide B, Martens A, Hassel JC et al. Baseline biomarkers for outcome of melanoma patients treated with pembrolizumab. *Clin. Cancer Res.* 2016; 22(22):5487–5496.
 154. Seo Y, Jalikis F, Jiang X et al. Combination T cell receptor immunosequencing and multiplex immunohistochemistry reveal novel insights into the immune response to human pancreatic cancer. *Proc. Am. Assoc. Cancer Res., Chicago*: 2018.
 155. Rosenbaum MW, Bledsoe JR, Morales-Oyarvide V et al. PD-L1 expression in colorectal cancer is associated with microsatellite instability, BRAF mutation, medullary morphology and cytotoxic tumor-infiltrating lymphocytes. *Mod. Pathol.* 2016; 29(9):1104–1112.
 156. Powles T, Eder JP, Fine GD et al. MPDL3280A (anti-PD-L1) treatment

- leads to clinical activity in metastatic bladder cancer. *Nature* 2014; 515(7528):558–562.
157. Blank CU, Haanen JB, Ribas A, Schumacher TN. The “cancer immunogram.” *Science* (80-.). 2016; 352(6286):658 LP-660.
 158. Seymour L, Bogaerts J, Perrone A et al. iRECIST: guidelines for response criteria for use in trials testing immunotherapeutics. *Lancet Oncol.* 2017; 18(3):e143–e152.
 159. Champiat S, Dercle L, Ammari S et al. Hyperprogressive disease is a new pattern of progression in cancer patients treated by anti-PD-1/PD-L1. *Clin. Cancer Res.* 2017; 23(8):1920–1928.
 160. Saâda-Bouزيد E, Defaucheux C, Karabajakian A et al. Hyperprogression during anti-PD-1/PD-L1 therapy in patients with recurrent and/or metastatic head and neck squamous cell carcinoma. *Ann. Oncol. Off. J. Eur. Soc. Med. Oncol.* 2017; 28(7):1605–1611.
 161. Ferrara R, Caramella C, Texier M et al. Hyperprogressive disease (HPD) is frequent in non-small cell lung cancer (NSCLC) patients (pts) treated with anti PD1/PD-L1 monoclonal antibodies (IO). *Ann. Oncol.* 2017; 28(suppl_5):mdx380.009-mdx380.009.
 162. Seith F, Forschner A, Schmidt H et al. 18F-FDG-PET detects complete response to PD1-therapy in melanoma patients two weeks after therapy start. *Eur. J. Nucl. Med. Mol. Imaging* 2018; 45(1):95–101.
 163. Cho SY, Lipson EJ, Im H-J et al. Prediction of Response to Immune Checkpoint Inhibitor Therapy Using Early Time-Point FDG-PET/CT Imaging in Patients with Advanced Melanoma. *J. Nucl. Med.* 2017;jnumed.116.188839.
 164. Sachpekidis C, Larribere L, Pan L et al. Predictive value of early 18F-FDG PET/CT studies for treatment response evaluation to ipilimumab in metastatic melanoma: preliminary results of an ongoing study. *Eur. J. Nucl. Med. Mol. Imaging* 2014; 42(3):386–396.
 165. Wong ANM, McArthur GA, Hofman MS, Hicks RJ. The Advantages and Challenges of Using FDG PET/CT for Response Assessment in Melanoma

- in the Era of Targeted Agents and Immunotherapy. *Eur. J. Nucl. Med. Mol. Imaging* 2017; 44:67–77.
166. Chen PL, Roh W, Reuben A et al. Analysis of immune signatures in longitudinal tumor samples yields insight into biomarkers of response and mechanisms of resistance to immune checkpoint blockade. *Cancer Discov.* 2016; 6(8):827–837.
 167. Riaz N, Havel JJ, Makarov V et al. Tumor and Microenvironment Evolution during Immunotherapy with Nivolumab. *Cell* 2017; 171(4):934–949.e15.
 168. Balachandran VP, Luksza M, Zhao JN et al. Identification of unique neoantigen qualities in long-term survivors of pancreatic cancer. *Nature* 2017; 551(7681):S12–S16.
 169. Reuben A, Gittelman R, Gao J et al. TCR Repertoire Intratumor Heterogeneity in Localized Lung Adenocarcinomas: An Association with Predicted Neoantigen Heterogeneity and Postsurgical Recurrence. *Cancer Discov.* 2017; 7(10):1088 LP-1097.
 170. Garcia-Diaz A, Shin DS, Moreno BH et al. Interferon Receptor Signaling Pathways Regulating PD-L1 and PD-L2 Expression. *Cell Rep.* 2017; 19(6):1189–1201.
 171. Patel SP, Kurzrock R. PD-L1 Expression as a Predictive Biomarker in Cancer Immunotherapy. *Mol. Cancer Ther.* 2015; 14(4):847 LP-856.